Isolation and Characterization of the Elusive Cyanoformate Ion and the Dependence of its Stability on Solvent Dielectric Constant

By
Luke Joseph Murphy

A Thesis Submitted to
Saint Mary's University, Halifax, Nova Scotia
in Partial Fulfillment of the Requirements for
the Degree of Master of Science in Applied Science

April 2014, Halifax, Nova Scotia

Approved:	Dr. Jason Clyburne Supervisor Departments of Chemistry & Environmental Science
Approved:	Dr. Jason Masuda Examiner Department of Chemistry
Approved:	Dr. Lisa Gannett Examiner Department of Philosophy
Approved:	Dr. Philip Jessop External Examiner Department of Chemistry Queen's University

Date: April 30, 2014

Isolation and Characterization of the Elusive Cyanoformate Ion and the Dependence of its Stability on Solvent Dielectric Constant

by Luke Joseph Murphy

The cyanoformate ion, speculated to be an intermediate by-product in the biosynthesis of ethylene in plants for decades but never observed, was successfully isolated for the first time as its tetraphenylphosphonium salt ($[PPh_4][NCCO_2]$). Full spectroscopic and crystallographic characterization of $[PPh_4][NCCO_2]$ is provided, including characterization of ^{13}C-labelled isotopologues. *In situ* infrared spectroscopic analysis of the decomposition of cyanoformate in various solvents has revealed that cyanoformate will dissociate into CN^- and CO_2 in higher dielectric media. The active site of 1-aminocyclopropane-1-carboxylic acid oxidase (ACC oxidase) bears an iron atom which may be protected from produced cyanide by its complexation with CO_2 as cyanoformate. When cyanoformate migrates out of the active site of the enzyme to the higher dielectric cytosol, it then dissociates, producing CN^- or HCN, which is subsequently metabolized.

April 30, 2014

Acknowledgements

Firstly I would like to thank my supervisor, Dr. Jason Clyburne. Years ago when I first started working in his lab, I had no idea that research, and even chemistry in general, would become such an important part of my life. Working with him has inspired me to continue on in this field and has provided me with so many amazing opportunities. I never would've imagined being first author on a paper in *Science*, let alone this early on.

Dr. Kathy Robertson has also been an enormous asset to myself and the rest of the research group over the years. Without seemingly inhuman ability to handle a million different things at the same time, in addition her skill and expertise, particularly with X-ray crystallography, none of this work would have been possible.

Dr. Heikki Tuononen and Dr. Jani Moilanen at the University of Jyväskylä in Finland are responsible for carrying out, and discussing, all of the computational work contained herein. Without their hard work to back up the experimental evidence this project could not have been as much of a success as it was. In addition I'd like to thank Dr. Ulrike Werner-Zwanziger at Dalhousie for all the time she spent troubleshooting NMR samples with me, for processing and explanation of the data, and also for not killing me when I nearly destroyed all of her rotors.

Scott Harroun and Dr. Christa Brosseau are responsible for all the Raman spectra contained in this work, without which likely nobody would believe we even made cyanoformate. Special thanks to Patricia Granados who spent weeks investigating methods to improve our EA data, and Canadian Microanalytical Service, Ltd. in BC who somehow managed to pull it off.

The other members of the Clyburne group have been a huge help both with getting things done in the lab, as well keeping me social and somewhat sane. The technicians at Saint Mary's have been a great help as well, particularly Elizabeth McLeod who procures all of our chemicals (even dangerous ones Canada did not seem to want us to have), and always seems to have every random thing I happen to be looking for. In addition I truly appreciate my supervisory committee (Dr. Jason Masuda, Dr. Lisa Gannett) and my external examiner (Dr. Philip Jessop) taking time out of their lives to read and evaluate all this.

Table of Contents

List of Figures

List of Schemes

List of Tables

Table of Symbols and Abbreviations

$[Bu_4N]^+$	tetrabutylammonium ion
$[N(CN)_2]^-$	dicyanimide ion
[EMIM]OAc	1-ethyl-3-methylimidazolium acetate
$[FCO_2]^-$	fluorocarbonate ion
$[H^+]$	concentration of hydrogen ion
$[HCO_3]^-$	bicarbonate ion
$[Me_4N]^+$	tetramethylammonium ion
$[NCCO_2]^-$	cyanoformate ion
$[P_{66614}]^+$	trihexyl(tetradecyl)phosphonium ion
$[PPh_4]^+$	tetraphenylphosphonium ion
$[TFSI]^-$	bis(trifluoromethylsulfonyl)imide ion
°	degrees
°C	degrees Celsius
µm	micrometer
Å	Angstrom
ACC	1-aminocyclopropane-1-carboxylic acid
AMU	atomic mass unit
Asp	aspartate/aspartic acid
ATP	adenosine triphosphate
br	broad
c	speed of light
CCS	carbon capture and sequestration/storage
cm^{-1}	wavenumber
CP	cross-polarization
CSD	Cambridge Structural Database
DBU	1,8-diazabicyclo[5.4.0]undec-7-ene
dec	decomposes
DETA	diethylenetriamine
$DETAH^+$	mono-protonated diethylenetriamine ion
DMC	dimethylcarbonate
DMF	dimethylformamide
DMSO	dimethylsulfoxide
FLP	frustrated Lewis pair

FTIR	Fourier-transform infrared
FWHM	full-width half-maximum
g	gram
HCN	hydrogen cyanide
His	histidine
Hz	Hertz (s^{-1})
IL	ionic liquid
IR	infrared
J	Joule/coupling constant
K	Kelvin
k	force (spring) constant
kcal	kilocalorie
kHz	kilohertz
km	kilometer
kPa	kilopascal
L	liter
m	medium
mA	milliamp
MAS	magic-angle spinning
MEA	monoethanolamine
MeCN	acetonitrile
MeOH	methanol
mg	milligram
MHz	megahertz
mL	milliliter
mM	millimolar (millimole per liter)
MOF	metal-organic framework
mol	mole
mp	melting point
mRNA	messenger ribonucleic acid
ms	millisecond
MS	mass spectrometry
mV	millivolt
MW	molecular weight/molar mass
mW	milliwatt
NADPH	nicotinamide adenine dinucleotide phosphate
NHC	*N*-heterocyclic carbene

NHC-CO_2	imidazol-2-carboxylate
NHO	*N*-heterocyclic olefin
NMR	nuclear magnetic resonance
nm	nanometer
NO_x	oxides of nitrogen
OCN	cyanate
P	pressure
P_0	initial pressure
PCP	porous coordination polymer
PEG 200	polyethylene glycol (MW = 200 g mol^{-1})
PEI	polyethyleneimine
PhMe	toluene
PMDBD	3,3,6,9,9-pentamethyl-2,10-diazabicyclo[4.4.0]dec-1-ene
ppm	parts per million
RO^-	general alkoxide
Rubisco	ribulose-1,5-bisphosphate oxidase/carboxylate
s	second/strong
SAM	*S*-adenosylmethionine
SCN	thiocyanate
T	Tesla
t	time
$T_{1/2}$	half-life
TBD	1,5,7-triazabicyclo[4.4.0]dec-5-ene
TGA	thermogravimetric analysis
THF	tetrahydrofuran
THP	1,4,5,6-tetrahydropyrimidine
v/v	volume/volume
vs	very strong
vw	very weak
w	weak
$\Delta_a G°$	Gibbs energy of activation
$\Delta_a H°$	enthalpy of activation
$\Delta_r G°$	reaction Gibbs energy
$\Delta_r H°$	enthalpy of reaction
μ	reduced mass

μL	microliter
$\nu_{as}CO_2$	asymmetrical carboxyl stretching frequency
ν-bar	vibrational frequency
νCN	cyano stretching frequency
$\nu_{s}CO_2$	symmetrical carboxyl stretching frequency

Overview of Thesis

The introduction to this thesis is divided into two major sections. In Chapter 1, carbon dioxide will be introduced in terms of the basics of its structure and properties. Its generation as a waste product in the burning of carbon-based fuels will be discussed along with the consequences of its increasing concentration in the atmosphere. Methods for storing carbon dioxide will be outlined, as will the main techniques being investigated for CO_2 capture from flue gas streams and from the atmosphere (*e.g.* solid sorbents, amines). A smaller-scale application for CO_2 capture will also be outlined.

In Chapter 2, the ethylene-forming enzyme (ACC oxidase) will be introduced, and the gradual progression of our understanding of the reaction it catalyses will be discussed at length. Particular focus will be on the final step of ethylene production, and the by-products of this reaction. Cyanoformate will be discussed as a postulated, but never observed, by-product which went largely uninvestigated due to its predicted rapid decomposition to cyanide and carbon dioxide. The coordination chemistry of carbon dioxide will be discussed in terms of crystallographically-characterized examples of inclusion complexes (*e.g.* MOFs), carbene-CO_2 adducts, carbamates, and carbamato and carboxylato complexes.

In the results and discussion sections, Chapter 3 will focus on CO_2 uptake from ambient air, comparing performances of an amine and an amine-based ionic liquid used as solutions in a polymeric solvent. Chapter 4, which comprises the bulk of this thesis, will focus on the preparation, characterization and investigation of the cyanoformate ion. Its stability in solution is of particular interest.

Chapter 1 – Carbon Dioxide Capture and Sequestration

1.1 Carbon Dioxide

Carbon dioxide, a simple linear triatomic molecule, is one of the most well-known and frequently studied species in a variety of scientific fields, such as chemistry, biology, geology and others. CO_2 represents a fully-oxidised form of carbon,[1] consisting of two oxygen atoms bound to a single carbon atom, each by a σ-bond and by a π-bond. The difference in electronegativity between carbon and oxygen leads to individually-polarized carbon-oxygen bonds (quadrupole moment),[2] while the symmetry of the molecule leads to its overall non-polar nature. The combination of these electronic features renders carbon dioxide susceptible to reaction with a variety of chemical species. The electrophilic central carbon atom may be subject to attack by Lewis bases, while the oxygen atoms may interact with Lewis acids, these interactions can be present individually or in conjunction with one another.

In addition, the physical properties of carbon dioxide have been, and are still being, thoroughly investigated. In particular, the phase behaviour of carbon dioxide has spawned much interest, the main uses of carbon dioxide lying in the gas phase, or in the solid phase as a coolant (dry ice). These are the only forms of carbon dioxide available at ambient pressure, but of CO_2 can also be condensed to a liquid form at elevated pressure, and can exist in the 'supercritical' phase above its critical point.[3] Supercritical CO_2 has been investigated primarily as a solvent.[4]

Our knowledge of the chemistry and properties of carbon dioxide is constantly growing, however, it is reasonable to believe that there is much still to be uncovered,

particularly regarding its potential use as a chemical feedstock. Various aspects of carbon dioxide will be explored in this thesis, from its accumulation in the atmosphere as a greenhouse gas, to the interesting interactions it participates in in biological, specifically enzymatic, systems.

1.2 Carbon Dioxide Emissions

Atmospheric concentrations of carbon dioxide continue to rise steadily. Mauna Loa Observatory in Hawaii has records of atmospheric CO_2 concentration dating back to 1958 when the concentration was still below 320 parts per million. Nearly six decades later concentrations have very recently surpassed 400 parts per million with no end to the increase in sight.[5] While it is true that atmospheric concentrations of carbon dioxide fluctuate with glacial cycles (ice ages), reaching maxima when the ice has melted, the fact remains that for the last eight glacial cycles, a period of about 650,000 years, concentrations have remained between 180 and 300 parts per million.[6]

The greenhouse effect and global climate change are typically cited as the reasons necessitating improved CO_2 management techniques. As CO_2 accumulates in the atmosphere, it traps heat provided by the sun, resulting in global climate change.[7] However, ocean acidification is another huge, and sometimes overlooked, consequence of the increase of CO_2 concentration in the atmosphere. Le Chatelier's principle tells us that increasing the concentration of a reactant in equilibrium with a product will shift that equilibrium toward the product. With respect to carbon dioxide concentrations and the ocean, the equilibria shown in Scheme 1 are relevant.[8]

1) $CO_{2\,(g)} \rightleftharpoons CO_{2\,(aq)}$

2) $H_2O_{\,(l)} + CO_{2\,(aq)} \rightleftharpoons H_2CO_{3\,(aq)}$

3) $H_2CO_{3\,(aq)} \rightleftharpoons H^+_{(aq)} + HCO_3^-{}_{(aq)}$

4) $HCO_3^-{}_{(aq)} \rightleftharpoons H^+_{(aq)} + CO_3^{2-}{}_{(aq)}$

Scheme 1: Relevant equilibria involved in the dissolution of carbon dioxide in water.

An increase in the $CO_{2(g)}$ concentration results in an increase in the H^+ concentration, $[H^+]$, causing a decrease in pH, which can have dire consequences for the marine ecosystem. It is estimated that pH levels in the ocean have decreased from 8.25 to 8.14 since the 18th century. This level is expected to drop to 7.85 by the end of the century, corresponding to a 2.5-fold increase in $[H^+]$ since 1751.[9] It isn't simply the increase in $[H^+]$ that is cause for concern in terms of ocean acidification, the ocean chemistry is based on delicate equilibrium between a number of ions, and molecules and small changes in pH can greatly disrupt these equilibria. For example, a decrease in ocean pH is expected to effect a greater transfer of ammonia from the atmosphere to the ocean, at the same time causing transfer of acidic species *from* the ocean to the atmosphere (aqueous acids typically HCl, HNO_3, H_2SO_3).

An increase in the partial pressure of CO_2 in seawater will also decrease the degree of calcium carbonate saturation, with direct consequences for calcification rates, and adversely affecting calcifying organisms like coral.[10] The effect of increased CO_2 concentration on other aquatic animals (e.g. fish) is still not well understood.[11] Ocean sequestration of CO_2 is one idea that has been proposed for long-term storage of CO_2, along with geological sequestration (either as gaseous CO_2 or as a mineralized carbonate),

however, each of these comes with its own set of disadvantages which will be discussed in the next section.

1.3 Carbon Dioxide Capture

In the energy sector, the burning of petroleum, fossil fuels, coal, biomass and virtually any other substance containing carbon all release enormous amounts of CO_2 into the atmosphere. According to the Intergovernmental Panel on Climate Change, global annual CO_2 emissions from fossil fuels have grown from 21 billion tons to 38 billion tons from 1970 to 2004.[12] Such an enormous volume limits possible storage solutions to geological sequestration, and ocean sequestration, which has clear disadvantages as outlined above. To counteract the sheer volume of CO_2 released into the atmosphere today, much research is being put into the field of CO_2 capture and sequestration/storage (CCS) technologies. The sequestration end of this process is arguably the more important to consider. Even with a hypothetical 'perfect' capture system that runs with 100% efficiency and requires no energy to regenerate the sorbent, the issue of where to put all the carbon dioxide is one that cannot be ignored.

Geological sequestration typically involves injection of gaseous CO_2 into depleted oil and gas wells, millions of which have been created in North America alone.[13] As with ocean sequestration, however, there are clear disadvantages. In this case, the most important disadvantage to consider is the potential for a leak. An example of the effects of a leak is a disaster that occurred on August 21st 1986 in Africa. A large pocket of naturally sequestered carbon dioxide was emitted from Lake Nyos, situated on an inactive volcano, in northwest Cameroon. Hundreds of thousands of tonnes of carbon dioxide

were rapidly expulsed from the lake, suffocating nearly two-thousand people living in nearby villages.[14] This incident was not caused by a man-made carbon dioxide sink which are more stable; but it does follow that without preventative measures in place, the occurrence of an incident such as Lake Nyos cannot be discounted as a possibility.

Rather than storing gaseous CO_2, another option would be to mineralize it and then store the resulting salt. This is admittedly a much safer process, but irreversibility aside, mineralizing CO_2 demands higher volumetric storage requirements. For example, CO_2 comprises less than 45% of the total mass of calcium carbonate, $CaCO_3$, which would be one of the most likely forms used to store CO_2 as a mineral.

It is the opinion of the author that complete capture of all anthropogenically produced carbon dioxide is simply not possible. Realistically the only way to decisively mitigate CO_2 emissions is to move away from combustion processes as our primary energy source. There is clearly much work to be done in this respect; in the meantime, carbon dioxide capture methods are perhaps the best tools we have to reduce the amount of CO_2 emitted into the atmosphere.

CO_2 capture techniques can typically be divided into three general categories, post-combustion processes, pre-combustion processes and oxy-combustion processes.[15] These categories generally refer to any pretreatment the gas stream undergoes before the CO_2 is captured using the chosen method. Post-combustion processes involve capture of CO_2 from a complex flue gas stream, typically containing contaminants such as oxides of nitrogen and sulfur (NO_X and SO_2 in particular). This category involves capture from an untreated stream and would typically be the most expensive and difficult to implement.

The pre-combustion method involves a reforming process (in the case of natural gas) or a gasification process (for coal). These processes produce ‘syngas’, a mixture of carbon monoxide and hydrogen gas. The subsequent shift-reaction converts the carbon monoxide to carbon dioxide which can then be captured with a decreased degree of difficulty due to the lower complexity of the gas mixture.

Finally, the oxy-combustion method refers to the combustion of fuels in an oxygen-rich atmosphere. The advantage of this technique is that a stream that is rich in carbon dioxide is produced. Purity of greater than 95% CO_2 by volume can be obtained, which means that subsequent separation is unnecessary and that the gas can be compressed and stored as-is. Inherent in this process, however, is prior scrubbing for removal of more prevalent impurities (mainly SO_2). Also, the requirement of an oxygen-rich combustion environment means that oxygen must itself be separated from air to use in this process, another energy-intensive step.

Membrane technology has been investigated for CO_2 separation, wherein the gas mixture is passed through a membrane driven by a pressure gradient. However, common issues are the fact that gases typically need to be cooled significantly prior to membrane separation, as well as the difficulty in designing a membrane resistant to the chemicals commonly contained in flue gas mixtures.[16] A particularly attractive advantage to membrane technology is the fact that no costly desorption step is required,[17] as with some of the other technologies which will be discussed in the next section.

1.4 Carbon Dioxide Capture Methods

1.4.1 Solid Sorbents

As mentioned earlier, one option for CO_2 sequestration is the storage of carbon dioxide as carbonate salts, prepared through a process known as mineral carbonation. By doing this, CO_2 can be obtained in solid form, and subsequently stored. The obvious advantages are the circumvention of changes in ocean acidity (ocean sequestration), or avoiding any danger of a leak that goes alone with storing gaseous CO_2 (terrestrial sequestration). The formation of carbonates is one of the major processes in the global carbon cycle already. It is estimated that a staggering majority (>99%) of the carbon on the planet (including that in the atmosphere) is present as carbonate minerals.[18] As a relatively new type of potential geological sequestration, there is much room for improvement and exploration as far as mineral carbonation is concerned. Despite the fact that the overall process is exothermic, the rate is incredibly slow.[19,20]

Pressure swing adsorption with molecular sieves and activated carbon has also been explored for carbon dioxide capture applications. This process involves pressurizing a gas mixture on the porous material (molecular sieve or activated charcoal, typically) which is capable of selectively adsorbing the carbon dioxide. Of course, the usual issues of selectivity and adsorption capacity arise under these circumstances.[21] The porous materials being used for adsorption of CO_2 are usually functionalized to add some degree of chemical absorption in addition to the physical adsorption. This often involves addition of some an amino moiety,[22,23] as amines are well known to form carbamate salts with carbon dioxide. For example, incorporation of polyethyleneimine (PEI) in mesoporous molecular sieves has been shown to greatly improve absorption and desorption rates of

CO_2, as well as enhancing selectivity, all at ambient pressure.[24] Unsurprisingly, sieves with larger pores and a higher surface density of amine have higher capacity for CO_2 absorption.[25]

Related to functionalized molecular sieves and zeolites are metal-organic frameworks (MOFs). MOFs are porous materials consisting of an array of metal centers supported by a molecular 'scaffold' of ligands. They can offer high thermal stability[26] and are can also be 'tuned' by varying the metals or ligands used.[27] This greatly enhances the ability to design a MOF for a particular use. The size of the resultant pores leads to size and shape selectivity. The geometry of the MOF can be predicted and controlled by using rigid ligands that can only bind in a limited number of conformations.[28] In terms of CO_2 capture, many MOFs are able to bind CO_2 effectively and selectively.[29] Some are even able to bind CO_2 very effectively even at low partial pressure and in the presence of moisture.[30] Using amine-functionalized ligands in the framework has been shown to enhance uptake as well.[31, 32] The field of MOFs for CO_2 capture has been reviewed fairly recently.[33]

One downside of MOFs is that their preparation typically involves the use of harmful solvents and they contain metals and ligands that may create additional environmental concerns.[34,35] Many MOFs do not retain their structure and porosity after repeated absorption and desorption cycles, which would be a vital aspect of their use for CO_2 capture. Some MOFs 'collapse' after removal of their absorbed molecules.[36] Thermal stability is also an issue[37] and as a result MOFs that exhibit both thermal stability and stable porosity are few and far between.[38]

1.4.2 Photosynthesis

Photosynthesis, or more specifically carbon fixation, can be considered the original carbon-capture process. Plants and other organisms have evolved to use available carbon dioxide as a feedstock, in conjunction with water and light, to produce sugars and other carbohydrate molecules. It is this process that is responsible for maintaining oxygen levels in the world.

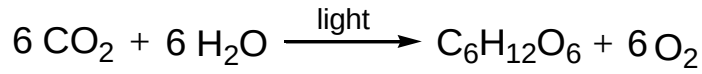

Scheme 2: Overall reaction scheme for the process of photosynthesis, generating carbohydrate and oxygen from carbon dioxide, water and sunlight.

The notion that the solution to carbon dioxide capture is being utilized by the plants we see every day is not a new one, development of closed photo-bioreactor systems has been in the works for over fifty years.[39] This is a particularly attractive idea, as the benefits aren't limited to the capture of CO_2 alone, but also include oxygen being produced as a by-product. Of course, to reach the efficiency needed to achieve fixation on an economically viable scale there are a number of factors that must be addressed. For instance, collection of sunlight (the energy source for this process) is an infamously inefficient process; thus various methods of light capture are being explored as well. For example, in the late 1990s Usui and Ikenouchi used fiber-optic technology to pass light into a microorganism-based bioreactor, resulting in a 55% increase in overall efficiency.[40] Despite findings such as this, research in the field has decreased markedly since the nineties after it was deemed unlikely to ever become an economically viable process, though there are still those that insist, perhaps wishfully, that bioenergy and other

renewable resources, as well as hydroelectric and nuclear power could completely replace fossil fuels as early as 2020.[41]

Another issue with implementing photosynthesis as a source of biomass (or as a CO_2 capture technique) is the mechanism by which it occurs. Ribulose-1,5-biphosphate carboxylase/oxygenase, commonly known as Rubisco, is the enzyme that catalyzes the first step of photosynthesis, capturing CO_2 so it can be incorporated in the preparation of 3-phospho-D-glycerate. It is also, unsurprisingly, the most abundant protein on the planet.[42] The first step of the reaction that Rubisco catalyses is the conversion of ribulose-1,5-biphosphate from its ketone form to its enediol form, a step necessary for the subsequent CO_2 addition to occur at the correct carbon atom.[43] Subsequent hydration of the produced β-ketoacid, followed by protonation of the same carbon the CO_2 added to, are the final steps before dissociation of the product, yielding two equivalents of 3-phospho-D-glycerate.

Perhaps surprisingly, this process is considered remarkably inefficient for a variety of reasons. Generally, the most important photochemical reactions that occur in photosynthesis require longer wavelengths of light, meaning that the shorter wavelengths (higher energy) are simply absorbed and re-emitted as heat or fluorescence, wasted in other words. Furthermore, significant energy is required to produce the nicotinamide adenine dinucleotide phosphate (NADPH) and adenosine triphosphate (ATP) required for the carbon fixation process. Rubisco can also accept oxygen as a substrate, rather than CO_2, resulting in oxygenation of the ribulose-1,5-biphosphate, a competing reaction that greatly diminishes photosynthetic efficiency. If photosynthesis is being considered as a carbon capture process, this competing reaction is indeed a very serious hurdle.[44] As a

result, many researchers are attempting to modify the enzyme itself to produce a more efficient model.[45] Others are focusing on emulating photosynthesis but avoiding the use of Rubisco altogether.[46]

1.4.3 Amines

The use of amines as carbon dioxide capture agents is the most well-understood and exploited technology in the field. It has been argued that of all the advanced technologies for carbon dioxide capture, the use of amines is the most likely to be able to balance energy-efficiency with timeliness as CO_2 emissions continue to rise.[47] The fact that the technology is already commercially available is also a clear advantage.[48]

As stated earlier, amines readily react with CO_2 to form carbamate salts.[49] The most widely used amine for carbon dioxide capture is monoethanolamine (MEA). The reaction between CO_2 and MEA is exothermic, and is thermally reversible;[50] however, regeneration of the absorbent is an energy intensive step for a number of reasons. MEA is utilized in a moderately dilute aqueous solution meaning that a great deal of energy is expended simply heating the water, which has a very high specific heat capacity. Typically in the regeneration step, the absorbent is heated to 100-120 °C at a pressure of 1.5-2.0 atm.[51] Furthermore, the reaction between CO_2 and monoethanolamine (and other amines) results in the formation of a very strong C-N bond, which, of course, must be cleaved in order to recycle the absorbent.[52]

The use of alternative amines for CO_2 capture has also been investigated. In particular, the use of polyamines has drawn much interest due to presence of additional sites for CO_2 coordination. It is rationalized that a higher uptake should be achieved using

polyamines such as polyethyleneimine,[23] or oligomers such as diethylenetriamine (DETA).[53] Previously, DETA has been shown to react with CO_2 in a 1:1 ratio affording a zwitterionic carbamate material, as shown in Scheme 3B, in contrast to monoethanolamine which reacts with CO_2 in a 2:1 ratio (Scheme 3A).

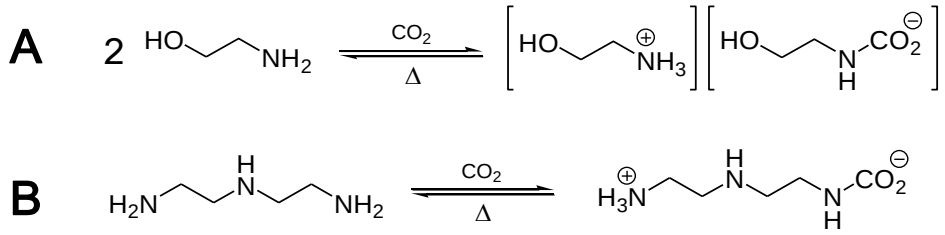

Scheme 3: Reaction of monoethanolamine with CO_2 (A) and reaction of DETA with CO_2 (B).

Using DETA in conjunction with a polymeric solvent or ionic liquid introduces the benefit of a solvent with a much lower specific heat capacity relative to water. ILs and polymeric solvents have been investigated for CO_2 capture applications repeatedly in the literature. The molar heat capacity of poly(ethylene glycol), MW = 200 g mol^{-1} (PEG 200) is 416.3 J mol^{-1} K^{-1} at 298.15 K,[54] equating to a *specific* heat capacity of 2.08 J g^{-1} K^{-1}, less than half of that of water. This could translate to enormous energy savings if it could be implemented on a large scale.

Simple salts of DETA can also be easily prepared, and Ilioudis, et al.[55] found that while attempting to prepare a mononitrate salt of DETA, they isolated crystals of its corresponding CO_2 adduct. The fact that there was no issue isolating the other simple salts of DETA without added CO_2 suggests that the nitrate salt in particular may have a higher affinity for CO_2,[56] perhaps higher than that of DETA alone as well. A direct

comparison of CO_2 uptake rates between DETA and $[DETAH]NO_3$ would prove useful in determining whether or not there is a higher affinity for one or the other.

1.5A Smaller-Scale Application of CO_2 Capture

While capture of CO_2 from flue gas streams is an expensive process, and the issue of sequestration a serious hurdle to overcome, there is the potential to capture CO_2 in other, smaller-scale, scenarios. In fact, CO_2 scrubbers are currently used during controlled-atmosphere storage of fruits and vegetables.[57] Nearly 50 years ago Burg and Burg[58] observed that both low (<1.8%) and high (>10%) levels of carbon dioxide result in the inhibition of ethylene production. Ethylene is a plant hormone often responsible for controlling the fruit-ripening process,[59,60] although ethylene-independent ripening pathways are known for other fruits.[61] The biosynthesis of ethylene will be discussed at length in Chapter 2. The inhibition of ethylene production at elevated CO_2 concentrations (20%) was investigated in tomatoes, and revealed a marked decrease in the mRNA levels of the enzymes responsible for the biosynthesis of ethylene, 1-aminocyclopropane-1-carboxylic acid synthase (ACC synthase) and 1-aminocyclopropane-1-carboxylic acid oxidase (ACC oxidase).[62] Another study attributes the decrease in ethylene production under high concentrations of CO_2 (20%) to the utilization of *S*-adenosylmethionine (SAM) for the production of polyamines (spermidine, spermine) rather than it being utilized in the stepwise conversion to ethylene.[63] It has also been found that very low levels of CO_2 can also delay the ripening process, not by regulating the synthesis of the ethylene-forming enzyme (ACC oxidase), which may be detrimental in the long-term, but by regulating its activity.[64]

Levels of CO_2 and O_2 need to be maintained at a particular level (rather than completely depleted) in order to effectively delay the fruit-ripening process without adversely affecting the produce.[65] The ability to regulate the concentrations of these gases is clearly a valuable tool. As far as CO_2 regulation is concerned (and, in turn, ethylene), amine-based CO_2 capture in non-traditional solvents is an ideal candidate.[66] The utilization of lower-energy alternatives to the typical aqueous MEA systems on a large scale is hampered mainly by the vast amounts of material required for these applications; however, for smaller-scale applications these alternative sorbents could prove invaluable, such as removing CO_2 from a produce-containing warehouse.

Chapter 2 – CO_2 Involvement in the Biosynthesis of Ethylene

2.1 The Ethylene-Forming Enzyme

As described in the previous section, the biosynthesis of the plant hormone, ethylene, plays an important role in the ripening process of many fruits. It is only fairly recently, however, that researchers have been able to uncover the mechanistic details of ethylene production. It was known from the 1960s that the production of ethylene stemmed from the metabolisation of the amino acid, methionine.[67] About ten years later, *S*-adenosylmethionine(SAM) was identified as an intermediate in the process.[68,69]

In 1979, Adams and Yang[70] identified another key intermediate in ethylene biosynthesis process. ^{14}C-labelled methionine was incubated with plugs of apple tissue, one sample in open air, one sample under nitrogen, and one sample under nitrogen and then exposed to air. They observed the build-up of an unknown ^{14}C-labelled compound in the samples kept under nitrogen, while the samples kept open to air produced ^{14}C-labelled ethylene. Furthermore, when a sample kept under nitrogen was subsequently exposed to air, production of ethylene followed, at a rate greater than that of the samples exposed to air the whole time. All of these observations pointed to the generation of an intermediate, which continuously built up until it was exposed to air. At that point it was metabolized into ethylene, indicating an oxygen-dependence. Adams and Yang identified this intermediate as the structurally unusual[71] amino acid, 1-aminocyclopropane-1-carboxylic acid (ACC), and proposed the following mechanism for its degradation into ethylene.

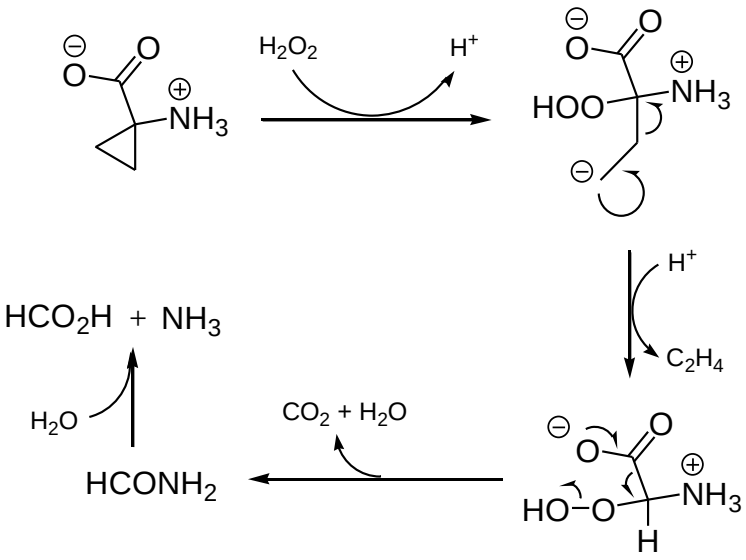

Scheme 4: Decomposition of ACC to produce ethylene, CO_2, formic acid and ammonia as proposed by Adams and Yang in 1979.

Not long after the identification of ACC as an intermediate in ethylene production, researchers were able to identify the enzymes catalyzing the final two steps of its production. The enzyme ACC synthase, was found to catalyze the production of ACC from SAM,[72-75] and the enzyme ACC oxidase, to catalyze the production of ethylene from ACC.[76,77]

Other than ethylene, the products of ACC degradation were not conclusively identified. The mechanism shown in Scheme 4 is merely the authors proposal, with no evidence of the production of formic acid and ammonia occurring during ethylene production. Many mechanisms had been suggested after the identification of ACC as the ethylene precursor, including the one shown in Scheme 4.[78,79] In 1981, Adams and Yang proposed another mechanism involving the oxidation of ACC to give a nitrenium intermediate, which subsequently fragmented into ethylene and cyanoformic acid.[80] Not long afterwards, Pirrung was able to show that the decomposition of ACC derivatives

yields ethylene, carbon dioxide and cyanide (or HCN), as determined by gas chromatography,[81]and proposed another mechanism involving two single-electron oxidation steps. In addition, ring-opening and β-fragmentation steps led ultimately to the same products, ethylene, CO_2 and cyanide.[82] The following year Peiser *et al.*[83] demonstrated, again using ^{14}C radioisotopic studies, that ACC itself does in fact decompose into cyanide and carbon dioxide during the biosynthesis of ethylene. These observations, particularly the decomposition to cyanide, were bolstered with ^{13}C-labelling studies.[84]

Investigation of the structure and activity of the ethylene-forming enzyme, ACC oxidase, have continued. *In vitro* isolation of the ethylene-forming enzyme revealed that both Fe^{2+} and ascorbate, an electron donor,[85] were required cofactors for enzyme activity.[86-89] Bicarbonate was also identified as an activator in the production of ethylene.[90,91] Further study began to unravel the structure of the enzyme active site, including the catalytic role of the iron center, as well as the amino acid residues anchoring it in place. These findings prompted further mechanistic studies, including investigation of the role of the iron-center and postulated iron-oxo complexes involved in the activation of oxygen and stepwise oxidation of ACC.[92-97]

2.2 – The active site of ACC oxidase

In 2004, Zhang, *et al.*[98] reported a crystal structure of uncomplexed ACC oxidase and structures of the enzyme complexed with iron(II) and cobalt(II), offering unprecedented insight into the structure and mechanistic workings of the ethylene-forming enzyme. Of the most interest, at least in the scope of this work, is the structure of the active site. The amino acid residues located on the inner face of the active site are

described as ‘mostly hydrophobic’, with the iron(II) (or cobalt(II)) center ligated by two histidine residues and one aspartate residue. This is the so-called 2-His-1-carboxylate facial triad, a structural motif common to iron-containing enzymes catalyzing the activation of molecular oxygen.[99] The crystal structure determination solidified much of the speculation concerning the nature of the enzyme, and prompted renewed interest in the reaction mechanism. In particular, the exact sequence of events leading to oxygen activation, and the nature of bicarbonate (or CO_2) as an activator were (and still are) still subject to scrutiny.

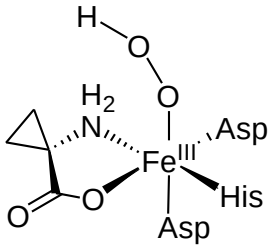

Figure 1: One of many postulated intermediates in the ACC oxidase-mediated conversion of ACC to ethylene.

Despite the headway that has been made in the last 30-40 years concerning the structure of ACC oxidase and the mechanism of ethylene formation, certain details are still under debate. These include the order in which substrates bind, how and what types of iron-oxo intermediates are produced in the process, and the roles of bicarbonate and ascorbate in the entire process.[100-102] It is now agreed that the process begins with the binding of ACC and oxygen to the iron(II) center located in the active site of ACC oxidase. A proximal ascorbate ion sequentially donates two electrons to the nitrogen of ACC, causing ring opening and β-fragmentation, and then release of ethylene, CO_2 and cyanide.[100]

2.3 The By-products of Ethylene Biosynthesis

It is now certain that carbon dioxide and cyanide are the ultimate by-products of the biosynthesis of ethylene. However, a short-lived precursor to these by-products, a complex of carbon dioxide and cyanide, has been repeatedly invoked in the process. This intermediate was first postulated in 1981.[80] Adams and Yang noted that the oxidation of a substituted cyclopropylamine to ethylene, via a nitrenium ion, had already been documented.[103] If a similar reaction were to occur with ACC, they rationalized that ethylene would be produced together with cyanoformic acid.[80]

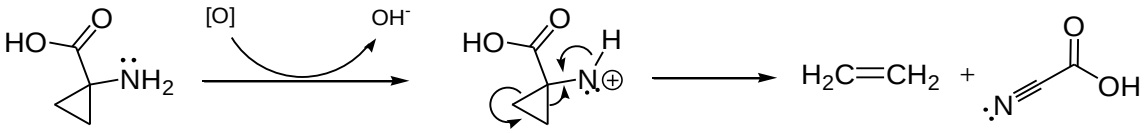

Scheme 5: Production of ethylene *via* a nitrenium intermediate to give ethylene and cyanoformic acid, as outlined by Adams and Yang in 1981.

Two years later, Pirrung[81] suggested that cyanoformic acid would undergo rapid decarboxylation to yield CO_2 and cyanide. Cyanoformic acid and its conjugate base, cyanoformate, are both oft speculated products in the ACC degradation pathway, though production of cyanoformic acid in most papers seems to be based on the assumption that the anion will be quickly protonated in aqueous media. Both species, however, are invariably described as unstable with respect to their constituents. Rapid decomposition is invoked to explain the repeated observation of cyanide and carbon dioxide as products of the ACC oxidase-catalyzed reaction.[94,104-106] Pirrung later pointed out the fact that cyanoformic acid had never been observed, alluding to erroneous citations in the literature. He also calculated cyanoformic acid to be only 5 kcal/mol (~20 kJ/mol) higher

in energy than its constituents, supporting its spontaneous decomposition.[107] Reich[108] later acknowledged that while cyanoformate is known to decompose to cyanide and carbon dioxide, it is not known whether or not this process occurs in solution or at the active site of the enzyme.

The production of cyanide in plant tissues has the potential to be quite harmful. For example, cytochrome c oxidase, a key enzyme in the electron-transport chain facilitating cellular respiration, is shut down upon binding of cyanide to the iron in the active site, the basis of cyanide poisoning.[109] It was understood that there must be a mechanism in place to deal with the produced cyanide.[110] The activity of the enzyme β-cyanoalanine synthase has been shown to closely mirror that of ACC oxidase, suggesting that the cyanide produced by the latter enzyme, may eventually be used in amino acid synthesis by the former. Metabolism by *β*-cyanoalanine synthase is the most common method of cyanide metabolism in biological systems.[111-113] It should be noted that that *β*-cyanoalanine synthase activity is mainly mitochondrial, while ethylene production is cytosolic,[114] however, there do exist less abundant forms of *β*-cyanoalanine synthase present in the cytoplasm.[115] Migration of cyanide *into* the mitochondria for metabolisation has also been suggested.[116]

Interestingly, an activating effect of cyanide on the biosynthesis of ethylene has been identified, after first being hypothesized by Pirrung and Brauman in 1987.[117] The mechanism by which this activation occurs is still speculative, but Dilley *et al.*[118] have suggested that cyanide is bound to the iron center in ACC oxidase, protecting the enzyme from inactivation before it is displaced by ACC, ascorbate and oxygen. Cyanide concentrations between 0.1 and 1 mM have been shown to be activating, while at cyanide

concentrations higher than 1 mM deactivation of the enzyme occurs. With the high binding affinity of Fe(II) and Fe(III) for cyanide,[119] both of which have been repeatedly implicated in the production of ethylene, it is indeed very curious that deactivation of ACC oxidase does not occur more often. The answer could quite possibly lie with the formation of the elusive cyanoformate intermediate, which may preclude binding of larger amounts of free cyanide to the iron center.

2.4 Solvent Effects on Complex Stability

Cyanoformic acid can decompose to HCN and CO_2, while the cyanoformate ion must decompose to cyanide ion and CO_2. It is likely both decompositions would be promoted in polar media as hydrogen cyanide or the cyanide ion would be better solvated. In both cases production of CO_2 would be expected to be thermodynamically favourable. But in the active site of ACC oxidase the amino acid residues are described as mainly hydrophobic,[99] and the medium likely less polar in nature than one might expect given that the dielectric constants (ε) inside proteins are quite low; Gilson and Honig,[120] for example, gave values as low as ε = 2-3. Coupled with the very high dielectric constant of water (~78.5[121]), they describe the interface between proteins and water as a boundary between dielectric media.

Recently Shoukry and Hassan[122] have investigated the effect of solvent on the coordination of ACC to Fe(II). They performed this study using water-dioxane mixtures, explaining that this mixture acts as a model for the lipophilic media of enzyme-containing solutions. They were able to show that an increase of the organic content (higher dioxane concentration and lower dielectric constant) resulted in a favoured interaction between the

ferrous ion and the ACC anion, leading to a more stable Fe(II)-ACC complex. This example of solvent effect on complex stability is the most relevant to this work; however, other conceptually similar studies have been performed. For example, Masoud and Abdallah found that the stability of monoethanolamine-metal complexes increased with higher relative concentration of organic solvent to that of water.[123] Similarly, Sigel *et al*.[124] found that the stability constants of 1:1 complexes between Cu(II) and Zn(II) and carboxylate salts increased with the organic content of the solvent (decreasing solvent polarity). More recently, the stability of Meisenheimer adducts (Scheme 6) has been shown to be considerably increased in non-polar solvents. The authors attribute this stability to a strong ion-pairing between the cation (not shown in the scheme) and generated product anion, as well as the fact that small anionic nucleophiles (the reactant) are difficult to solvate in non-polar media, resulting in increased nucleophilicity.[125]

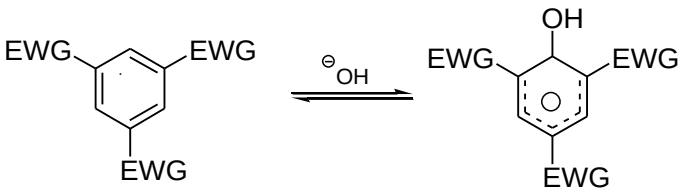

Scheme 6: Formation of a general Meisenheimer adduct from an electron-deficient aromatic compound and an anionic nucleophile, hydroxide in this case (EWG = Electron-withdrawing group).

Expanding these findings to cyanoformate, it is reasonable to believe that cyanoformate may be stable at the low-dielectric active site of ACC oxidase. Though cyanoformic acid is generally accepted to be unstable with respect to its constituents,[94] the same may not be true for cyanoformate. The closest related species in the literature is the fluorocarbonate ion which was prepared and crystallographically characterized by

Zhang *et al*. in 1995.[126] The fluoride affinity to CO_2 was calculated to be -110.7 kJ/mol. Fluoride affinities to other similar molecules to CO_2 were also calculated, however, their magnitudes were found to be so low that their affinities competed with that of the cation or solvent, meaning no reaction would be expected to occur. As a result the authors describe the fluoride affinity of CO_2 as the approximate lower limit for a reaction.

2.5 Coordination Chemistry of Carbon Dioxide

In the realm of the coordination chemistry of carbon, the vast majority of the literature deals with carbon donor-species binding to Lewis acids to generate complexes. Many of these complexes are described as having a dative bond (where both electrons are donated from the same atom) with carbon as the donor, as is prevalent in the field of *N*-heterocyclic carbenes.[127] Examples of coordination complexes wherein a carbon atom accepts the lone pair of electrons rather than donating it are indeed rare.[128,129] In the case of carbon dioxide acting as the acceptor, few examples of coordination complexes of a so-called 'naked' CO_2 fragment appear in the literature, and will be discussed herein.

The formation of a strong covalent bond between the Lewis acidic carbon atom of CO_2 and a donating Lewis base are the most prevalent examples of CO_2 complexes in the literature. Prime examples are the carbamates formed by the reaction of CO_2 with amines as outlined earlier, which are almost always formed with a concomitant proton transfer. However, the ability to bind CO_2 through the formation of low-energy, easily-broken bonds could indeed prove invaluable in a variety of contexts. For example, weaker bonds to CO_2 in a carbon-capture setting would greatly reduce costs of the energy-intensive sorbent-regeneration step common to most CCS technologies. Furthermore, exploration

of this field has the potential to lead to the discovery of novel CO_2 chemistry, particularly involving its use as a chemical feedstock for the preparation of value-added products.

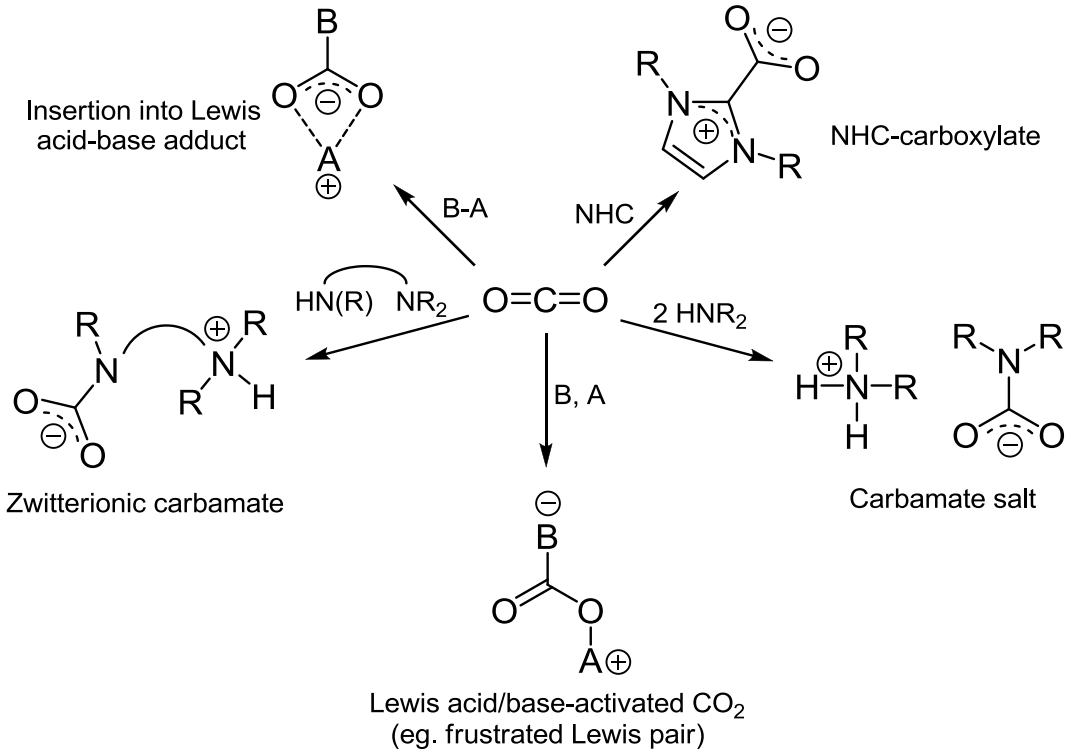

Scheme 7: Various general structures of some CO_2 complexes discussed in this section. Bonding modes are variable, particularly for CO_2 insertion products (top left). (B = Lewis basic species, A = Lewis acidic species, R = any side chain, including hydrogen)

2.5.1 Inclusion Complexes of CO_2

The physical adsorption of carbon dioxide and other gases into porous materials, without drastically altering its structure, has been extensively studied for potential applications in separation technologies. The incorporation of CO_2-reactive fragments (e.g. amino groups), coupled with high-surface areas, has allowed MOFs and porous coordination polymers (PCPs) to be designed with very high gas-loading capacities. The inclusion of gaseous molecules into such frameworks, coupled with characterization

techniques such as X-ray crystallography, has offered unprecedented insight into the structure and behaviour of these species. In the early 1980s, Gies *et al*. crystallographically characterized two forms of melanophlogite (naturally occurring silicate minerals), which were determined by mass spectrometry to include methane, nitrogen and CO_2 as guest molecules.[130,131] Later Tabushi, Yamamura and Nonoguchi determined the crystal structure of a macrocyclic heterocyclophane with CO_2 incorporated into its hydrophobic core.[132] These are the earliest known examples of CO_2 inclusion complexes, whose structures were determined using X-ray diffraction.

Since that time, the number of known inclusion complexes of carbon dioxide has increased markedly. The manner in which the gas is actually adsorbed varies from system to system in terms of placement and stabilizing interactions. CO_2 can adsorb in the central 'hole' of a large cyclic molecule, which often form channels when stacked in the solid state, or it may adsorb inside a 'cage'-like molecule (e.g. carcerands, hemicarcerands). Adsorption into the space generated *between* the molecules in the solid-state is also quite common. Of course, there are an enormous number of systems that have been shown to physically adsorb carbon dioxide (and other gases), without the structure having been crystallographically determined. These will not be discussed in this work; many reviews are available on this topic.[133-136]

Adsorption of CO_2 into a framework generated by octahedral manganese(III) atoms bridged by formate ions has been shown to be favourable. The crystal structure reveals the formation of close C-H…O contacts between carbon dioxide and the hydrogen atom of formate, likely a driving factor in its adsorption.[137] In fact, several other CO_2

inclusion complexes of metal formates feature this interaction.[138] Hydrogen bonds (H-bonds) to CO_2 were observed again in a rhodium(II)benzoate-pyrazine complex where CO_2 is adsorbed between molecules of the organometallic complex (Figure 2). In addition, interactions with the π-orbitals of the aromatic rings help to stabilize the structure,[139,140] which is another recurring feature in complexes of this type.[141-143] Particularly these π-orbital interactions appear in other porous materials where there are no other stabilizing factors available.[144]

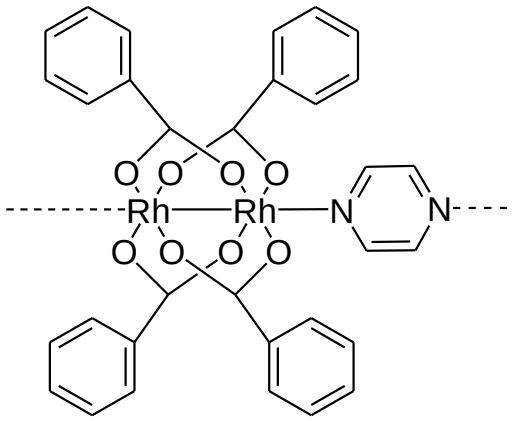

Figure 2: Structure of one repeating unit of the rhodium(II) benzoate-pyrazine complex prepared by Takamizawa *et al.*[139]

It should be noted that the adsorption of CO_2 into these latter complexes is accompanied by a transformation of the crystal system (monoclinic to triclinic in both cases). Crystal-to-crystal transformations have been observed in other complexes[145, 146] and the increased flexibility of these frameworks are thought to have advantages over their more rigid analogues in terms of molecular recognition, separation and sensing applications.[147] In one such system, the formation of CH/O interactions between the sorbent and CO_2 was deemed necessary for its adsorption.[148] However, in the case of another copper complex, complete desorption of carbon dioxide was not possible,

illustrating the very strong stabilizing effect H-bonds can have.[149] The presence of H-bonds to the oxygen atoms of CO_2 are common features in the structures of many other MOFs and inclusion complexes of CO_2.[150,151]

Crystallographically-characterized examples of porous materials that do not contain metals, but do include adsorbed CO_2, are quite rare in comparison to their metal-containing cousins. The earliest such examples have already been mentioned above. In 2002, an inclusion complex of CO_2 and decamethylcucurbit[5]uril (a macrocyclic *N*-heterocycle-containing compound) was reported,[152] and so too was a complex of *p-tert*-butylcalix[4]arene and CO_2 several years later (Figure 3).[153] The latter was obtained in two forms, with 1:1 and 2:1 loadings. The 2:1 compound was observed to release its extra CO_2 molecule over time. This CO_2 molecule was found to be located in the interstitial space between the arene molecules, while the other CO_2 molecule was localized inside the cavity. Its increased stability was presumably due to π-orbital stabilizing interactions of the type previously mentioned.

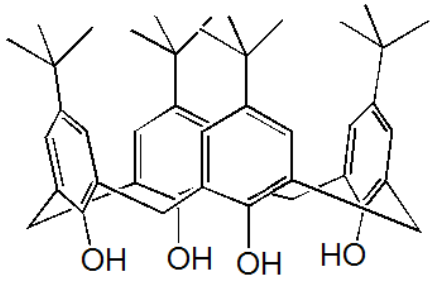

Figure 3: Structure of *p-tert*-butylcalix[4]arene. In the study by Udachin *et al.*[153] CO_2 adsorbs in the cavity between the aromatic rings.

As for decamethylcucurbit[5]uril, it is likely that the CO_2 was stabilized by interactions between its carbon atom and lone pairs from the various nearby nitrogen

atoms. Interactions such as these have been observed in other complexes of nitrogen-containing porous materials with CO_2,[32,154-156] and they have been studied computationally.[157] The stabilizing effect of nitrogen is unsurprising considering the known reactivity of CO_2 towards basic nitrogen atoms, and amines in particular. Interactions between the carbon atom of CO_2 with oxygen atoms of host-guest complexes have also been repeatedly observed as stabilizing factors,[32,158,159] as have similar interactions with halogens.[160]

End-on (η^1) coordination of carbon dioxide through oxygen directly to the nickel center of a MOF, nickel(II) dihydroxyterephthalate, has been observed.[161] This coordination-mode of CO_2 is exceedingly rare, having only been observed for the first time in 2004 in a uranium complex.[162] In the nickel case, an interaction with a neighbouring oxygen atom of a terephthalate ion to the carbon atom of CO_2 likely aids in its stabilization, as a deviation from linearity is observed in the O-C-O angle, which is 162(3)°. Coordination of CO_2 oxygen to lithium in MOFs has also been suggested, though not through direct observation of the binding modes *via* X-ray crystallography.[163]

2.5.2 Imidazol-2-Carboxylates and Related Complexes

It was not until nearly a decade after the first stable crystalline carbene was isolated and characterized by Arduengo[164] that the first NHC-carboxylate was prepared by Kuhn.[165] Reaction of 2,3-dihydro-1,3-diisopropyl-4,5-dimethylimidazol-2-ylidene (Me_2I^iPr) with carbon dioxide generated the corresponding imidazol-2-carboxylate (Scheme 8). The authors also reported that the carboxylate was found to be reactive

toward thionyl chloride giving the cationic acid chloride, which was then converted to its corresponding methyl ester with methanol.

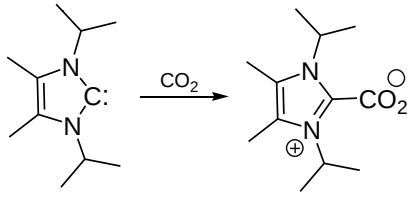

Scheme 8: The preparation of the first NHC-carboxylate, 2,3-dihydro-1,3-diisopropyl-4,5-dimethylimidazol-2-ylidene, as reported by Kuhn *et al.*[165]

NHC-carboxylates, also known as imidazol-2-carboxylates, are a major class of CO_2 coordination complexes. The carbene precursor donates its lone pair to the electrophilic carbon atom of CO_2 to generate the zwitterionic carboxylate, as shown in Scheme 8. There are other methods that can be used to prepare these complexes. For example, Tkatchenko and Rogers[166] were able to synthesize an NHC-CO_2 through the reaction of the imidazole precursor with dimethylcarbonate (DMC), which they proposed occurred *via* generation of a carbene intermediate, as shown in Scheme 9.

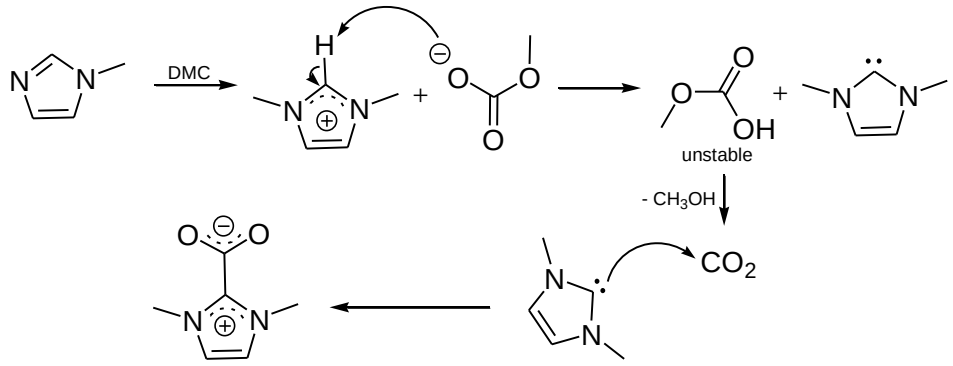

Scheme 9: Proposed mechanism of NHC-CO_2 synthesis from the imidazole precursor and dimethylcarbonate (DMC), proceeding through a carbene intermediate.[166]

The earliest work with NHC-carboxylates, namely with Me_2I^iPr, was focused on investigating their ability to ligate to transition metal centers, the most common application of their carbene precursors. Kuhn found that the rather weak interaction of NHC-carboxylates to titanium centers was more akin to those of dithiocarboxylates, rather than those of the more structurally similar classic carboxylates, probably due to the charge-neutral nature of NHC-carboxylates.[167] It should be noted that a carbene-like (carbodiphosphorane) adduct of CO_2 has also been prepared.[168] It has a C-C bond length similar to that found in Kuhn's first NHC-carboxylate. It also displayed better metal-coordinating abilities,[169] though it was also found to be more sensitive to hydrolysis.[170]

The utility of NHC-CO_2 adducts as ligands being limited, focus was instead turned to investigating the nature of the generated C-C bond between the carbene and CO_2. Louie[171] was the first to address the issue of bond stability. Complexes of CO_2 with 1,3-dimesitylimidazol-2-ylidene (IMes) or 1,3-bis(2,6-diisopropylphenyl)imidazol-2-ylidene (IPr) could be prepared as air-stable solids, but decomposed in aerated solution. Furthermore, exchange of the carboxylate with $^{13}CO_2$ was observed by NMR, and thermal decarboxylation by TGA. Finally, crossover experiments were conducted with IMes-CO_2, IPr-CO_2 and Me_2I^iPr-CO_2. Addition of Me_2I^iPr to either IMes-CO_2 or IPr-CO_2 generated *i*Pr_2Im-CO_2 and the other, decarboxylated, carbene. Addition of IMes to IPr-CO_2 gave IMes-CO_2 and IPr. The relative stability of these particular NHC-carboxylates could be ordered based on these observations alone: Me_2I^iPr-CO_2 > IMes-CO_2 > IPr-CO_2. NHC-carboxylates were also found to be sensitive to decarboxylation by protic acids such as HPF_6, HCl, H_2SO_4 and picric acid, generating the corresponding imidazolium salts of the

conjugate base of the acid, and exposing a novel route for the synthesis of imidazolium-based ionic liquids.[172] It is also interesting to note that imidazolium-based ionic liquids have been converted electrochemically to the corresponding carbene with simultaneous addition of CO_2 to generate NHC-carboxylates. Decarboxylation in this case was achieved by heating, giving the carbene.[173]

Louie[174] also investigated the underlying factors responsible for the decarboxylation of NHC-carboxylates and proposed a number of relationships between decarboxylation temperature (as determined by TGA) and the structural features of the complexes. Additional electron density in the imidazolium ring, provided by methylation of the backbone, was found to have a stabilizing effect. Furthermore, the dihedral angle between the plane of the imidazolium ring and the plane of the carboxylate group directly correlated with the temperature required for decarboxylation. As the bulkiness of the *N*-substituents increases, the carboxylate group is typically oriented more perpendicularly to the ring, lengthening the C-C bond and lowering the decarboxylation temperature as a result of decreased orbital interaction between the carboxylate and the imidazolium ring. A subsequent computational study by Suresh[175] supported these findings, and also found that the inclusion of *N*-substituents containing H-bond donors markedly increased the binding affinity of CO_2 to the carbene.

The dynamic nature of NHC-carboxylates, coupled with their surprising air-stability in the solid state, was soon recognized as advantageous in terms of their use as protected versions of NHCs. NHCs are air-sensitive, but have also been demonstrated to be useful ligands and catalysts in a variety of applications. As a result, the generation of

carbenes, *in situ*, from decarboxylation of the NHC-carboxylate precursor, was found to be a fruitful endeavour. It has been utilized in the coupling of CO_2 with epoxides or aziridines,[176-178] polyurethane synthesis,[179] transcarboxylation,[180] transesterification and benzoin condensation reactions,[181,182] and ring-opening polymerization.[183] In fact, in one study[184] a remarkable solvent effect was observed. Yields increased and reaction times decreased as the solvent polarity was increased (e.g. 71% yield over 300 minutes for toluene, compared to 95% yield over 150 minutes for DMSO) for the IMes-CO_2 catalysed polymerization of *rac*-*β*-butyrolactone, even though the authors claim that dissociation of IMes-CO_2 is not promoted in polar solvents. Contrarily, in an earlier work decarboxylation of a nitronyl carboxylate, structurally similar to an imidazol-2-carboxylate (Figure 4), was found to proceed readily in polar solvents, suggested by the authors to be due to the weak C-C bond.[185]

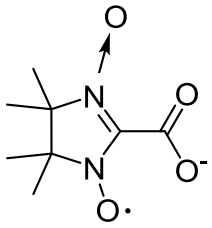

Figure 4: Structure of a nitronyl carboxylate as reported by Tretyakov *et al*.[185]

As with the inclusion complexes of gaseous CO_2, H-bonding interactions are observed in many imidazol-2-carboxylate complexes, undoubtedly playing a vital role in their stabilization.[186] These interactions are especially common in the crystal structures of benzimidazol-2-carboxylates. The added stability provided by their fused ring structures allows the *N*-substituents to be hydrogen atoms, as opposed to the bulky groups required

in most NHCs.[187-190] In the realm of ionic liquids, Gurau *et al.*[191] found that bubbling CO_2 into the ionic liquid 1-ethyl-3-methylimidazolium acetate, [EMIM]OAc, promoted the deprotonation of the cation by the acetate anion, generating acetic acid, with subsequent addition of CO_2 to the generated carbene. The complex was crystallized as the [EMIM]OAc solvate, with stabilizing H-bonds between the $[EMIM]^+$ cation and the carboxylate group, as well as an acetate-acetic acid dimer, shown in Figure 5.

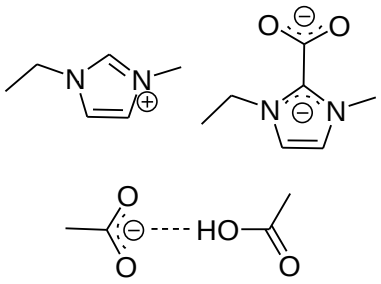

Figure 5: Main structural components of the reaction product obtained through addition of CO_2 to [EMIM]OAc. Depicted are the $[EMIM]^+$ cation (top-left), the acetate-acetic acid dimer (bottom) and the NHC-carboxylate product (top-right).

Finally, on a related note, *N*-heterocylic olefins (NHOs) have also been found to display remarkable reactivity towards CO_2. NHOs can be thought of as derivatives of NHCs. The main difference is the presence of an exocyclic double bond at the, formerly, carbeneic carbon atom. Because the imidazolium ring can delocalize a positive charge, this exocyclic double bond is highly polarized. There are significant contributions from several different resonance structures (Scheme 10), making the exocyclic carbon nucleophilic.

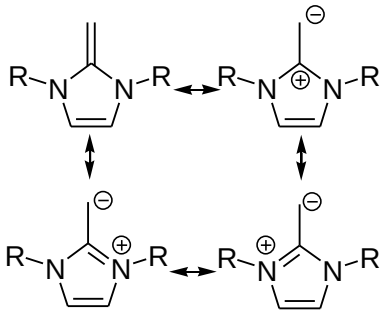

Scheme 10: Various resonance structures of a general *N*-heterocyclic olefin (NHO).

NHO-CO_2 adducts have been prepared by Wang *et al.*[192] and they feature C-CO_2 bond lengths that are significantly longer than those in corresponding NHC-CO_2 adducts, which the authors suggest leads to easier decarboxylation. Indeed, they do observe decarboxylation in dichloromethane. And, these NHO-CO_2 adducts were found to be 10-200 times more effective at catalyzing the formation of cyclic carbonates than the corresponding NHC-CO_2 adducts, again supporting facile decarboxylation to generate the active NHO catalyst.

2.5.3 – Carbamates and Carbamato Complexes

As described earlier, it has been known for decades that CO_2 can undergo nucleophilic attack by amines.[193] The species which result are carbamate zwitterions with a small charge-separation. However, because of the instability of these species, rapid proton transfer from the attacking nitrogen to another available basic site occurs. In the vast majority of examples, the base that abstracts the acidic proton is a second equivalent of the attacking amine, such as in the case of MEA, which generates a discrete cation/anion pair (see Scheme 11A). If there is a moiety within the same molecule that is sufficiently basic, a zwitterionic species may be formed, such as in the case of DETA. A

special, and rather rare, case of the second scenario is proton transfer to the carboxylate group, generating a carbamic acid (Scheme 11B). Carbamic acids are notoriously unstable towards hydrolysis (as are carbamates), however, they have been isolated and characterized in a few cases.[194-197]

In an aqueous environment, or even simply in the presence of moisture, the ultimate products of many reactions between amines and CO_2 are bicarbonate salts. For example, Kuhn and Meyer[198] found that commercial samples of what was supposed to be ammonium carbonate actually contained ammonium carbamate, which was found to hydrolyze readily to ammonium bicarbonate. It is also likely that in high pH aqueous systems (such as an aqueous amine solution), the presence of a high concentration of hydroxide ions would lead to their direct reaction with CO_2 to generate bicarbonate, bypassing the carbamate stage altogether.

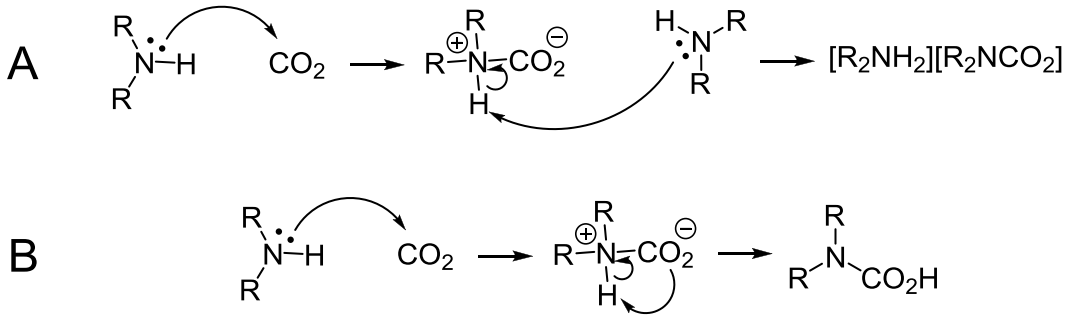

Scheme 11: Reaction of an amine with carbon dioxide followed by a proton-transfer to a second equivalent of amine to generate a carbamate salt (A) or to the carboxylate group to generate a carbamic acid (B).

As stated earlier, the product of the reaction shown in Scheme 11A represents the majority of what is found in the literature concerning carbamates. The simplest such salt, ammonium carbamate, was crystallographically characterized for the first time in 1973[199]

(and re-determined in 2006[200] and 2007[198]), revealing two different polymorphs (α and β). The original structure, α-$[NH_4][CO_2NH_2]$, features an extensive hydrogen bonding array and a short C-N bond length of 1.361(5) Å. This bond length is indicative of partial double-bond character and stems from the delocalization of the lone pair on the nitrogen into the carboxylate group. This shortened bond length, relative to other C-N single bonds, is characteristic of all carbamates.

Sterically-hindered 2-amino-2-methyl-1-propanol has been proposed as an alternative to MEA for CO_2 capture. The crystal structure of its CO_2-derived carbamate salt was first reported by Jo *et al*. in 2010.[201] The authors suggest it might be superior to MEA based on the weaker nature of its bond to CO_2 and the reduced energy requirement that would go along with releasing the captured CO_2. They inferred the bond was weaker bond from theoretical calculations, however, as no crystal structure of the MEA-CO_2 complex has been reported. They also observed the hydrolysis of the carbamate to a bicarbonate salt. Interestingly, in another spectroscopic and computational study, it was shown that increased steric bulk around the amino group (in amines such as *t*-butylaminoethanol or *t*-butylaminopropanol) resulted in CO_2 addition to the hydroxyl end of the molecule rather than the amino end, forming an oxygen-bound CO_2 adduct (a carbonate).[202]

Zwitterionic carbamates, while less common than discrete carbamate salts, have still been prepared and crystallographically characterized. The first such example, *N*-(2-ammonioethyl)carbamate (Figure 6), was published in 1983. The original paper described two different polymorphs both of which featured O…H-N hydrogen bonds between

neighbouring molecules.[203] Later, the structure of the monohydrate was published with, as one might expect, a more extensive hydrogen bonding network.[204] Crystal structures of structurally similar zwitterionic carbamates are known as well.[53, 205, 206] All of these feature H-bonding to the carboxylate group in some form.

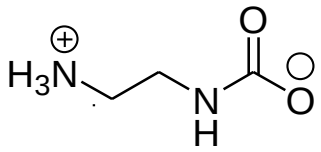

Figure 6: Structural diagram of *N*-(2-ammonioethyl)carbamate.

There is a general trend that emerges when examining the crystallographically-characterized carbamate species appearing in the literature, zwitterionic or otherwise. As the C-N bond length of the carbamate fragment decreases, there is typically an concomitant decrease in the O-C-O bond angle. Furthermore, as the C-N interaction strengthens, the C-O bond lengths increase. This observation does not come as a surprise. When the C-N bond length increases, it should also gradually become weaker, meaning that the carboxylate fragment begins to adopt a structure much closer to that of CO_2. The O-C-O bond angles widen (to approach linearity), and the C-O bonds become shorter. Teague and Jiang[207] illustrated this effect by calculating interaction energies of Lewis basic species (RO^-, cyclohexanolate and phenolate ions in this case) with carbon dioxide. Varying the degree of fluorination of the cyclohexanolate and phenolate anions was found to have a direct influence on the calculated CO_2-anion interaction energies, and the resulting geometries around the CO_2 fragment. As expected, a lower calculated interaction energy, caused by increased fluorination, led to longer C-O(R) bond distances

and wider O-C-O bond angles in the CO_2 fragment. These calculated species ranged from inarguably covalent (O-C = 1.506Å) to more physical, van der Waals interactions (O-C = 2.429Å), such as those observed in the inclusion complexes of CO_2 described earlier.

Of course this trend is only general, and there are many exceptions to be found. Most of these stem from the fact that in every available crystal structure of carbamate species, there is a, sometimes highly elaborate, array of H-bonding which varies greatly from one structure to another. It is quite difficult to draw comparisons and predict how the H-bonding might affect the bond lengths and angles. However, it may be assumed that without these stabilizing interactions, the bond between the amine and carbon dioxide might even be weaker, and more easily broken, unless of course there are other factors influencing its stability.

H-bonding is not the only interaction that can stabilize carbamates. Coordination of the carboxylate oxygen atoms to metals or main group elements has been observed in a variety of complexes. Most of these carbamato complexes are produced through formal insertion of CO_2 into a bond between nitrogen and, most commonly, a metal atom. In this regard, insertion of CO_2 into Mg-N bonds has been reported most frequently, resulting in the formation of polynuclear Mg-carbamato complexes. Metal-oxygen interactions such as these may form if no other H-bonding options are available to the oxygen atoms of CO_2. The investigation of these complexes is often geared towards CO_2 activation.[208, 209] Others have drawn comparisons between these complexes and the complexes that may be generated in the magnesium-containing active site of the enzyme Rubisco (Ribulose-1,5-biphosphate carboxylase/oxygenase) during the biochemical fixation of CO_2.[210] Various

binding modes have been identified in Mg-carbamato complexes,[211, 212] some of which are shown in Figure 7, but the C-N bond lengths and O-C-O bond angles generally remain typical, in comparison to the H-bonded carbamate salts and zwitterions, suggesting that these species are no less stable.

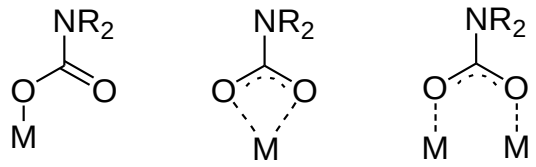

Figure 7: Some examples of binding modes of carbamato ligands to metal centers.

Insertion of carbon dioxide into Li-N,[213-215] B-N,[216]Al-N,[217,218] and Ga-N[219] bonds has also been reported, all resulting in the generation of polynuclear carbamate complexes with multiple O-M (where M = Li, B, Al or Ga) interactions. Insertion of CO_2 into Cu-N,[220] Zn-N,[220] Sb-N[221] and Sn-N[221] bonds has been shown to give multiple carbamato ligands around the same atom, and in the case of tin, bridging carbamato ligands are sometimes present as well.[221, 222] Finally, only two phosphorus-carbamato complexes have been reported, both from Lewis acidic P(V) compounds, with fluorinated ligands (or fluoride itself) bound to the phosphorus to increase its electrophilicity, certainly helping to stabilize these species.[223,224]

2.5.4 Carboxylato Complexes Derived from CO_2

CO_2 insertion reactions are not limited to the production of carbamato complexes. Moving to phosphorus, a number of CO_2 insertion complexes have been prepared, resulting in the formation of P-C bonds. This normally occurs in conjunction with oxygen

coordination to a Lewis acidic center, again typically a metal or a group 13 element. Similar complexes of activated CO_2 that do not stem from true insertion reactions are also well known, most of these coming from the rapidly expanding field of frustrated Lewis pair (FLP) chemistry. These latter complexes are typically derived from attack of the sterically bulky Lewis base on the electrophilic carbon atom of CO_2, while simultaneously an interaction forms between oxygen of the CO_2 and the Lewis acid (most often boranes or alanes).

These reactions are often touted as reversible, and sometimes mildly so, which suggests some degree of instability relative to their carbamato cousins which are often quite stable. In carbamate complexes the orbital overlap between CO_2 and the lone-pair bearing nitrogen, results in a relatively strong C-N bond, with partial double-bond character. Due to the mismatch of orbitals that is introduced on moving down the periodic table to phosphorus, the C-P bond-shortening is not as pronounced, resulting in a generally weaker interaction. For instance, Dickie *et al.*[225] generated a bridging CO_2 complex through insertion into a tin-phosphorus bond. The P-C bond lengths were significantly longer than the other P-C single bonds in the structure, and the adduct was found to release its CO_2 on heating. A zinc-phosphorus insertion product was also prepared. Although its stability was not specifically investigated, the corresponding CS_2 adduct was found to dissociate readily in solution.[226] Binding of carbon dioxide between aluminium and phosphorus centers has been observed, and here it could be reversed by simple exposure to a nitrogen atmosphere.[227] Insertion of CO_2 between Pb-O bonds in

lead alkoxides was found to be reversible depending on the nature of the alkoxide (e.g. reversible under reduced pressure with a *tert*-butyl alkoxide, but not *iso*-propyl).[228]

Activation of carbon dioxide is one of the typical 'tests' performed to investigate potential FLP activity. With the vast number of Lewis acidic and Lewis basic species available for these applications, there are many FLP systems that should be capable of activating carbon dioxide. In terms of Lewis bases, phosphines, amines and carbenes have all been used, while boranes and alanes remain the acids of choice. The increased acidity of alanes relative to boranes is seen as an attractive feature. It diminishes the need for highly-fluorinated groups around the group 13 center, whose preparations can be rather costly, while still maintaining reactivity. However, while alane-based FLPs are quite capable of activating CO_2, the resultant adducts are known to be quite stable,[229,230] and the reaction has been deemed irreversible in some cases.[231] Because of this stability, reactions at the CO_2 center can be accomplished without its release, facilitating its reduction to, for example, carbon monoxide[232, 233] and methanol.[234]

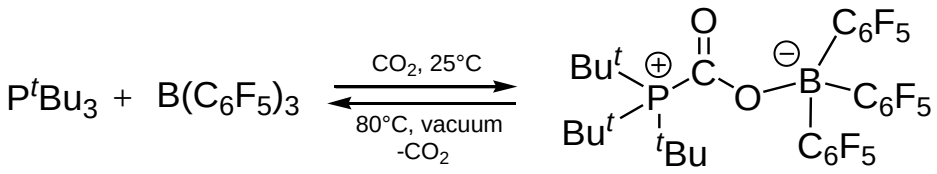

Scheme 12: One example of an FLP activating CO_2 to generate a complex. This particular reaction is reversed through heating under vacuum.[235]

Many borane-based FLPs bind CO_2 to form stable adducts as well, requiring forcing conditions (typically high temperature and vacuum) to release the CO_2.[236,237] Again, the fact that these complexes are so stable is not necessarily a disadvantage, depending on what the ultimate aim is regarding their use. For reversible binding of

carbon dioxide, on the other hand, formation of weak interactions between the Lewis acid and the base is a necessity, and there are already examples of FLPs that bind CO_2 and release it at remarkably low temperatures (~ -20°C).[235, 238] The variety of combinations makes drawing useful comparisons between FLP systems quite difficult as there simply aren't enough complexes of a single 'type' to reliably identify trends. For instance a bridged-FLP $(Me_3C_6H_2)_2P\text{-}CH_2CH_2\text{-}B(C_6F_5)_2$ was found to bind CO_2, but released it above -20 °C in dichloromethane.[235] Meanwhile, another bridged-FLP not dissimilar in structure, tBu$_2$P-CH$_2$-BPh$_2$, was stable to CO_2 loss even at 100°C under vacuum.[236] The increased stability of the latter was attributed to its smaller bite angle (one less carbon in the chain). The fact that a non-fluorinated borane was able to activate CO_2 in an FLP system, however, was unprecedented at the time.

The vast majority of the Lewis bases used in FLP chemistry (with the exception of carbenes) do not react with carbon dioxide on their own. It is the presence of the Lewis acid that stabilizes adduct formation, as with the CO_2 adducts described in previous sections. For instance, tertiary amines are not known to react with carbon dioxide on their own, nor are phosphines. There is one report of a crystallographically characterized phosphonoformate, obtained as a trisodium salt and as a hexahydrate,[239] however, this is the only reported complex of such a species and recent attempts to crystallize similar materials have been unsuccessful.[240]

One example of an FLP combination that was found to activate CO_2 clearly stands above the others in terms of the potential fragility of the produced complex. The FLP combination of *N*,*N*-dimethylaniline (a tertiary amine) and tris(pentafluorophenyl)borane

reacts with carbon dioxide at low temperatures (-32 °C) to give the corresponding adduct (Figure 8A). As with some other FLP combinations, CO_2 is released at low temperatures (> -20°C), but it is not this fact alone that makes this particular example so remarkable. The crystal structure of the adduct reveals an O-C bond length in the CO_2 fragment of only 1.193(3)Å, remarkably close to that of gaseous CO_2 (1.1602(8) Å[241]). Furthermore, the O-C-O angle of the fragment was found to be an astonishing 133.06(18)°, which is not only wider than that of any carbamate yet reported, but is also wider than that of any NHC-CO_2 adduct, with the sole exception of the super-bulky imidazol-2-carboxylate shown in Figure 8B (O-C-O = 133.852°).[184]

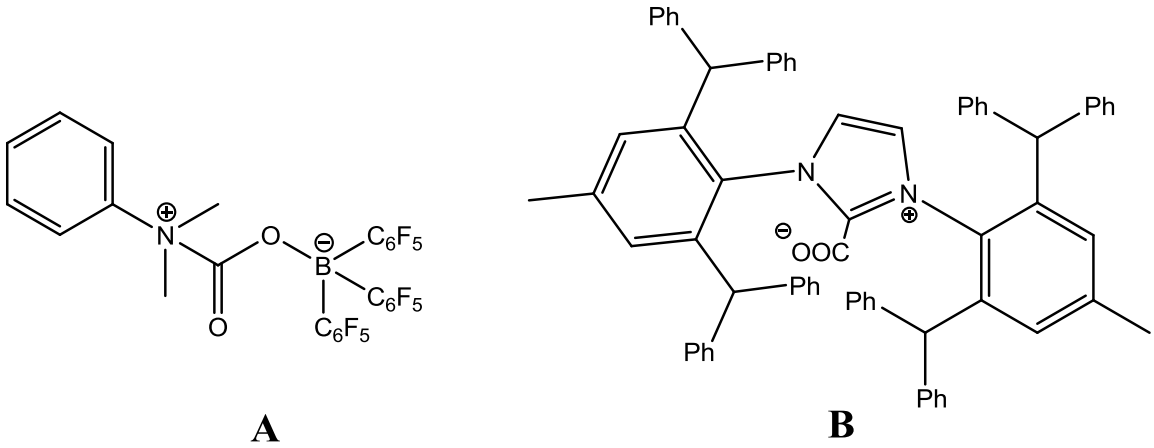

Figure 8: Structures of (A) CO_2 complex of the FLP combination of tris(pentafluorophenyl)borane and *N*,*N*-dimethylaniline, and (B) the carboxylate adduct of the super-bulky carbene 1,3-bis(2,6-dibenzhydryl-4-methylphenyl)imidazol-2-ylidene.

2.5.5 Cyclic Amidines and Guanidines

Common to all the structures described above is the presence of stabilizing interactions which help to keep the carbon dioxide bound to whatever molecule has managed to complex it. At one end of the spectrum are the inclusion complexes of carbon dioxide described in Section 2.5.1. These materials are able to bind carbon dioxide

without significantly altering its structure (i.e. CO_2 is not bent). Of course, outside the realm of simple capture-and-release applications of carbon dioxide, bending/activating carbon dioxide for its use as a chemical feedstock is an unavoidable step. In this regard, nucleophiles which take advantage of the fact that the carbon atom of CO_2 is weakly electrophilic have proven time and again quite capable of binding CO_2, breaking a π-bond between carbon and oxygen to generate a σ-bond between carbon and the attacking species.

The issue with these activating reactions lies with the difficulty in reversing them. While breaking the bond to the carbon atom of CO_2 is clearly the dominating interaction that must be overcome to reverse the reaction, other interactions must be broken as well. H-bonding or coordination through oxygen to Lewis acidic sites are prevalent in all the structures described above, though admittedly the nature of these interactions in solution is not known. Eliminating these interactions may render the CO_2 adducts less stable, so a balance must be struck, minimizing stabilizing interactions in order to potentially access novel chemistry about the carbon atom of CO_2.

In the literature, examples of CO_2 adducts with minimal stabilizing interactions are not common. The properties of a complex, *vis-à-vis* observed stability, and particularly crystal metrics around the carboxylate fragment, are helpful in deducing whether or not a CO_2 adduct is abnormally weak. Thus far, one of the best (crystallographically characterized) examples of such a complex is the adduct formed between carbon dioxide and 1,5,7-triazabicyclo[4.4.0]dec-5-ene (TBD), which was characterized, after repeated failures, by Villiers, *et al*.[242] in 2010.

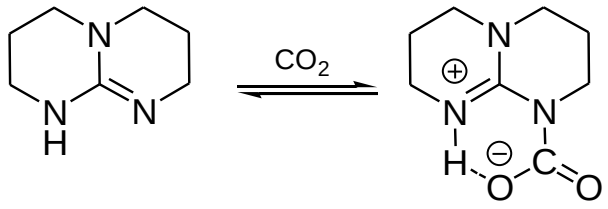

Scheme 13: Reaction of carbon dioxide with TBD to generate a zwitterionic adduct.

Unlike the Lewis acid stabilized carboxylate fragments, the only apparent stabilizing factor in the TBD-CO_2 adduct, other than the charge delocalization in the ring, is a sole hydrogen bond (1.70Å, derived from N2…O1 = 2.535(2) Å and N2-H2 = 0.95 Å) between the carboxylate and the protonated nitrogen in the same molecule. Although there are other, intermolecular, hydrogen bonds present in the solid state structure, they are quite long (H…X ranging from 2.50-2.55Å). The adduct is, unsurprisingly, sensitive to hydrolysis, giving the corresponding bicarbonate salt, as was repeatedly isolated during the earlier attempted preparations of the zwitterion. This adduct not only has the widest O-C-O angle of any characterized carbamate (128.59(19)°) it also has the longest N-C bond (1.480(3)Å). Short N-C lengths (~1.35Å) are typical of carbamates due to the delocalization effect of the carboxylate group described earlier.

The isolation of this adduct provided justification for previously proposed mechanisms for the TBD catalyzed production of organic carbonates. This had been speculated to proceed *via* the generation of the zwitterionic species shown in Scheme 13.[243] Zwitterion formation between CO_2 and 1,8-diazabicyclo[5.4.0]undec-7-ene (DBU), as well as between CO_2 and 3,3,6,9,9-pentamethyl-2,10-diazabicyclop[4.4.0]dec-1-ene (PMDBD), both of which have similar catalytic activity to TBD, have been proposed, and supported with NMR evidence. However, to date no crystal structures of these particular

adducts have been obtained, instead all attempts at crystallization have led to bicarbonate salts.[244,245] 1,4,5,6-tetrahydropyrimidine (THP) and its derivatives have also been speculated to form such adducts.[246,247] Still, the only cyclic guanidine-CO_2 adduct that has been crystallized successfully is TBD-CO_2, a testament to their instability (and sensitivity to hydrolysis).

TBD has been subsequently used as a base, promoting reductive, and reversible, insertion of CO_2 into O-H and N-H bonds.[248] These latter reactions are important in the field of switchable solvents. The first ambient pressure switchable solvent discovered was the combination of a nitrogen base and an alcohol, both neutral molecules. It gave an ionic liquid with markedly altered physical properties upon the simple addition of CO_2. This was achieved through the formation of an alkoxide salt of the protonated base, and the reaction could be reversed under incredibly mild conditions (e.g. bubbling nitrogen to remove the CO_2).[249] Other switchable solvent systems have been discovered since then.[250]

While highly exothermic reactions can be useful in a variety of contexts, in terms of catalysis, the ability to reversibly form adducts with almost no energy barrier in either direction is an incredibly valuable tool. The complexes and subsequent reactions outlined in this section illustrate the remarkable advantages that come along with the generation of weakly bound CO_2 species. While many of these species are highly sensitive, particularly to hydrolysis, others have proven to be more robust and are already finding impressive uses in a multitude of applications (e.g. switchable solvents). Further investigation of weak complexes of carbon dioxide will surely uncover new methods to more reliably prepare and handle these fragile species in terms of their use in the catalytic conversion of

CO_2 to useful products, as well as in carbon capture and release technologies. The elusive cyanoformate ion, as an incredibly rare example of a weak adduct of CO_2 with a small anion, if better understood, could play an important role in this respect.

Results & Discussion

Chapter 3 - CO_2 Uptake from Air Using DETA and $[DETAH]NO_3$

CO_2 uptake studies were performed on solutions of diethylenetriamine (DETA) in PEG 200, as well as solutions of the ionic liquid $[DETAH]NO_3$ in PEG 200, by bubbling the atmosphere (ambient air) of a closed 90 L container into the uptake solution of interest. Concentrations of 5, 10, 15 and 20% (v/v) were investigated. A blank run of PEG 200 alone was also performed, and while there was an observed decrease in CO_2 concentration it was insignificant in comparison to the solutions containing amine or ionic liquid (10 ppm over 100 minutes). PEG 200 was chosen as the solvent mainly due to its desirable properties, such as low-volatility and low-toxicity. To illustrate the low-volatility of PEG 200 (and solutions of DETA in PEG 200), vapour pressure measurements were performed between 50-130 °C, as shown in Figure 9.

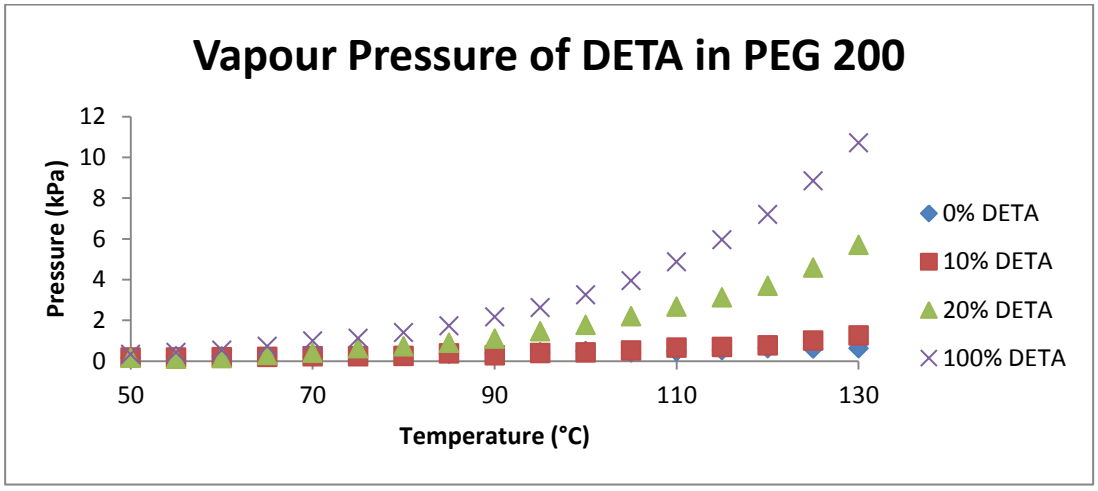

Figure 9: Vapour pressure of solutions of DETA in PEG 200 at varying concentration, from neat PEG 200 (0%) to neat DETA (100%).

While PEG 200 does exhibit a measurable vapour pressure at higher temperatures,[251] it is still remarkably low (i.e. less than 1 kPa at 130 °C). Another advantage of PEG 200 is its non-reactivity toward DETA, its nitrate salt and their CO_2 addition products. PEG 200 shows some ability to solubilise CO_2 itself without the addition of a sorbent based on the measured CO_2 concentration decrease in the blank run. The solubility of CO_2 in PEG 200 has been previously reported.[252] Finally the specific heat capacity of PEG 200 (2.08 J g^{-1} K^{-1} at 298.15 K[53]) is less than half of that of water (4.184 J g^{-1} K^{-1}), the most commonly used solvent in amine-based carbon capture today. Less than half the energy is required to heat a particular mass of PEG 200 than is required to heat the same mass of water. The ionic liquid trihexyl(tetradecyl)phosphonium chloride, $[P_{66614}]Cl$, which was used in a previous study with DETA,[53] was also considered as a solvent for this comparison study but it was found to react with $[DETAH]NO_3$ through, presumably, an anion exchange reaction producing the solid chloride salt of DETA. Therefore PEG 200 was the only solvent used for this study.

Initial rates of CO_2 capture obtained for each solution were investigated through linear regression analysis of the first ten minutes of data for each run, with the slope taken as the rate. The results are represented in Figures 10 through 18, and pertinent results are tabulated in Table 1.

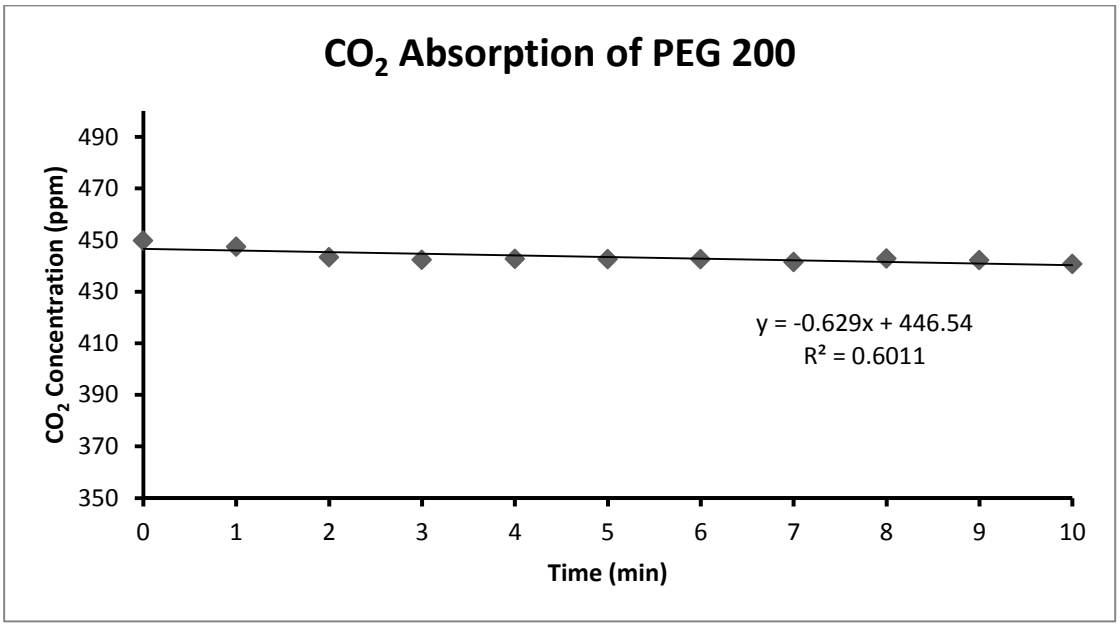

Figure 10: Rate of CO_2 uptake in PEG 200.

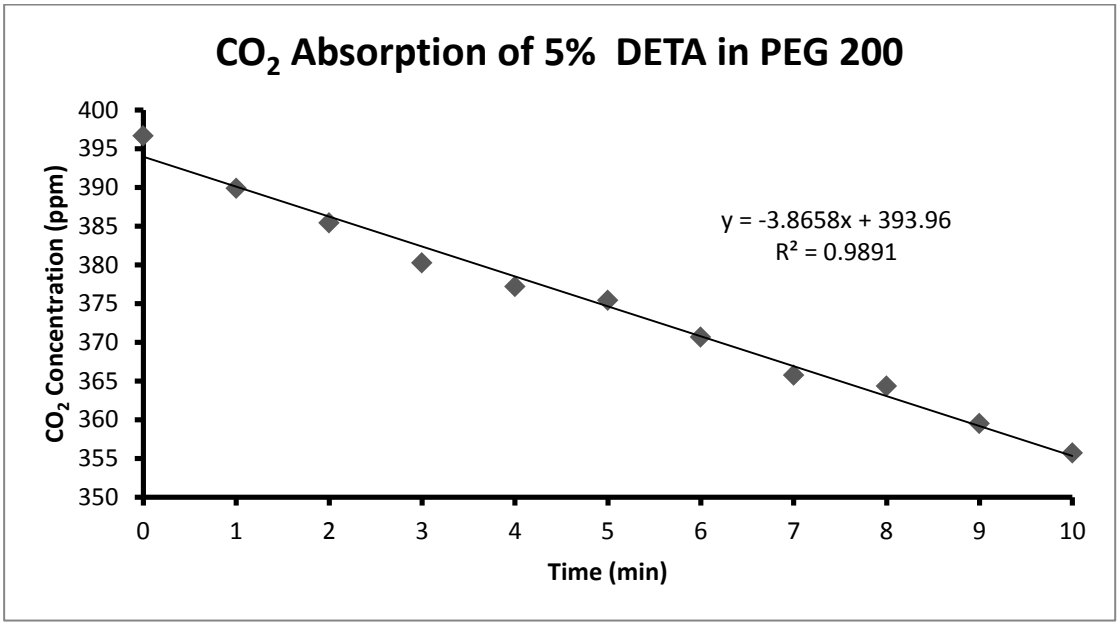

Figure 11: Rate of CO_2 uptake in a 5% (v/v) solution of DETA in PEG 200.

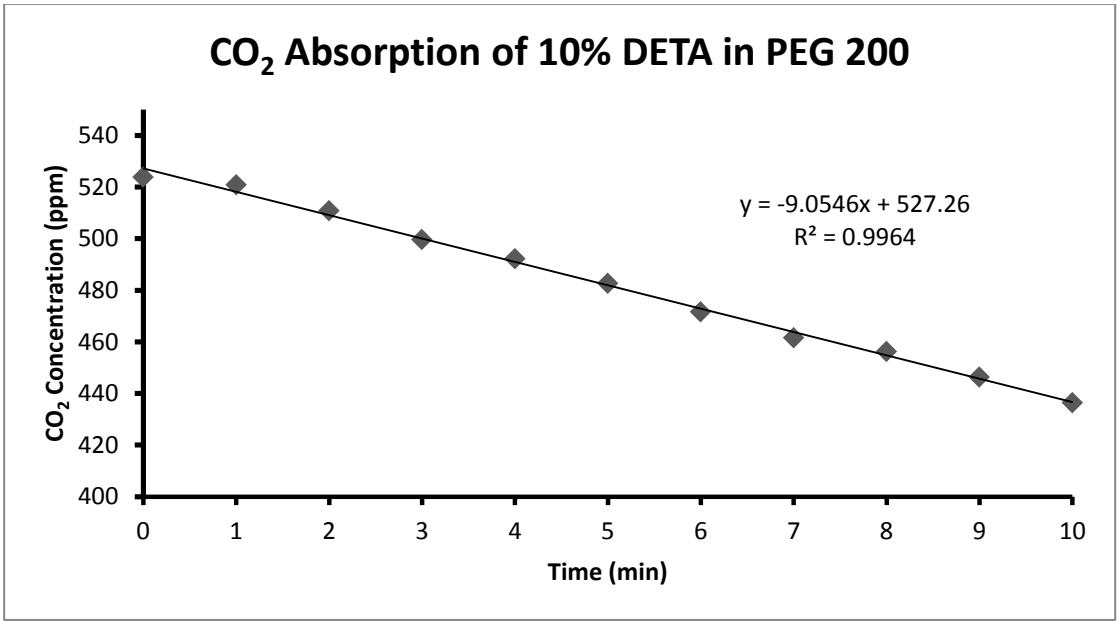

Figure 12: Rate of CO_2 uptake in a 10% (v/v) solution of DETA in PEG 200.

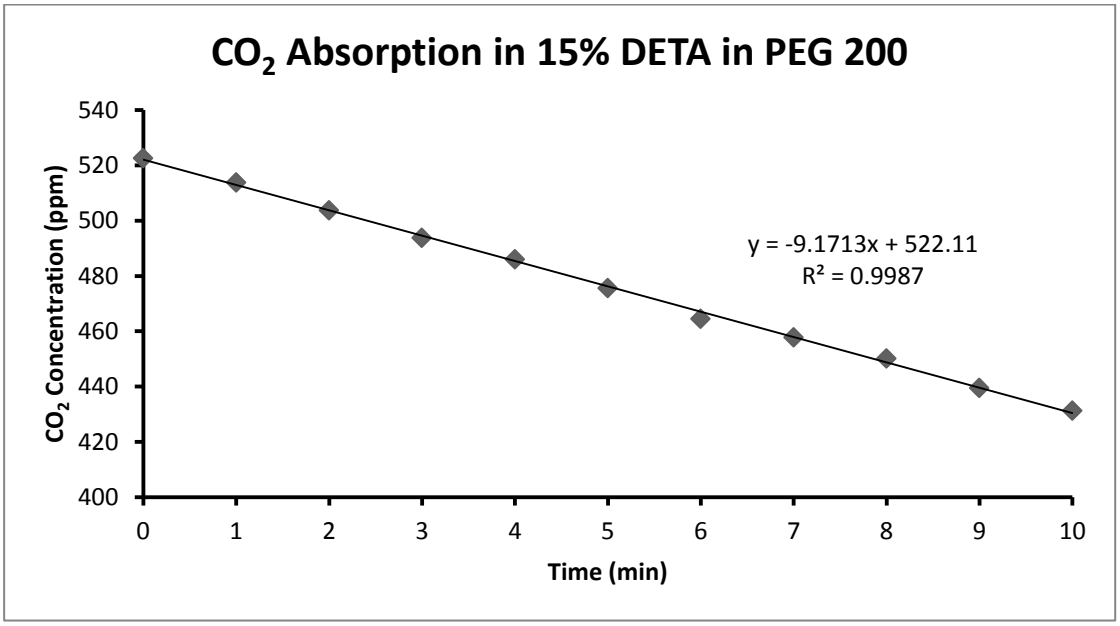

Figure 13: Rate of CO_2 uptake in a 15% (v/v) solution of DETA in PEG 200.

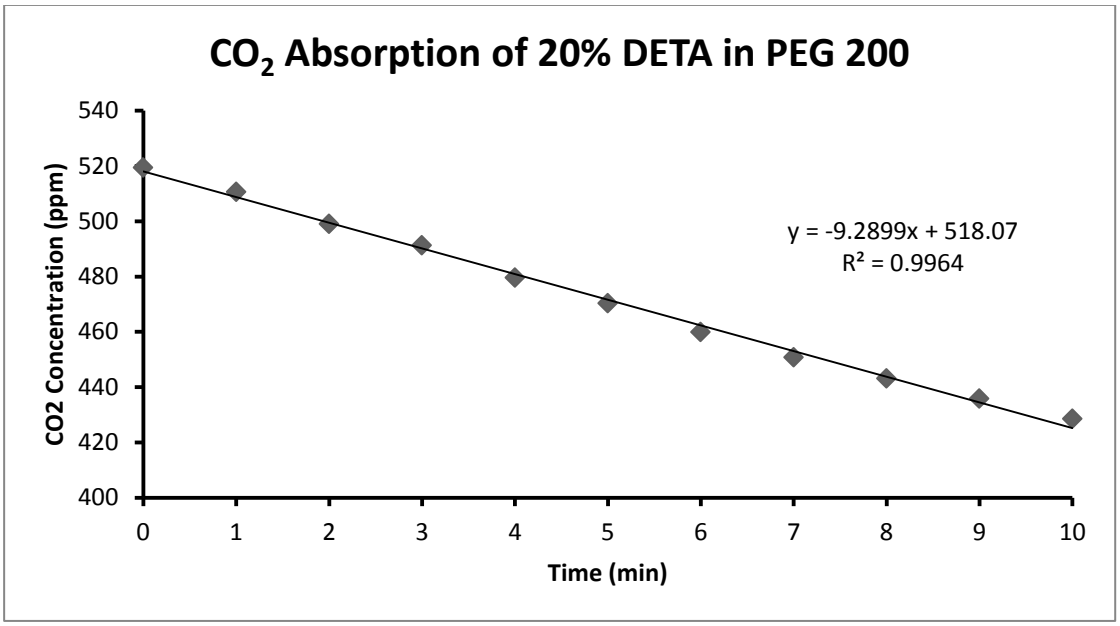

Figure 14: Rate of CO_2 uptake in a 20% (v/v) solution of DETA in PEG 200.

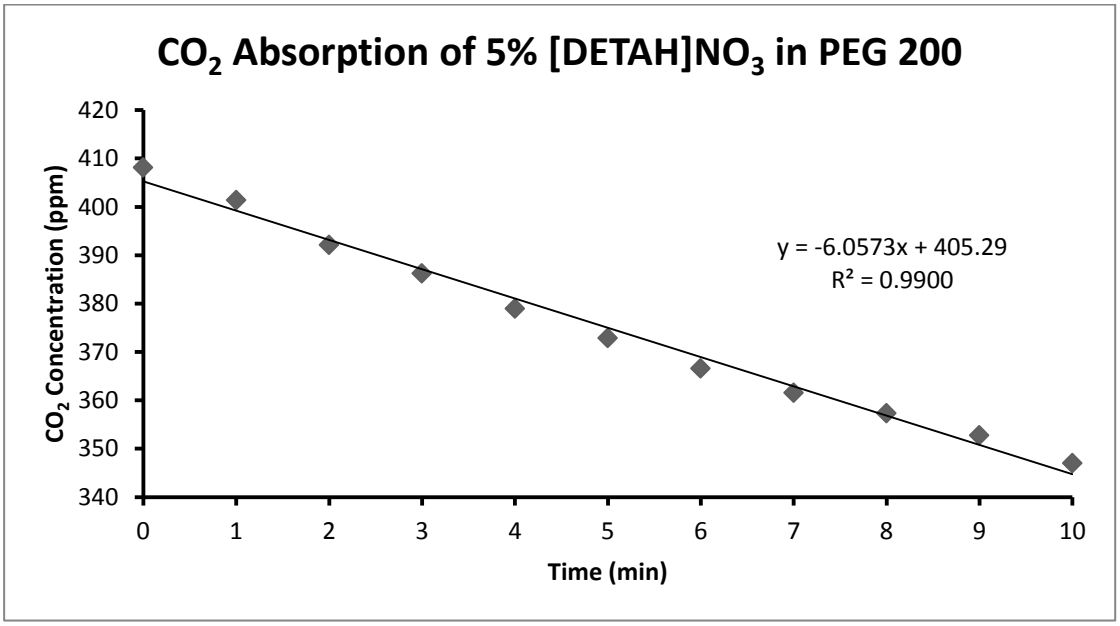

Figure 15: Rate of CO_2 uptake in a 5% (v/v) solution of $[DETAH]NO_3$ in PEG 200.

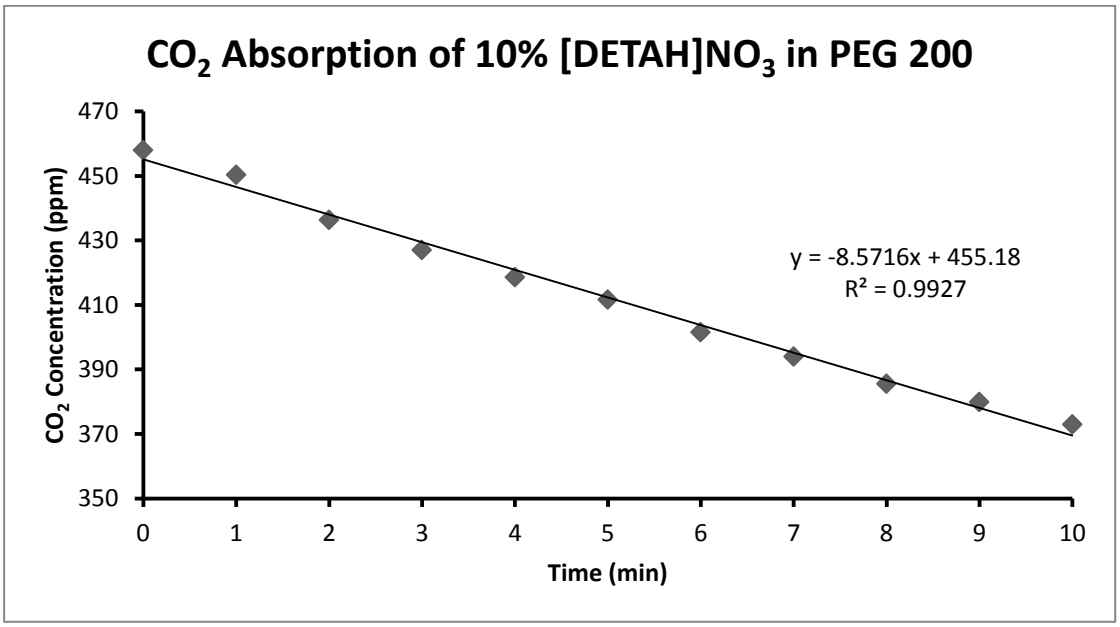

Figure 16: Rate of CO_2 uptake in a 10% (v/v) solution of $[DETAH]NO_3$ in PEG 200.

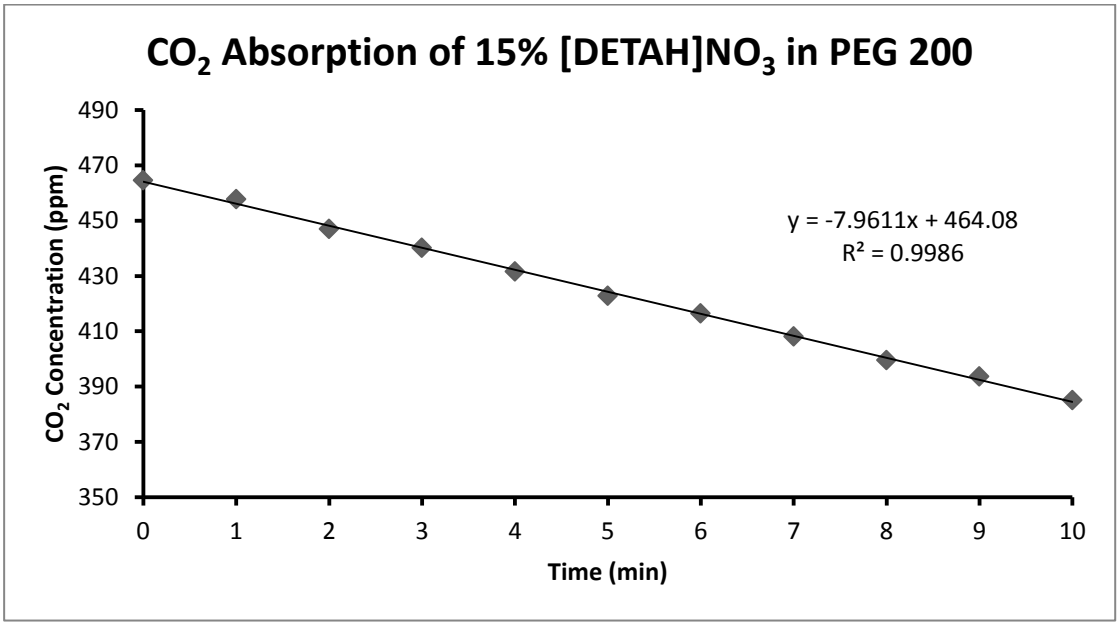

Figure 17: Rate of CO_2 uptake in a 15% (v/v) solution of $[DETAH]NO_3$ in PEG 200.

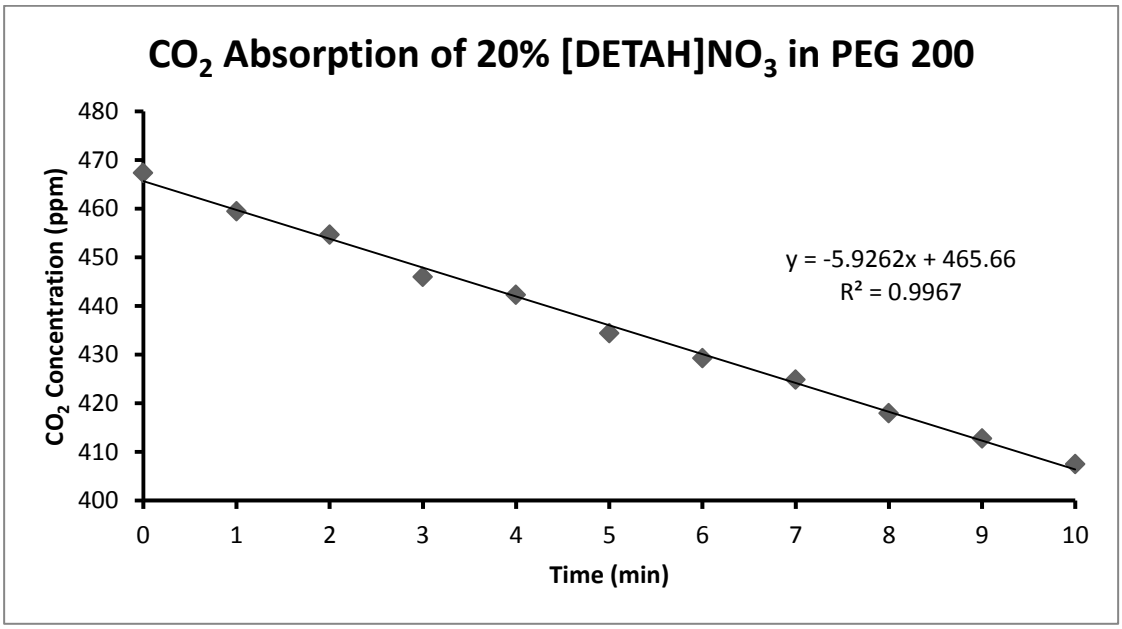

Figure 18: Rate of CO_2 uptake in a 20% (v/v) solution of $[DETAH]NO_3$ in PEG 200.

An estimated standard error (ESD) for the experiment was obtained through comparison of two CO_2 uptake runs of the same solution, 10% DETA in PEG 200. Initial rates of 9.1

ppm/min (Figure 12) and 8.6 ppm/min were obtained, giving a sample standard deviation of 0.4 ppm/min, equating to an ESD of 0.3 ppm/min. These are in agreement with statistically calculated standard deviations of the initial rate as determined through ordinary least-squares regression analysis of each set of data using Microsoft Excel 2010 (see Tables 1 and 2). Obtaining statistical data from two runs is not ideal, thus additional runs should be performed to obtain results at a higher confidence level.

Table 1: Initial rates of CO_2 concentration decrease, the total amount of time taken for CO_2 concentrations to decrease to 50 ppm and standard deviations for tested solutions of DETA and $[DETAH]NO_3$ in PEG 200.

	DETA			
Concentration (v/v%)	**Initial Rate (ppm/min)**	**Time decrease to 50 ppm (min)**	**Standard Deviation of Initial Rate (ppm/min)**	**Standard Deviation of CO_2 Concentration (ppm)**
5	3.9	274	0.14	1.42
10	9.1	150	0.31	3.21
15	9.2	149	0.11	1.20
20	9.3	146	0.19	1.95
	$[DETAH]NO_3$			
Concentration (v/v%)	**Initial Rate (ppm/min)**	**Time decrease to 50 ppm (min)**	**Standard Deviation of Initial Rate (ppm/min)**	**Standard Deviation of CO_2 Concentration (ppm)**
5	6.1	204	0.20	2.13
10	8.6	163	0.24	2.57
15	8.0	162	0.10	1.03
20	5.9	194	0.10	1.03

It was found that [DETAH]NO_3 exhibited a higher affinity for CO_2 (as determined by the initial rate of CO_2 uptake) up to a concentration of 10% (v/v) [DETAH]NO_3, at and after which neutral DETA had a higher affinity for CO_2. The concentration increase from 10% to 15% to 20% for DETA did not result in an appreciable increase in the CO_2 uptake rate (~0.1 ppm/min increase), and for [DETAH]NO_3 the same increase in concentration actually resulted in a decrease in the uptake rate (~2 ppm/min). At the lowest concentration (5%), [DETAH]NO_3 clearly outperforms DETA alone, with an uptake rate 2.2 ppm/min higher than that of DETA at a concentration of 5%.

It is worth looking at the total time taken for CO_2 concentrations to reach a certain (low) value as rates of CO_2 uptake were observed to decrease exponentially over time in each case. There are small deviations in the trends obtained from examining rates alone, as compared to examining uptake times alone. For instance, even though the initial CO_2 uptake rate was higher for 10% [DETAH]NO_3, 15% [DETAH]NO_3 reduced CO_2 concentrations to 50 ppm marginally faster. It is possible that the observed day-to-day fluctuations in CO_2 concentration (i.e. starting concentration of CO_2) are the source of these discrepancies. Furthermore, as no air was allowed to enter the box during the analysis, a net pressure decrease as the CO_2 is captured is implied. However, since the observed initial CO_2 concentrations were relatively low (~450 ppm in most cases) this pressure decrease is not likely to affect uptake rates significantly, causing a decrease in the uptake rates if it were to affect them at all. This effect would also be similar for all runs. Overall, despite these discrepancies, useful conclusions can still be derived from this study.

Clearly the optimal concentrations for CO_2 uptake in [DETA]HNO_3 lie in the 5-15% range, while in DETA this optimum concentration appears to lie close to 20%. Although in very large scale applications (e.g. CO_2 capture from flue gases) using a sorbent at such a low concentration may not be seen as advantageous due to the increased amount of material required, the same is not necessarily true for smaller scale applications. Because PEG 200 is available in such large quantities at a low cost, is of low volatility and low-toxicity, it lends itself quite well to application as a solvent in CO_2 capture, even in high relative concentrations as compared to the sorbent. It is especially advantageous over water in this latter regard, due mainly to its much lower specific heat capacity (less than half of that of water as stated earlier).

Furthermore, the use of lower concentrations of the amine-based sorbent, which of course can be assumed to be more detrimental to the environment than water or PEG 200, is another advantage. As these systems are being investigated for smaller-scale applications, it also follows that required amounts will be far lower than what is needed for CO_2 capture from fossil-fuel burning plants, which obviously will have a much larger CO_2 output than a warehouse containing CO_2-generating produce. Furthermore, the use of a reversible system such as those investigated in this study allows for recycling of the sorbent, which is not always possible, particularly when using stoichiometric reagents for capture[253] (such as hydroxides, which are commonly employed[254]). Further investigation of these two capture systems is required. For example, it would be useful to investigate rates of CO_2 uptake in higher concentrations of DETA in PEG 200 to identify at what concentration the CO_2 uptake rate is at its highest.

Chapter 4 – Preparation and Characterization of the Elusive Cyanoformate Ion

4.1 – Preliminary Calculations and Preparation

In 1995, Zhang *et al.*[126] prepared and characterized the first, and thus far, only, halide-CO_2 adduct, tetramethylammonium (and hexamethylpiperidinium) fluorocarbonate. This fluorocarbonate salt is a closely-related cousin to cyanoformate, and as a result data pertaining to its characterization will be drawn upon repeatedly for comparison purposes throughout this thesis. The structure of the fluorocarbonate ion is shown in Figure 19. It should be noted that there is one report[255] involving generation of the cyanoformate ion at low pressure in the gas phase though there are no comparable results between that and this study.

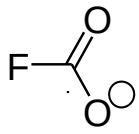

Figure 19: Structural diagram of the fluorocarbonate ion.

It seemed prudent to first determine whether or not a reaction between carbon dioxide and cyanide was even feasible, due to the described instability of the fluorocarbonate complex. All quantum chemical calculations and subsequent interpretations in this and subsequent sections were performed by Dr. Heikki Tuononen and Dr. Jani Moilanen at the University of Jyväskylä in Finland. Quantum chemical calculations at the PBE0/aug-cc-pVTZ, ωB97X-D/aug-cc-pVTZ, MP2/aug-cc-pVTZ and CCSD(T)/aug-cc-pVTZlevels of theory were performed to generate an optimized

structure for cyanoformate, as well as fluorocarbonate for comparison purposes (geometrical parameters can be found Table 2). Furthermore, calculations of thermochemical data for the formation of cyanoformate *in vacuo* from its constituents were also performed at the CCSD(T)/CBS, CCSD(T)/aug-cc-pVTZ, MP2/aug-cc-pVTZ, PBE0/aug-cc-pVTZ and ωB97X-D/aug-cc-pVTZ levels of theory, and are tabulated in Table 3. The details of all computational methods can be found in the experimental section (Chapter 6.9).

Table 2: Optimised geometrical parameters of cyanoformate, $[NCCO_2]^-$, and fluorocarbonate, $[FCO_2]^-$ at different levels of theory (in vacuum).

$[NCCO_2]^-$					
Method	**C-C [Å]**	**C-N [Å]**	**C-O [Å]**	**C-C-O [°]**	**O-C-O [°]**
PBE0 / aug-cc-pVTZ	1.536	1.155	1.235	113.3	133.3
ωB97X-D / aug-cc-pVTZ	1.548	1.152	1.233	133.3	133.5
MP2 / aug-cc-pVTZ	1.530	1.176	1.247	113.5	133.0
CCSD(T) / aug-cc-pVTZ	1.544	1.159	1.236	113.3	133.4
$[FCO_2]^-$					
Method	**C-F [Å]**	**C-O [Å]**	**F-C-O [°]**	**O-C-O [°]**	
PBE0 / aug-cc-pVTZ	1.468	1.219	111.7	136.6	
ωB97X-D / aug-cc-pVTZ	1.468	1.219	111.7	136.6	
MP2 / aug-cc-pVTZ	1.485	1.227	111.3	137.3	
CCSD(T) / aug-cc-pVTZ	1.467	1.228	111.7	136.6	

Table 3: Calculated thermochemical data [kJ/mol] for the reaction CO_2 (g) + CN^- (g) → $[NCCO_2]^-$ (g) at different levels of theory (in vacuum).

	CCSD(T)/ CBS	**CCSD(T)/ aug-cc-pVTZ**	**MP2/ aug-cc-pVTZ**	**PBE0/ aug-cc-pVTZ**	**ωB97X-D/ aug-cc-pVTZ**
$\Delta_a H°$	-30.1	-31.1	-30.4	*	-29.7
$\Delta_a G°$	3.0	2.0	2.2	*	1.3
$\Delta_r H°$	-74.2	-74.5	-76.3	-91.3	-73.2
$\Delta_r G°$	-36.1	-36.4	-38.1	-53.1	-35.0
* No transition state could be found as the reaction is spontaneous at this level of theory.					

As shown in Table 3, the thermochemical data indicates that, at least in the gas phase, a reaction between carbon dioxide and cyanide is theoretically possible. The reaction Gibbs energies ($\Delta_r G°$) are negative at all levels of theory, with low activation energies ($\Delta_a G°$) of 1.3-3.0 kJ mol^{-1}. In vacuum, the reaction begins with the formation of an ion-dipole complex that slightly lowers the Gibbs energy of the system. Subsequent shortening of the C-C bond affects an increase in free energy and leads to a transition state with $\Delta_a G°$ = 2.0 kJ mol^{-1} at the CCSD(T)/aug-cc-pVTZ level of theory. Based on these data, the formation of $[NCCO_2]^-$ is concluded to be spontaneous in the gas phase, whereas the reverse reaction (breaking the C-C bond) involves an energy barrier of 38.4 kJ mol^{-1} at the CCSD(T)/aug-cc-pVTZ level. The reaction profile for the formation of cyanoformate in the gas phase can be found in Figure 20.

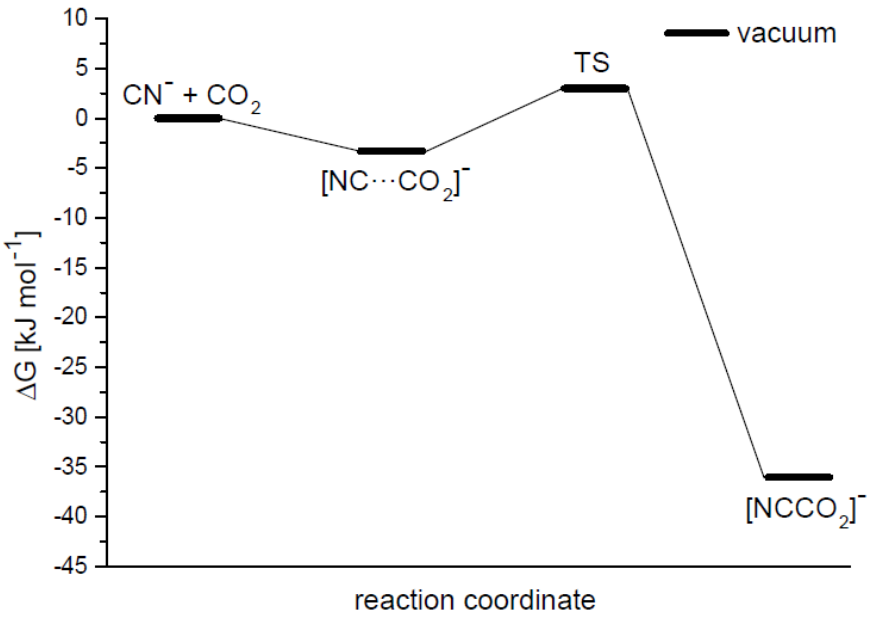

Figure 20: Calculated reaction profile for the formation of $[NCCO_2]^-$ from CN^- and CO_2 *in vacuo* at the CCSD(T)/CBS level.

Of course, the addition of carbon dioxide to the nitrogen end of cyanide to produce isocyanoformate, $[CNCO_2]^-$, could be envisaged, however, the optimized structure of $[CNCO_2]^-$ was found to be 56.2, 51.9, 61.5 and 54.9 kJ mol^{-1} higher in Gibbs energy than $[NCCO_2]^-$ at the PBE0, ωB97X-D, MP2 and CCSD(T) levels, respectively. It is worth noting, however, that all of these energies are higher than that of the reaction between CO_2 and fluorocarbonate, indicating that if cyanoformate did exist it would be even *less* stable than the fluorocarbonate ion.

Since the data found in Table 3 did seem to indicate that a marginally, stable complex could be prepared, attempts to isolate cyanoformate were made. Tetraphenylphosphonium, $[PPh_4]^+$, was chosen as the cation due to recent successes isolating novel tetraphenylphosphonium salts of organic zincates,[256] as well as isolation of

halosulfite salts (SO_2X^-), which will be reported soon. Tetraphenylphosphonium cyanide, $[PPh_4]CN$, was prepared by the metathesis of tetraphenylphosphonium bromide, $[PPh_4]Br$, with excess potassium cyanide, KCN, in methanol, as per a literature procedure reported by Gloaguen et al.[257] (Scheme 14A). It was found during this first step that, while tempting, heating the reaction to encourage KCN dissolution resulted in the generation of triphenylphosphine oxide. Presumably this occurs through attack of cyanide on a phenyl ring of the cation, followed by oxidation. This decomposition pathway was not investigated further, however, decomposition of tetraphenylphosphonium halide salts to phenylphosphine compounds at high pH has been described previously in the literature.[258] To avoid this decomposition, reaction temperatures were kept below 30 °C at all times.

After metathesis in methanol, the solvent was removed by rotary evaporation (< 30 °C), and the $[PPh_4]CN$ was extracted with acetonitrile. It is likely that some amount of unreacted $[PPh_4]Br$ remained after the preparation of $[PPh_4]CN$ despite the fact that excess KCN was used; it is not known the degree of completion the metathesis reaction reached. As the bromide ion was not expected to interfere chemically or spectroscopically no attempts were made to quantify its concentration.

To prepare tetraphenylphosphonium cyanoformate, $[PPh_4][NCCO_2]$, a concentrated solution of $[PPh_4]CN$ in acetonitrile was exposed to an atmosphere of carbon dioxide in a 250 mL Schlenk flask. Crystallization was observed immediately and the solvent was decanted to obtain X-ray quality crystals of the cyanoformate salt in low to moderate yield. It was observed that if the solution of $[PPh_4]CN$ was not sufficiently concentrated, crystallization did not occur immediately. Subsequent cooling of the

reaction mixture was found to give tetraphenylphosphonium bicarbonate, rather than cyanoformate. This presumably occurs through hydrolysis and will be discussed in Section 4.5.

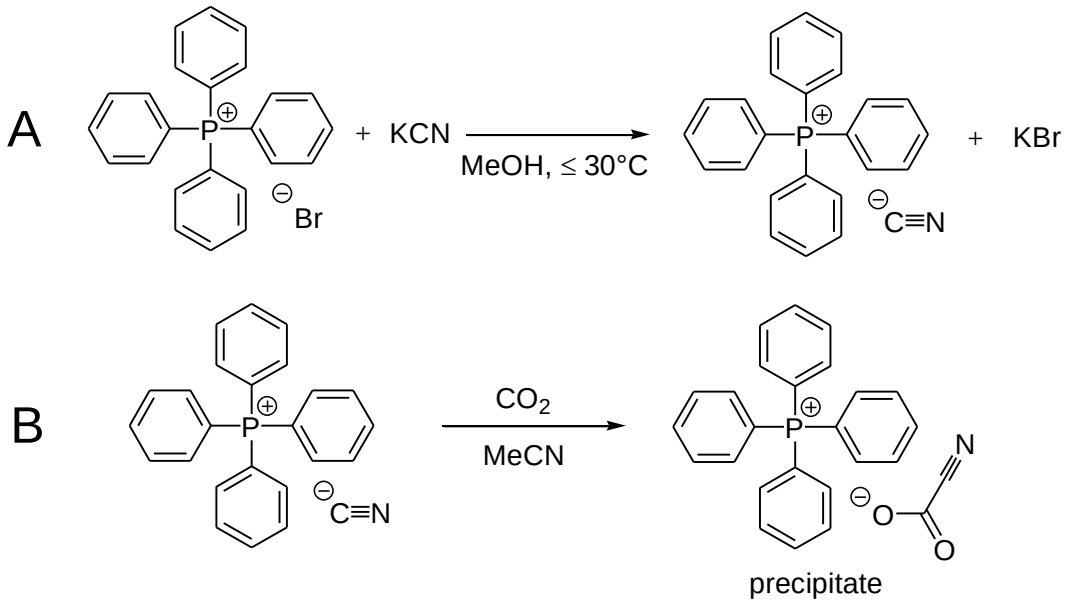

Scheme 14: (A) Preparation of $[PPh_4]CN$ from $[PPh_4]Br$ and KCN, and (B) reaction of $[PPh_4]CN$ with CO_2 to give the cyanoformate salt, $[PPh_4][NCCO_2]$, which precipitates from solution immediately.

4.2 Crystal Structure of $[PPh_4][NCCO_2]$

All X-ray crystallographic data for $[PPh_4][NCCO_2]$ and $[PPh_4][HCO_3]\cdot H_2O$ (see section 4.5) were collected and interpreted by Dr. Katherine Robertson at Saint Mary's University.

Crystals of tetraphenylphosphonium cyanoformate, suitable for X-ray diffraction, grew in the form of thick, clear and colourless plates. Figure 21 shows the crystal structure of $[PPh_4][NCCO_2]$, with the disorder of the anion shown on the left of the arrow,

and deconvoluted on the right. Figure 22, meanwhile shows a packing diagram of $[PPh_4][NCCO_2]$ viewed down the *Z* axis.

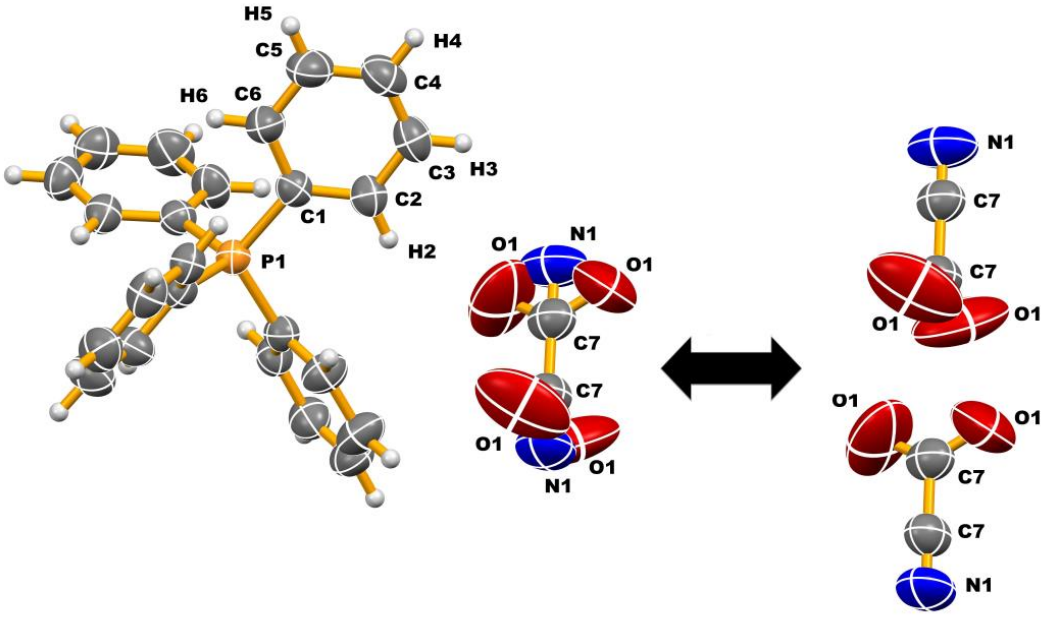

Figure 21: Structural diagram of $[PPh_4][NCCO_2]$. Ellipsoids are drawn at the 50% probability level. Unique atoms of the cation and all atoms of the anion are labelled. The anion is comprised of only three unique atoms, carbon and oxygen atoms with site occupancies of 0.50 and nitrogen with a site occupancy of 0.25. The remainder of the anion is generated by symmetry. To the right of the arrow the anion has been deconstructed into its two overlapping components, both of which are 50% occupied in the structure.

The cation of the salt is quite typical, similar to those observed in other tetraphenylphosphonium salts. The anion, however, is just the opposite. Due to symmetry and disorder only *three* atoms of the anion are crystallographically unique. The anion in the crystal structure is a composite of two complete cyanoformate anions, each at 50% occupancy, superimposed on one another in a head-to-tail fashion. The cyano carbon of one anion occupies the same position as the carboxyl carbon of the other anion, and vice versa. Furthermore, the planes of the carboxylate groups in each anion are oriented

perpendicularly to one another. A more detailed crystallographic description can be found in Chapter 6.10.

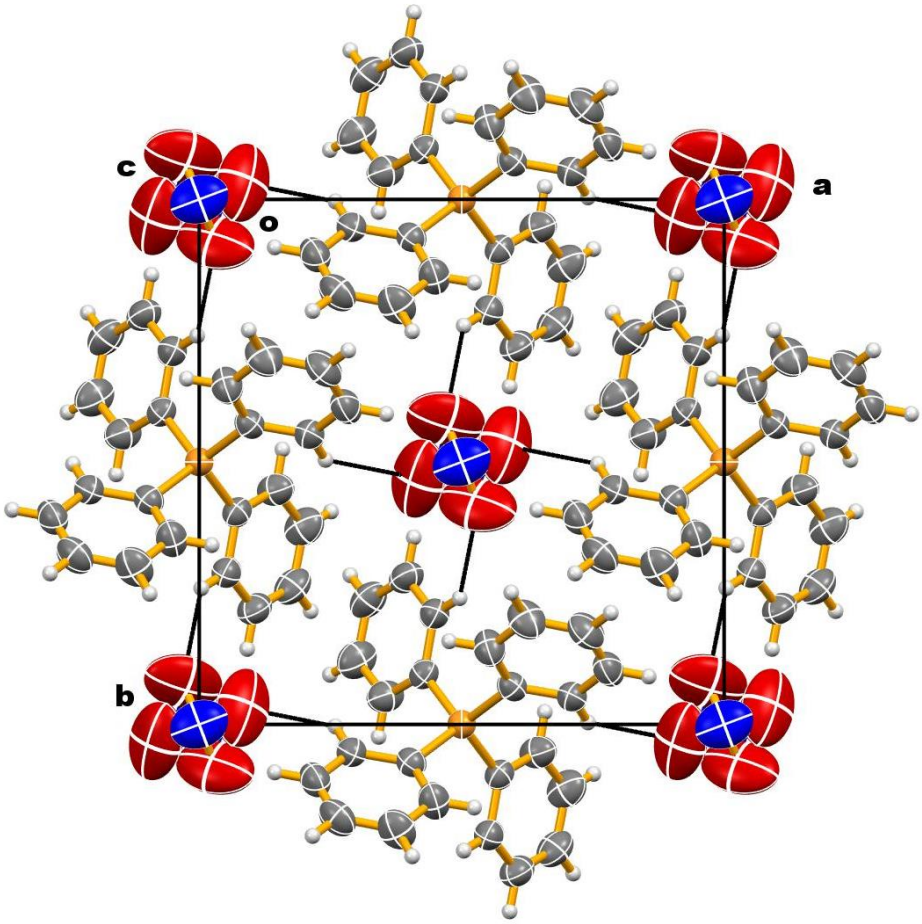

Figure 22: Packing diagram of $[PPh_4][NCCO_2]$ viewed down the *Z*-axis. Ellipsoids are drawn at the 50% probability level. The solid lines illustrate the strongest C-H…O interaction in the structure.

As a whole, the theoretically predicted metrical parameters of $[NCCO_2]^-$ (Table 2) are in good overall agreement with the results from the X-ray structural study. There is little, however, in the crystallographic literature with which to compare these results. The only structure containing a similar anion is the aforementioned fluorocarbonate anion, deposited in the Cambridge Structural Database (CSD)[259] as hexamethylpiperidinium

fluorocarbonate acetonitrile solvent (ZAQBIE) by Zhang *et al*., separate from their paper[126] which does not contain crystallographic results. Their study pertained to a different salt, tetramethylammonium fluorocarbonate. Using the data deposited in the CSD it is easily determined that the fluorocarbonate structure crystallises in a lower symmetry monoclinic unit cell with an ordered anion lying on general positions. Calculated bond lengths and angles for fluorocarbonate, as well as bond lengths and angles for cyanoformate are given in Table 4.

Table 4: Bond lengths and angles for the anions of hexamethylpiperidinium fluorocarbonate and tetraphenylphosphonium cyanoformate.

Fluorocarbonate		**Cyanoformate**	
Bond Length (Å)		**Bond Length (Å)**	
C-F	1.367	C-C	1.480(9)
C-O	1.261	C-N	1.056(12)
C-O	1.236	C-O	1.181(9)
Angle (°)		**Angle (°)**	
F-C-O	116.63	N-C-C	180
F-C-O	116.62	C-C-O	117.3(6)
O-C-O	126.75	O-C-O	125.4(12)

The CO_2 portions of the two anions are quite similar, although the one unique C-O bond length in $[NCCO_2]^-$ is slightly shorter than those in $[FCO_2]^-$. This may be due to the thermal motion the disordered anion can undergo in the cavity formed by the arrangement of the PPh_4 cations in the first structure. The large thermal ellipsoid of the oxygen atom shows that it is more able to vibrate/rotate in the off-axis position it occupies. The equivalent C-C-O angles are both smaller than the O-C-O angle, which is opened up by the larger, more electronegative oxygen atoms.

A CSD search was undertaken for structures similar to the current anion, in particular for those having an *sp* carbon of a cyanide bound to an sp^2 carbon such as in cyanoformate. The only compound located was cyanoformamide (Figure 23), described in a study published by Drück *et al*. in 1984.[260]

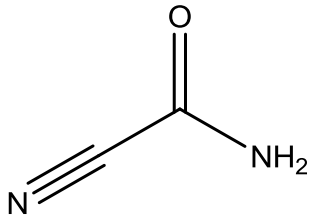

Figure 23: Structural diagram of cyanoformamide.

The authors report that a C-C length of 1.477(8) Å, which they report as expected for a bond between *sp* and sp^2-hybridised carbon atoms, and which is identical to that found in cyanoformate (1.480(9) Å). The length of the C-N bond, 1.056(12) Å, is shorter than the reported in cyanoformamide (1.141(8) Å). Thus another CSD search was undertaken for structures containing solvating acetonitrile, CH_3CN, for comparison. An informal search of the database revealed 13317 structures with 15648 values having an average C-N bond length of 1.138 Å, similar to that in cyanoformamide. However, 617 acetonitrile solvates did contain reported C-N bond lengths of less than 1.06 Å, indicating that the rather short C-N bond length observed in cyanoformate is not uncommon.

One might expect that a shorter C-N bond would reflect a stronger ionic component to the bond and a weaker interaction with the remainder of the adduct (a weak C-C bond). Again, looking to the CSD, bond lengths for free cyanide were sought. In the 12 bonds of the 9 structures obtained, the average C-N bond length was 1.093 Å, and they ranged from 0.966 to 1.323 Å. The C-N bond length of cyanoformate of 1.056(12) falls

well within this range and reinforces the notion of it containing only a weak carbon-carbon bond.

The packing of the cations and anions in the structure of $[PPh_4][NCCO_2]$ in the tetragonal space group *I*-4, is similar to that observed in many other simple $[PPh_4]X$ salts, where X = Br, I, SCN, OCN, $N(CN)_2$, etc.[261-264] Viewed down the *Z* axis (Figure 22) the cations and anions form discrete stacked columns, with the cations passing through the midpoints of the unit cell axes, and the anions centred at the unit cell corners and the midpoint of the cell, occupying the channels formed between the stacked columns of cations. There are no close contacts between the cation columns in the structure and there are also few interactions between the cations and the anions. Those that are present are generally weak, with only one H···O distance of less than 2.5 Å, at 2.37 Å. The lack of strong interactions between the cations and anions likely results in the relatively free rotation of the anion about the S_4 rotation axis, in the channels formed by the cations. The position of cyanoformate nestled in the channels created between the tetraphenylphosphonium cations, likely aids in stabilizing the anion.

4.3 Infrared and Raman Spectroscopy

The most useful vibrational modes of the cyanoformate ion in terms of structure confirmation are the cyano stretch, *ν*CN, and the symmetric and asymmetric carbonyl stretches (ν_sCO_2 and $\nu_{as}CO_2$), respectively. Cyano stretches conveniently lie in a region with very little interference, while the asymmetric carbonyl stretch is typically one of the strongest bands in the spectra of carbonyl compounds.

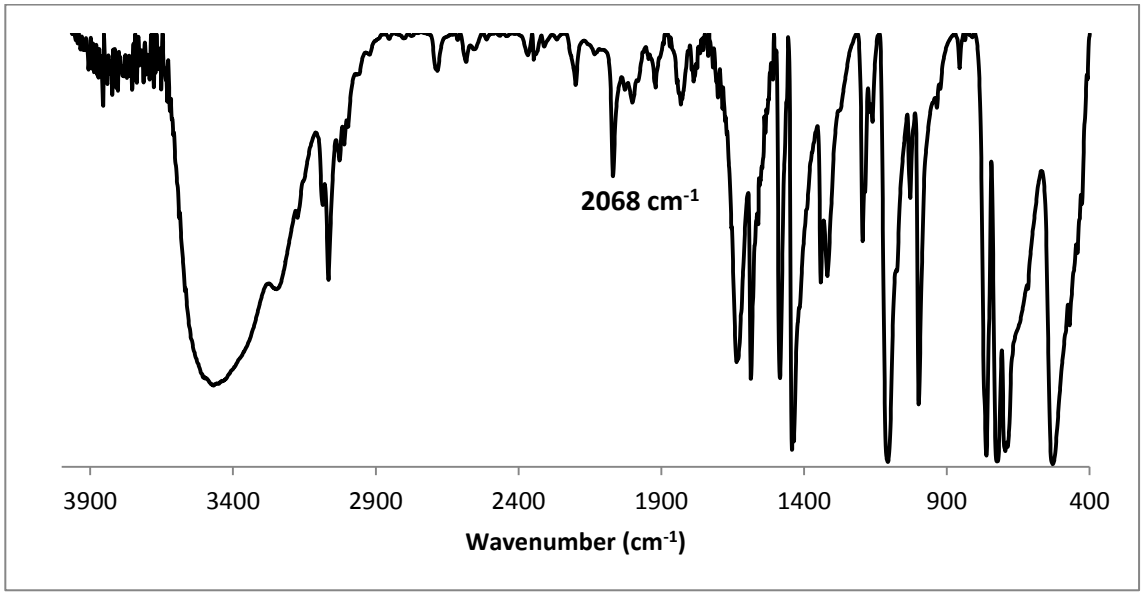

Figure 24: Infrared spectrum of tetraphenylphosphonium cyanide hydrate.

The infrared spectrum of the precursor material, tetraphenylphosphonium cyanide, is shown in Figure 24. The prominent OH band arises because the cyanide salt is obtained as a hydrate.[265] During our preparations crystals of both the monohydrate and the dihydrate have been obtained (confirmed by X-ray diffraction). Samples were difficult to dry completely, and it also appeared that heating the sample promoted a reaction between the anion and the cation to generate triphenylphosphine oxide; thus samples were kept under 30 °C at all times and stored at -15 °C. The majority of the bands observed in the spectrum are absorbances due to the cation. The νCN stretch of tetraphenylphosphonium cyanide appears at 2068 cm^{-1} as a medium-sharp peak.

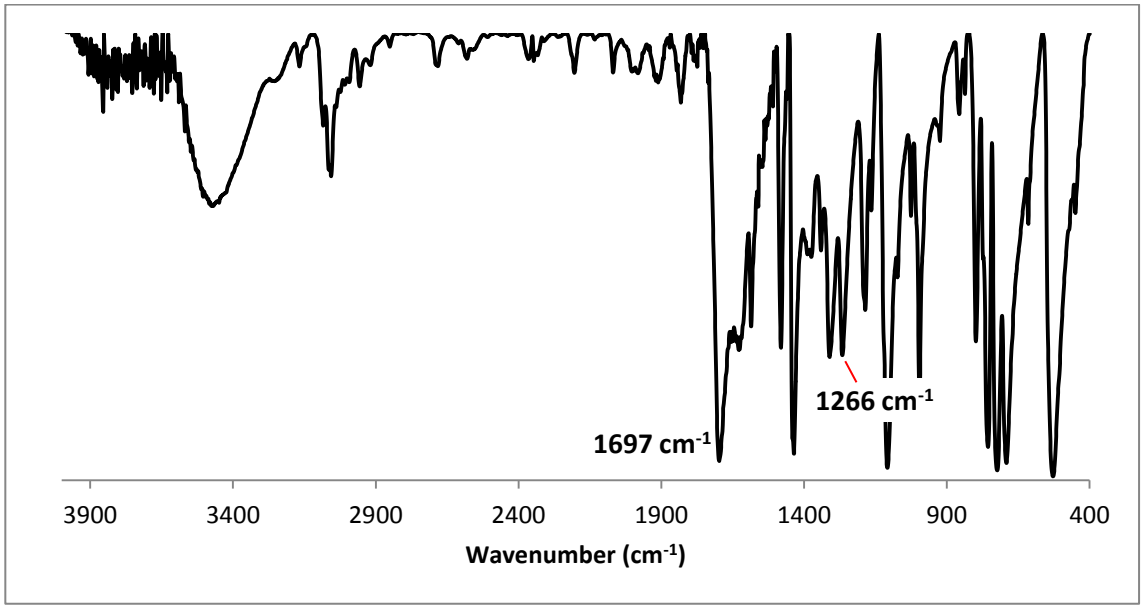

Figure 25: Infrared spectrum of tetraphenylphosphonium cyanoformate.

In the IR spectrum of tetraphenylphosphonium cyanoformate, there is still an OH band visible, although it is lower in intensity than that in the starting material. This band is probably due to residual water from the starting material. The cyano stretch is greatly diminished as compared to that of the starting material. However, bands associated with the carboxyl portion of cyanoformate do appear. The higher energy $\nu_{as}CO_2$ is readily apparent at 1697 cm^{-1}, and so is ν_sCO_2 at 1266 cm^{-1}. Of course, the appearance of a shifted cyano stretch is expected, but it is not visible in the IR. The missing stretch is, however Raman active. The Raman spectrum of tetraphenylphosphonium cyanoformate is shown in Figure 26, with the diagnostic νCN stretch appearing at 2196 cm^{-1}.

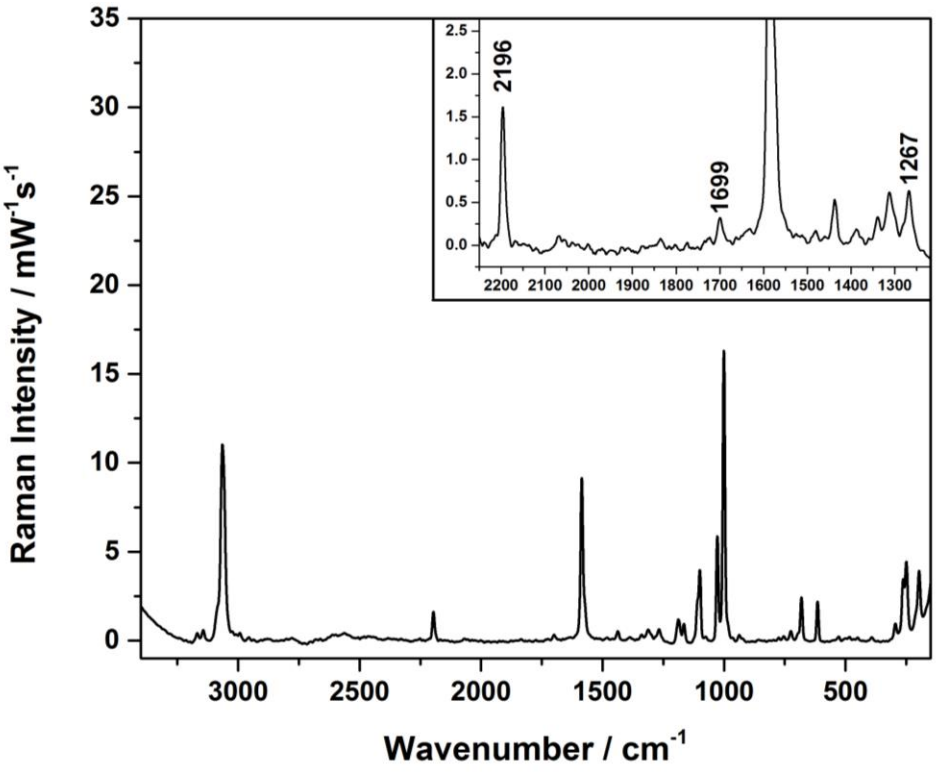

Figure 26: Raman spectrum of tetraphenylphosphonium cyanoformate.

Vibrational frequencies, IR intensities and Raman activities of the cyanoformate ion were computationally determined for comparison purposes, and can be found in Table 5. These calculated values indicate that while the ν*C*N is not symmetry-forbidden in the IR, its intensity is nonetheless extremely low (0, 7 and 10 km mol^{-1} at the levels of theory employed). While $\nu_s CO_2$ and $\nu_{as} CO_2$ are also visible in the Raman, their intensities are quite low as compared to that of ν*C*N. The ν*C*N stretch (2196 cm^{-1}) appears at a rather low frequency when compared to other nitriles (e.g. ν*C*N of acetonitrile is found at 2253 cm^{-1}). Free cyanide anions typically absorb at a considerably lower frequency compared to molecular nitriles; for example, ν*C*N occurs at 2068 cm^{-1} for $[PPh_4]CN$. The lower

νCN for cyanoformate may, as with the short C-N bond length, indicate some partial ionic character to the cyano group.

Table 5: Vibrational frequencies, IR intensities and Raman activities for the cyanoformate ion at the MP2/aug-cc-pVTZ, CCSD(T)/aug-cc-pVTZ, PBE0/aug-cc-pVT ωB97X-D/aug-cc-pVTZ levels of theory.The intensity/activity data is not readily available at the CCSD(T) level.

MP2/aug-cc-pVTZ (CCSD(T)/aug-cc-pVTZ)			
Vibrational mode	**Frequency [cm^{-1}]**	**IR int. [km/mole]**	**Raman act. [$Å^4$/AMU]**
νCC	797 (791)	112	3
$\nu_s CO_2$	1289 (1295)	211	47
$\nu_{as} CO_2$	1739 (1737)	655	22
νCN	2115 (2203)	0	80
PBE0/aug-cc-pVT			
Vibrational mode	**Frequency [cm^{-1}]**	**IR int. [km/mole]**	**Raman act. [$Å^4$/AMU]**
νCC	803	127	1
$\nu_s CO_2$	1330	240	29
$\nu_{as} CO_2$	1782	680	14
νCN	2294	10	120
ωB97X-D/aug-cc-pVTZ			
Vibrational mode	**Frequency [cm^{-1}]**	**IR int. [km/mole]**	**Raman act. [$Å^4$/AMU]**
νCC	801	12	1
$\nu_s CO_2$	1335	260	28
$\nu_{as} CO_2$	1792	736	12
νCN	2312	7	108

In order to unambiguously assign the νCN, $\nu_{as}CO_2$ and ν_sCO_2 bands, and for NMR studies (see next section), ^{13}C-labelled analogues of tetraphenylphosphonium cyanide and tetraphenylphosphonium cyanoformate were prepared. According to Hooke's Law, the infrared energy required to induce a vibration between two atoms *decreases* with the mass of the atoms on either end of the bond. This relationship is approximated by a

formula derived from Hooke's Law, Equation 1, wherein ν-bar is the vibrational frequency, μ, the reduced mass of the system, k, the force constant (spring constant) of the bond and c, the speed of light.

$$\bar{\nu} = \frac{1}{2\pi c}\sqrt{\frac{k}{\mu}} \qquad [1]$$

Following the relationship shown in Equation 1, a sample of a ^{13}C-enriched cyanide salt, for example, will have a CN stretch lower than that of an unenriched sample, leading to a red-shift. This is illustrated nicely in the Raman spectrum collected for ^{13}C-enriched (~75%) tetraphenylphosphonium cyanide, $[PPh_4]^{13}CN$, shown in Figure 27.

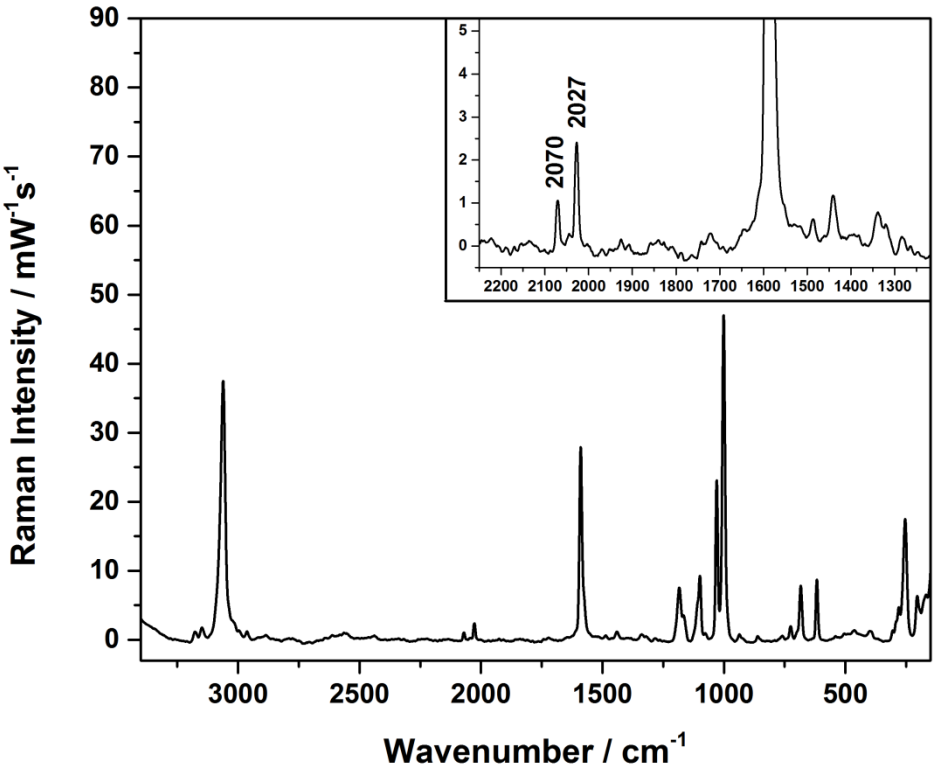

Figure 27: Raman spectrum of approximately 75% ^{13}C-enriched tetraphenylphosphonium cyanide.

The inset in Figure 27 clearly shows two absorptions for cyanide. The higher-energy band at 2070 cm^{-1} corresponds to unenriched cyanide, while the lower energy band (2027 cm^{-1}) belongs to the ^{13}C-enriched portion of the sample. The differing intensities are due to different relative concentrations of the ^{12}C- and ^{13}C-containing samples. Moving to the cyanoformate salt itself, samples were prepared wherein only the carboxyl fragment was ^{13}C-enriched or where both the cyano and carboxyl fragments were ^{13}C-enriched. Figure 28 shows the IR spectrum of the doubly-enriched sample, while Figure 29 shows the Raman spectrum of the same sample. It is important to note that cyanide enrichment was only ~50-60%, while the reactions were performed under an atmosphere of $^{13}CO_2$, leading to a fully ^{13}C-enriched carboxyl fragment.

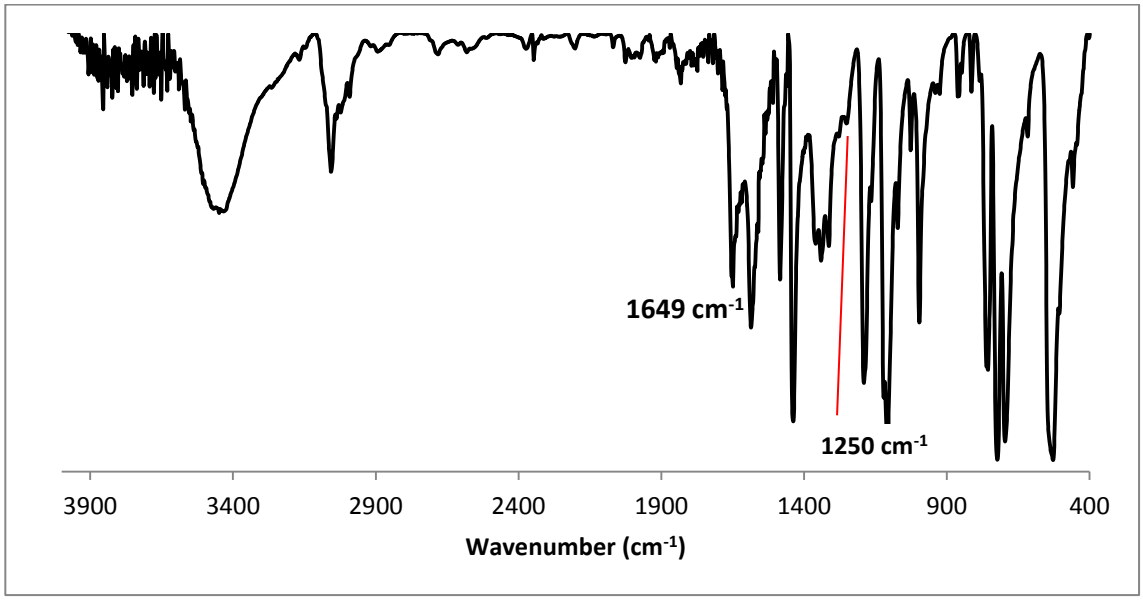

Figure 28: Infrared spectrum of doubly ^{13}C-enriched tetraphenylphosphonium cyanoformate, $[PPh_4][N^{13}C^{13}CO_2]$. Enrichment of ^{13}CN was approximately 60%, while $^{13}CO_2$ enrichment was approximately 100%.

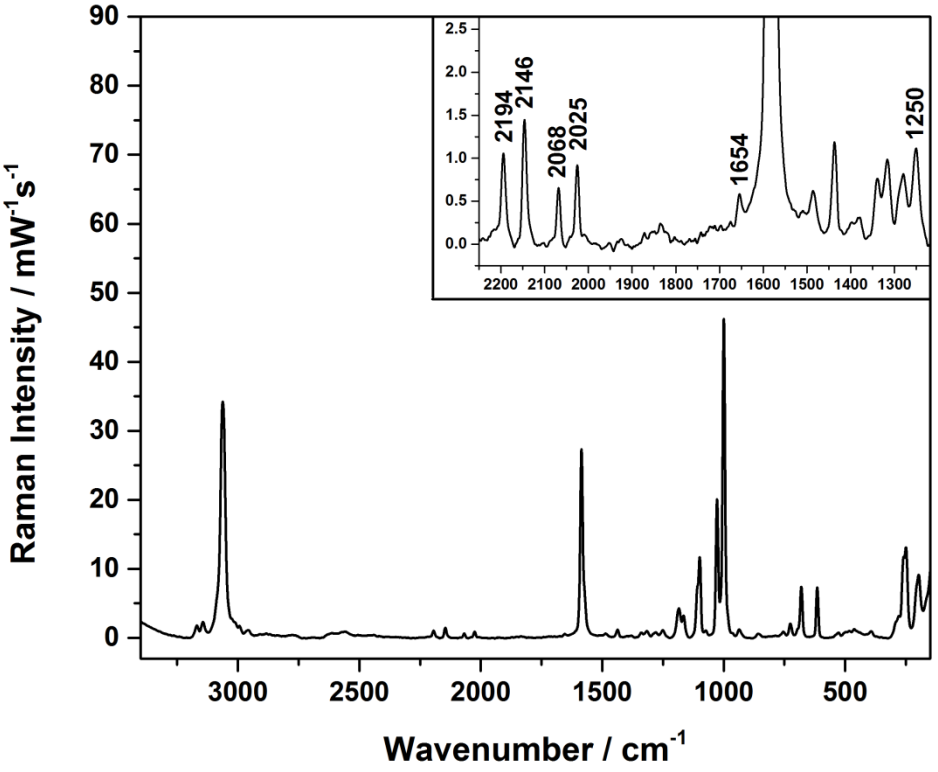

Figure 29: Raman spectrum of doubly ^{13}C-enriched tetraphenylphosphonium cyanoformate, $[PPh_4][N^{13}C^{13}CO_2]$. Enrichment of ^{13}CN was approximately 60%, while $^{13}CO_2$ enrichment was approximately 100%.

The IR spectrum of doubly enriched cyanoformate is of limited utility as νCN is very weak, essentially invisible. However, the $\nu_{as}CO_2$ and ν_sCO_2 peaks (1649cm^{-1} and 1250cm^{-1}, respectively) are both visible and are significantly red-shifted from the unenriched analogue, as expected from Hooke's law. The Raman spectrum of this sample is very informative, due to the presence of unreacted starting material, as well as unenriched portions of the cyanide and cyanoformate salts. The red-shifted weak $\nu_{as}CO_2$ and ν_sCO_2 stretches are also visible in this spectrum. In the cyano region of the spectrum four prominent peaks are visible (see the inset of Figure 29). The highest energy peak (2194cm^{-1}) corresponds to the partially enriched ion, $[NC^{13}CO_2]^-$; the peak at 2146cm^{-1}

on the other hand belongs to the doubly-enriched portion, $[N^{13}C^{13}CO_2]^-$. The lower energy bands, 2068 cm^{-1} and 2025 cm^{-1}, correspond to unreacted starting materials, $[PPh_4]CN$ and $[PPh_4]^{13}CN$, respectively. Similar results were observed in the IR and Raman spectra of a sample of singly ^{13}C-enriched tetraphenylphosphonium cyanoformate, $[PPh_4][NC^{13}CO_2]$. These spectra are shown in Figure 30 (IR) and Figure 31 (Raman).

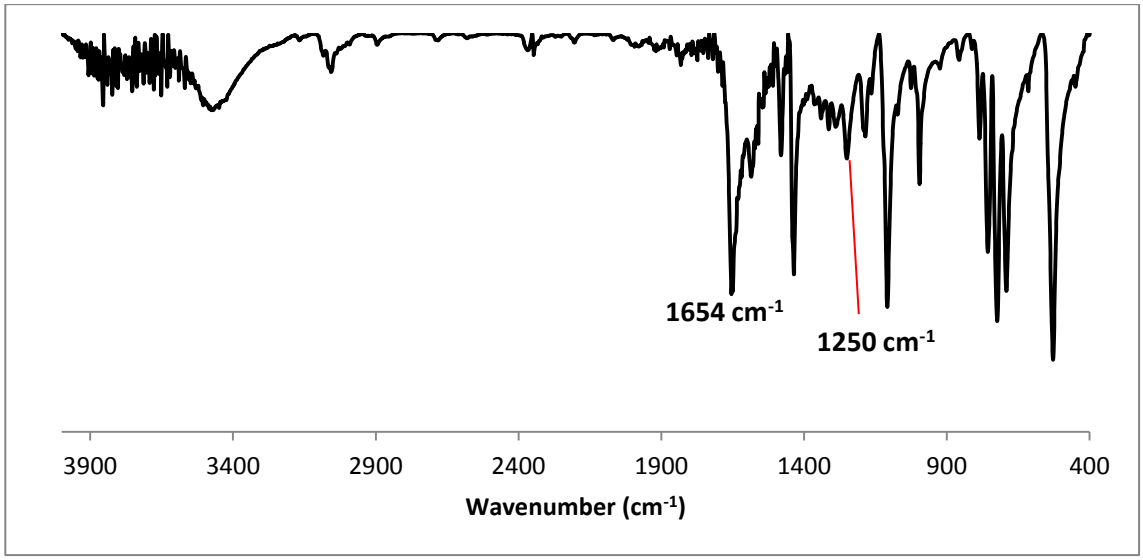

Figure 30: Infrared spectrum of singly ^{13}C-enriched tetraphenylphosphonium cyanoformate, $[PPh_4][NC^{13}CO_2]$. Enrichment of $^{13}CO_2$ was approximately 100%.

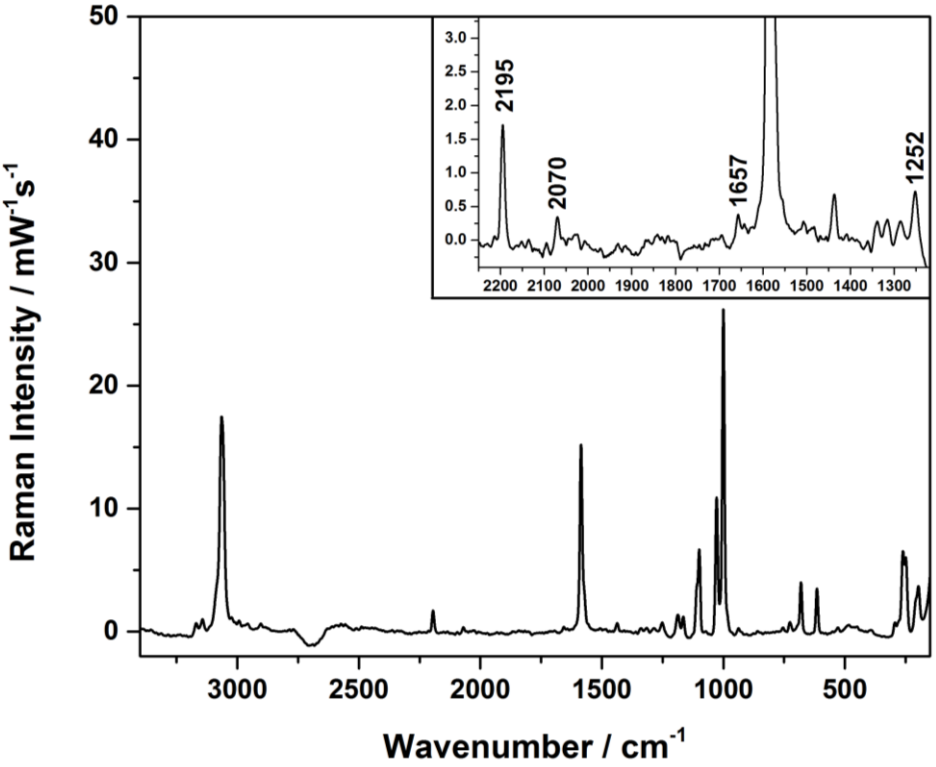

Figure 31: Raman spectrum of singly ^{13}C-enriched tetraphenylphosphonium cyanoformate, $[PPh_4][NC^{13}CO_2]$. Enrichment of $^{13}CO_2$ was approximately 100%.

Only the asymmetric and symmetric CO_2 stretches ($\nu_{as}CO_2$ and ν_sCO_2) of cyanoformate can be compared to the previously characterized fluorocarbonate ion. The frequencies obtained from the IR of $[Me_4N][FCO_2]$ were 1798cm^{-1} and 1275cm^{-1} for $\nu_{as}CO_2$ and ν_sCO_2, respectively.[126] The asymmetric stretch in particular deviates a great deal between the two ions, with the fluorocarbonate asymmetric C-O stretch being more in line with the theoretically predicted results found in Table 5. The authors explain their high $\nu_{as}CO_2$ (and low νCF) values as resulting from the wide O-C-O angle and weak C-F bond. Unfortunately, the spectroscopic data they supply is not for the crystallographically characterized fluorocarbonate salt found in the CSD; the IR of a different salt is reported. This is important to note as an O-C-O angle of 126.7° is found for the structure in the

CSD, while they report much larger calculated O-C-O angles, in the range of 136.6-137.3°, for the tetramethylammonium salt. Similarly, the calculated values for cyanoformate in Table 2 overestimate the O-C-O bond angle (133.0-133.5°), while the crystal structure reveals an angle of 125.4(12) °. It is not readily apparent what causes this discrepancy; it is possible that the packing in the hexamethylpiperidinium fluorocarbonate salt results in a smaller O-C-O angle, while the smaller cation in tetramethylammonium fluorocarbonate may allow a wider angle. Packing effects would not be present in the gas phase, which could explain the wide calculated O-C-O angles. Inclusion of solvation in the measurement of O-C-O bond angles was observed in one study to lead to narrower angles in comparison to the same structure in a vacuum,[266] so it may be expected that this effect will be even more pronounced in the solid state.

Overall, despite the discrepancy between the calculated and experimental frequencies, the vibrational spectroscopic data is in complete agreement with the formulation of the obtained product as tetraphenylphosphonium cyanoformate, generated through the formation of a carbon-carbon bond between carbon dioxide and cyanide. Table 6 summarizes the most relevant results of this section.

Table 6: Relevant IR and Raman data for ^{13}C-enriched and unenriched samples of tetraphenylphosphonium cyanide and tetraphenylphosphonium cyanoformate. Literature data for fluorocarbonate are also included.

Sample	$\nu_{as}CO_2$ (cm^{-1})	$\nu_s CO_2$ (cm^{-1})	νCN* (cm^{-1})
$[PPh_4]CN$	-	-	2068
$[PPh_4]^{13}CN$	-	-	2027
$[PPh_4][NCCO_2]$	1697	1266	2196
$[PPh_4][N^{13}C^{13}CO_2]$	1649	1250	2146
$[PPh_4][NC^{13}CO_2]$	1654	1250	2195
$[Me_4N][FCO_2]$[126]	1798	1275	-
$[Me_4N][F^{13}CO_2]$[126]	1748	1261	-
*νCN stretches were taken from Raman spectra, all other data were taken from IR spectra.			

4.4 Solid-State ^{13}C NMR Spectroscopy

To further characterize the prepared salt and confirm its structure as tetraphenylphosphonium cyanoformate, NMR studies were completed. All NMR spectra were collected and processed by Dr. Ulrike Werner-Zwanziger at Dalhousie University.

The cyanoformate salt was found to be insoluble in all conventional solvents (except dichloromethane with which it reacted rapidly, see Section 4.5), thus, solution state NMR could not be obtained. Instead, samples of isotopically-labelled cyanoformate were prepared for solid-state cross-polarization magic-angle spinning ^{13}C NMR studies (CP/MAS ^{13}C NMR). The technique does not typically allow for the collection of useful ^{1}H NMR spectra, however, this was not a significant issue as there were no protons in the anion. The cation of course does contain protons, but the other data obtained (crystal structure, vibrational spectroscopy) was enough to safely confirm its structure as $[PPh_4]^+$. All peaks found in the ^{13}C CP/MAS NMR spectra in this section have been confirmed experimentally to resonate at their isotropic chemical shift.

Figure 32 shows ^{13}C NMR spectra for (A) tetraethylammonium cyanide, (B) tetraphenylphosphonium cyanide (~50% ^{13}CN enriched), (C) tetraphenylphosphonium cyanoformate (~100% $^{13}CO_2$ enriched), and tetraphenylphosphonium cyanoformate (~50% ^{13}CN and ~100% $^{13}CO_2$ enriched) at 9.4 T (D) and 16.4 T (E) magnetic field strengths.

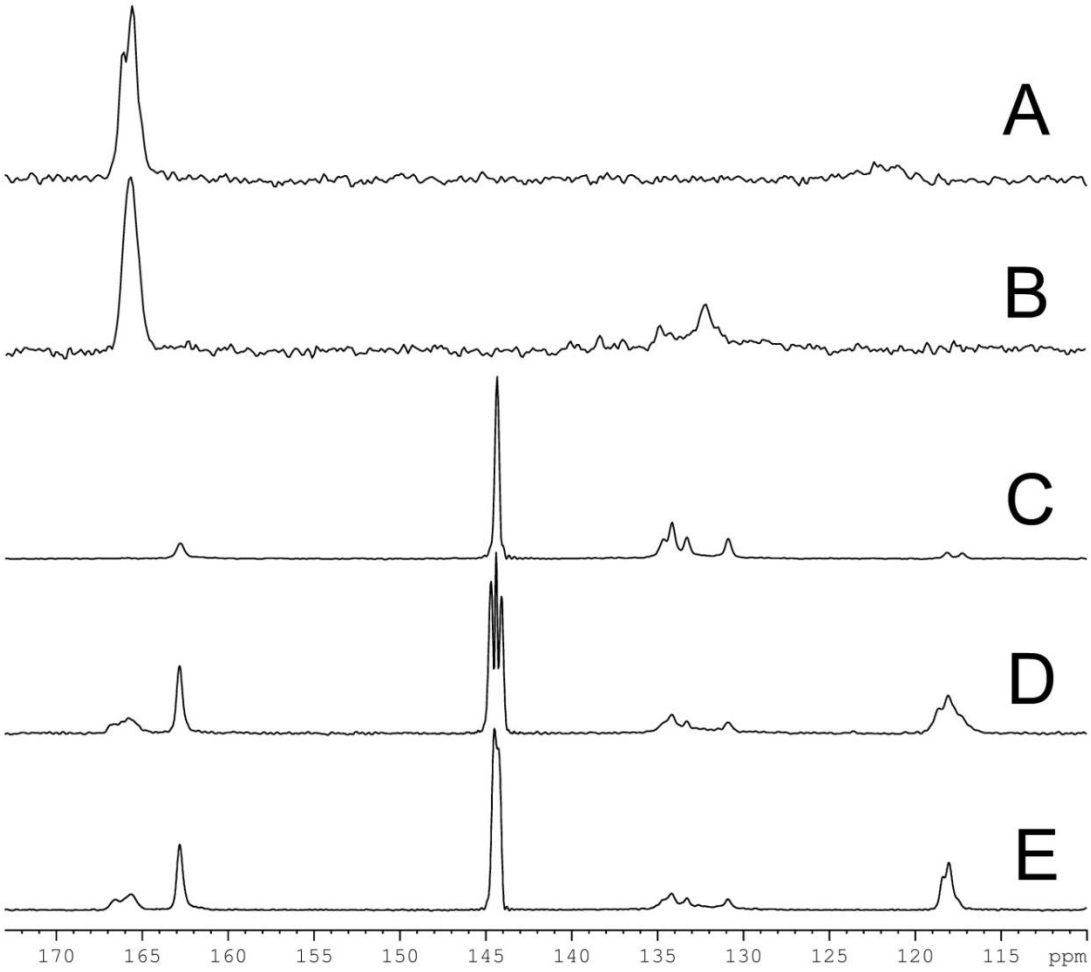

Figure 32: ^{13}C CP/MAS NMR spectra of (A) tetraethylammonium cyanide, $[Et_4N]CN$, (B) ^{13}CN enriched (~50%) tetraphenylphosphonium cyanide, $[PPh_4]^{13}CN$ and (C-E) tetraphenylphosphonium cyanoformate, $[PPh_4][NCCO_2]$. Specifically shown are in (C) $[PPh_4][N^{12}C^{13}CO_2]$, $^{13}CO_2$ (~100%), (D and E) $[PPh_4][N^{13}C^{13}CO_2]$, $^{13}CO_2$ (~100%) and ^{13}CN (~50%) enriched at 9.4 T (D) and 16.4 T (E) field strengths.

The spectrum of commercial tetraethylammonium cyanide (Figure 32A) was collected, in addition to those of the tetraphenylphosphonium cyanide and cyanoformate salts, in order to confirm the position of the cyanide carbon signal of the starting material, which, in the case of $[Et_4N]CN$, appears at 165.6 ppm. Figure 32B shows the ^{13}C CP/MAS NMR spectrum for tetraphenylphosphonium cyanide. This sample is partially (~50%) enriched with ^{13}CN to enhance the signal of the cyanide carbon, which is the most intense signal in the spectrum, appearing at 165.8 ppm. This is consistent (within 0.2 ppm) of that observed for $[Et_4N]CN$. The signals centred at 132.3 ppm and 128.8 ppm were assigned to the aromatic carbon atoms of the cation.

The ^{13}C CP/MAS NMR spectrum of a sample of tetraphenylphosphonium cyanoformate, prepared from $^{13}CO_2$, is shown in Figure 32C. A dominating single line at 144.4 ppm in this spectrum corresponds to the carbonyl carbon of the $^{13}CO_2$-enriched cyanoformate. Its shift is consistent with that of the fluorocarbonate anion reported previously, ca. 142 ppm.[126] Tetraphenylphosphonium cyanoformate, with a doubly ^{13}C-labelled anion, was prepared and its ^{13}C solid state NMR spectra measured at 9.4 T and 16.4 T magnetic field strengths. The resultant spectra are shown in Figure 32D and Figure 32E, respectively.

The apparent triplet of the carbonyl carbon centred at 144.4 ppm actually results from the overlap of a doublet with J-coupling of 61(±4) Hz and a singlet. Since the cyano portion of the anion was only partially enriched (~50%), the signal for the neighbouring carbon (carbonyl) is split in this fashion, with the singlet for the $[N^{12}C^{13}CO_2]^-$ ion and the doublet for the $[N^{13}C^{13}CO_2]^-$ ion. The apparent triplet is not resolved in the spectrum acquired in the higher magnetic field but its apparent narrowing when plotted on the

chemical shift scale (Figure 32E) and similar width, when plotted on a frequency scale (not shown) confirms the origin of the J-coupling.

The peaks around 165.8 ppm stem from unreacted starting material, while the peak centered around 162.3 ppm can be attributed to a bicarbonate impurity. This value correlates well to those of other bicarbonate salts reported in the literature.[267] This impurity will be discussed in Section 4.5. The signals in the range of 128.8-132.3 ppm correspond to the carbons of the aromatic rings of the cation and, finally, the broad signal at 118.1 ppm can be attributed to the cyano carbon of the anion.

The latter signal was troubling as the cyano group of acetonitrile (the solvent used for the reaction) should appear at almost exactly the same chemical shift. The ^{13}C CP/MAS NMR spectrum acquired at 16.4 T (Figure 32E) confirms that the signal at 118.1 ppm is J-coupled to the enriched carbonyl, since the peak narrows when displayed on the chemical shift scale. Also supporting the assignment of this signal to the cyano group and not acetonitrile is the fact that the corresponding methyl signal for acetonitrile, which would normally appear at approximately 1.4 ppm, is not observed. Furthermore, the infrared spectrum for $[PPh_4][N^{13}C^{13}CO_2]$ (Figure 28) lacks the characteristic absorption bands for acetonitrile, which appear at 2293 cm^{-1} (CCN bend) and 2253 cm^{-1} (CN stretch). Finally, the larger intensity of the peak at 118.1 ppm, relative to the cation peaks, support the notion that it belongs to a ^{13}C-enriched fragment, not acetonitrile, which would be at natural abundance.

All peak assignments are summarized in Table 7. Full individual spectra, including peak labels, for $[Et_4N]CN$, $[PPh_4]^{13}CN$ and $[PPh_4][N^{13}C^{13}CO_2]$ can be found in

Figures 33, 34 and 35, respectively. In these spectra all unlabeled peaks have been experimentally determined to be spinning side-bands.

Table 7: Summary of ^{13}C CP/MAS NMR data collected for tetraethylammonium cyanide, tetraphenylphosphonium cyanide and tetraphenylphosphonium cyanoformate.

Chemical Shift(s) (ppm)	**Assignment**
$[Et_4N]CN$	
166.1, 165.6	$\underline{C}N^-$
54.0, 52.8, 51.5	$[\underline{N}(\underline{C}H_2CH_3)_4]^+$
11.1, 10.1, 9.1, 6.5	$[N(CH_2\underline{C}H_3)_4]^+$
$[PPh_4]CN$ (~50% ^{13}CN-enriched)	
128.8, 132.3	$[P(\underline{C}_6H_5)_4]^+$
165.8	$\underline{C}N^-$
$[PPh_4][NCCO_2]$ (~50% ^{13}CN, ~100% $^{13}CO_2$-enriched)	
165.8	$\underline{C}N^-$
162.8	$H\underline{C}O_3^-$
144.6, 144.4, 144.0	$[NC\underline{C}O_2]^-$
134.2, 133.3, 130.9	$[P(\underline{C}_6H_5)_4]^+$
118.1	$[N\underline{C}CO_2]^-$

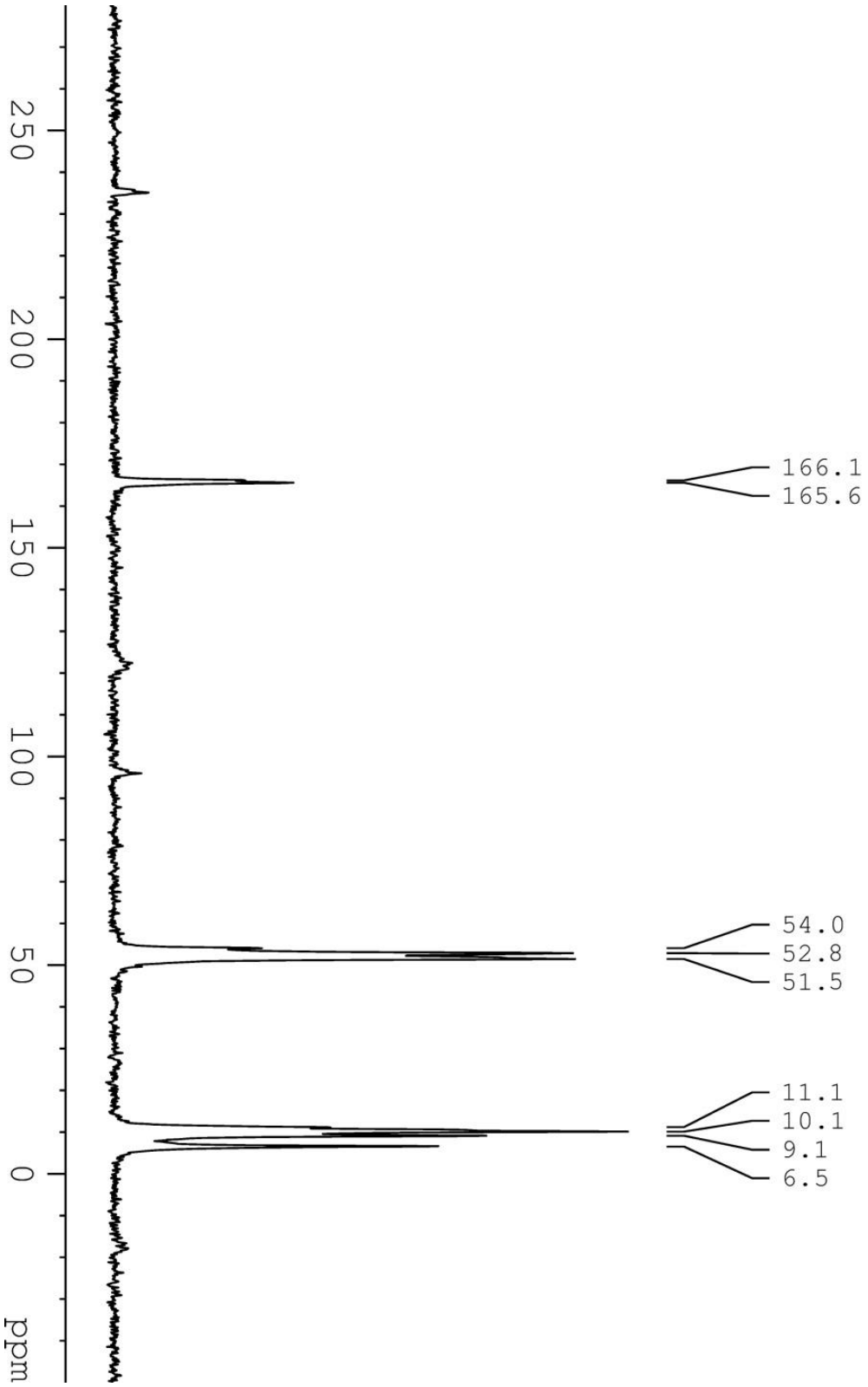

Figure 33: ^{13}C CP/MAS NMR spectrum for tetraethylammonium cyanide, $[Et_4N]CN$.

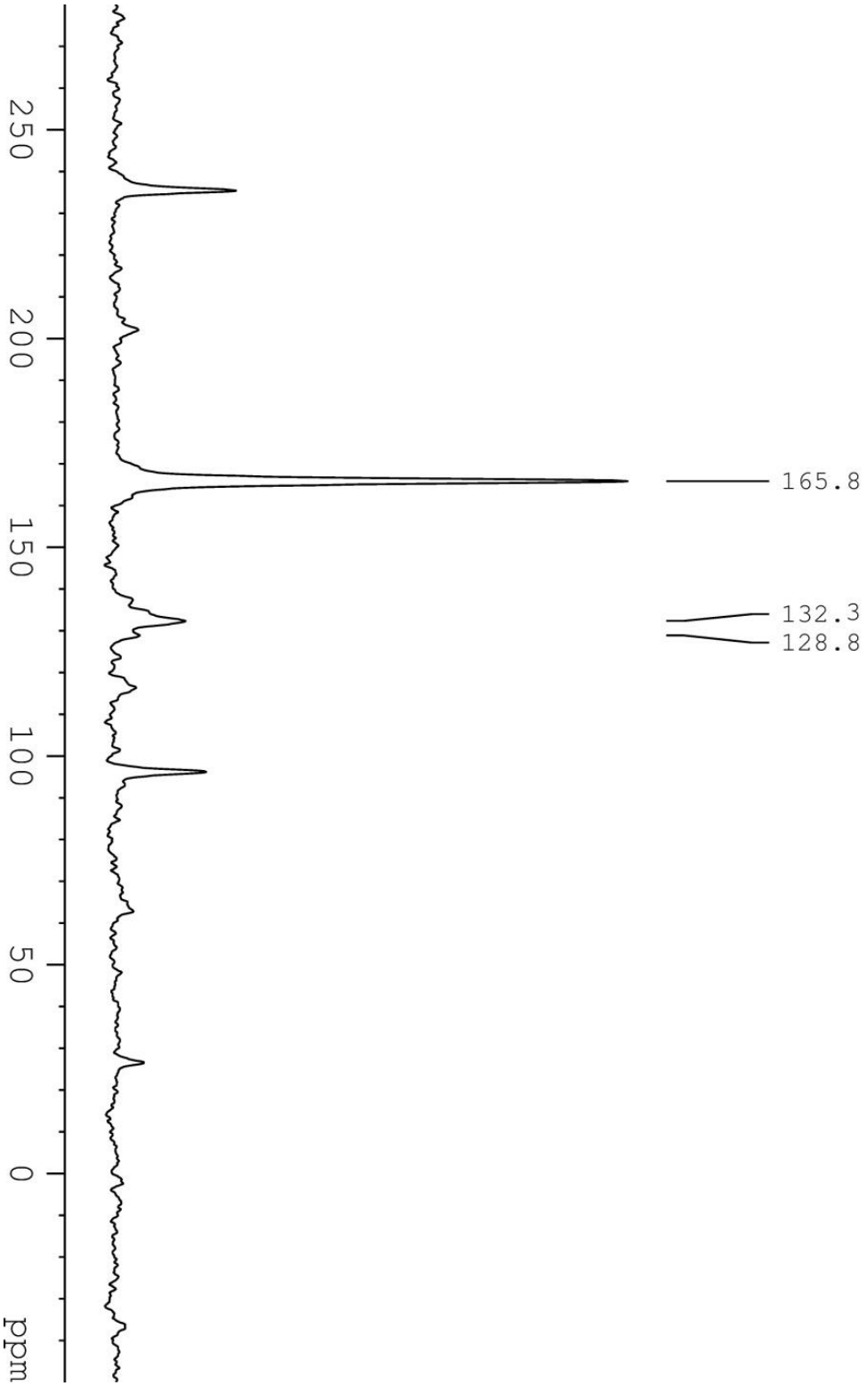

Figure 34: ^{13}C CP/MAS NMR spectrum for ^{13}CN enriched (~50%) tetraphenylphosphonium cyanide, $[PPh_4]^{13}CN$.

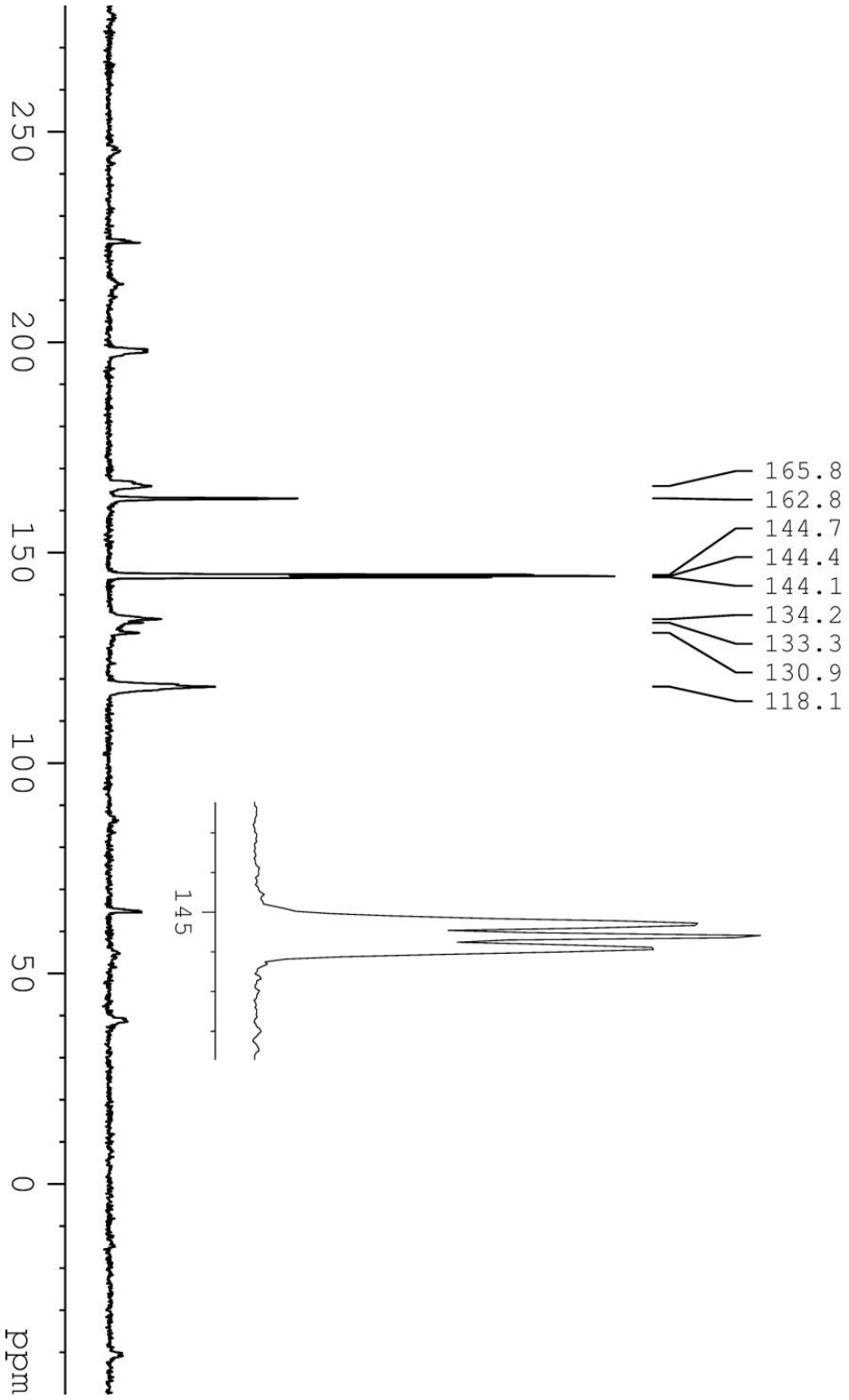

Figure 35: ^{13}C CP/MAS NMR spectrum for $^{13}CO_2$ (~100%) and ^{13}CN (~50%) enriched tetraphenylphosphonium cyanoformate, $[PPh_4][N^{13}C^{13}CO_2]$.

4.5 Stability in Solution and Thermal Stability

$[PPh_4][NCCO_2]$ was found to be insoluble in all but one of the conventional solvents tried, including acetonitrile, benzene, chlorobenzene, diethyl ether, hexane, toluene and water. The salt was soluble in dichloromethane, however, it was observed to subsequently undergo rapid decomposition. Although the product of decomposition could not be conclusively characterized (giving a brown tar-like substance), it is speculated that the cyanoformate ion decarboxylates to give cyanide ion, which then attacks the carbon center of dichloromethane to displace chloride. Nucleophilic displacement of chloride by cyanide has precedence in the literature.[268]

In order to investigate the stability of cyanoformate in solution, a precursor cyanide solution that was sufficiently stable and miscible with the other solvents to be studied was essential. After some investigation, a solution of tetrabutylammonium cyanide, $[Bu_4N]CN$, dissolved in an ionic liquid (IL), trihexyl(tetradecyl)phosphonium bis(trifluoromethylsulfonyl)imide, $[P_{66614}][TFSI]$, was found to be suitable. A stock solution of 3.4 g $[Bu_4N]CN$ was prepared in 47 mL of the IL and then diluted in the chosen solvent for each measurement. The stock solution was stored under a nitrogen atmosphere and CO_2 was bubbled into each aliquot for 10 minutes at ambient temperature and pressure prior to analysis. The IL was dried by diluting it with toluene to reduce the viscosity. Toluene and water were then removed by rotary evaporation and the isolated IL was dried under high-vacuum at 50-60 °C for several hours prior to use. Tetrabutylammonium cyanide was also dried *in vacuo* for several hours prior to use and both IL and reagent were stored under nitrogen.

The presence of cyanide and/or cyanoformate in the stock IL solution was confirmed using FTIR and Raman spectroscopy. In the Raman spectrum, a peak at 2051 cm^{-1}, corresponding to νCN, was observed for the cyanide containing solution. For the same solution saturated with CO_2, the peaks observed at 2051 cm^{-1} and 2193 cm^{-1} correspond to νCN of cyanide and cyanoformate, respectively. An overlay of these two spectra is shown in Figure 36. The symmetric CN stretch of the cyanoformate ion is not observed in the FTIR, consistent with the same peak in the spectrum of the tetraphenylphosphonium salt. The weak absorption of νCN of the cyanide in the IR and the relatively low concentration of cyanide in the solution meant that this peak was not observed either. However, $\nu_{as}CO_2$ of cyanoformate was plainly visible, appearing at 1689 cm^{-1} in the IL solution, and it is this absorbance that was monitored throughout each kinetic study.

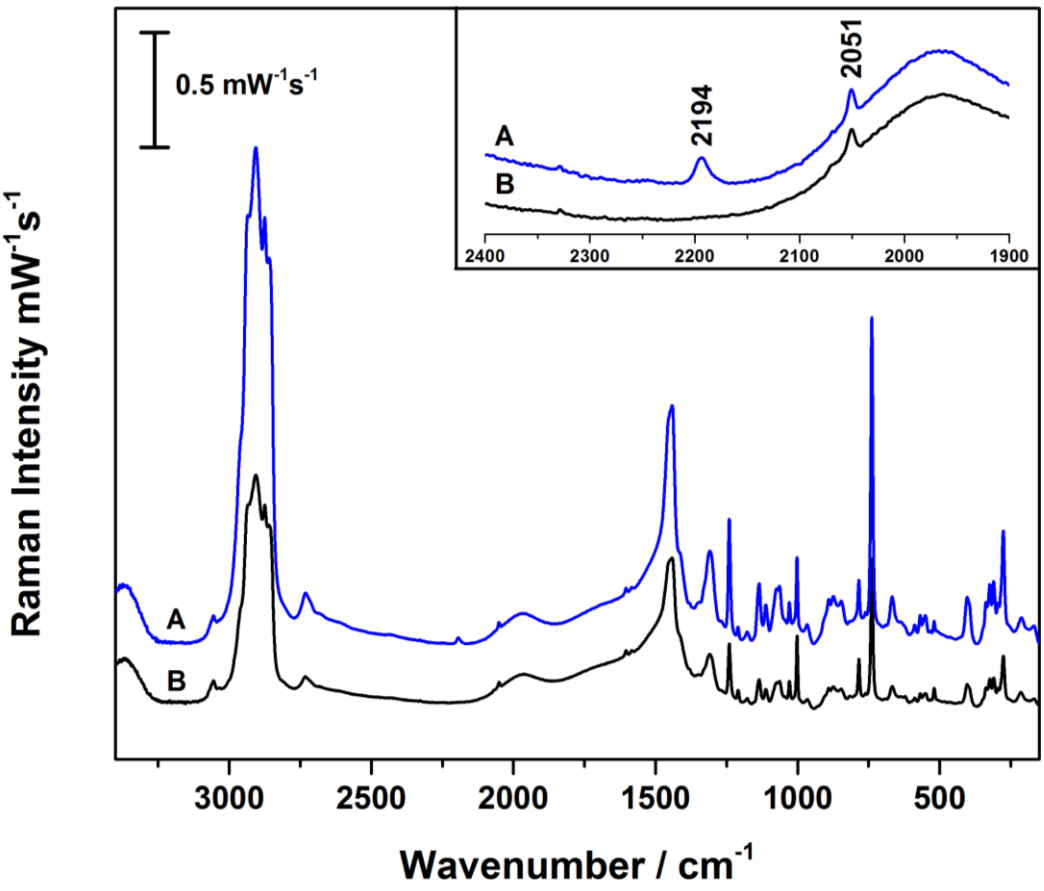

Figure 36: Overlay of the Raman spectra of a solution of $[Bu_4N]CN$ in $[P_{66614}][TFSI]$ (A) with and (B) without added CO_2. The appearance of νCN at 2194 cm^{-1} in A indicates the presence of cyanoformate.

The solvent to be studied (9 mL of toluene, acetonitrile or THF) was added to a 50 mL Mettler-Toledo EasyMax glass reactor vessel. The reactor was then continuously purged with argon as the ReactIR probe and EasyMax stirrer were connected to the system. The reactor was stoppered and kept under argon for the duration of the measurements. 1 mL of the $[Bu_4N]CN$ solution, saturated with CO_2, was quickly added to the reactor *via* syringe, to give a 10% IL solution by volume in the studied solvent. The solution was stirred initially to ensure adequate mixing, but during data collection the

stirrer was turned off. The solid state value of $\nu_{as}CO_2$ (1697 cm^{-1}) was observed to shift depending on the solvent used; in toluene $\nu_{as}CO_2$ = 1689 cm^{-1}, in THF $\nu_{as}CO_2$ = 1686 cm^{-1}, and in acetonitrile $\nu_{as}CO_2$ = 1697 cm^{-1}. Rates of decomposition were measured as a function of the $\nu_{as}CO_2$ peak height versus time. These results are plotted in Figures 37, 39 and 41, for toluene, acetonitrile and THF, respectively.

Peak heights were determined from the difference between the peak maximum and an appropriately chosen baseline position nearby. Peak heights in each experiment were adjusted by subtracting the minimum peak height from all measured values to facilitate the calculation of half-lives. This adjustment does not affect the calculated rate, but is necessary in order to obtain a linear plot passing through the origin for fitting of the equation shown below.

$$\ln\left(\frac{P}{P_0}\right) = -\left(\frac{\ln 2}{T_{1/2}}\right)t$$

Half-lives were determined by plotting $\ln(P/P_0)$, the ratio of peak height (P) to initial peak height (P_0), versus time (t). Linear plots were obtained, as shown in Figures 38, 40 and 42. Linear regression, fixing the y-intercept at the origin to obtain a relationship equivalent to that of Equation 1, allowed calculation of the half-life, $T_{1/2}$, of the cyanoformate ion in each solvent. Only data from t = 0 to the time corresponding to 10 % of the initial peak height remaining were included in the regression analyses. Half-lives of 110 minutes, 55 minutes and 17 minutes were obtained for toluene, tetrahydrofuran and acetonitrile, respectively. Table 8 summarizes the results obtained,

including the calculated half-life of cyanoformate in each of the solvents studied as well as the dielectric constant of the solvent. It is important to note that the dielectric constant of the reaction mixtures (i.e. 90% ionic liquid, 10% organic solvent) should be slightly different from those of the pure solvents; the general trends observed hold despite this slight difference.

Table 8: Experimentally determined half-lives of cyanoformate ion in toluene, tetrahydrofuran and acetonitrile and dielectric constants and polarity indices for each solvent studied.

Solvent	Half-life of Cyanoformate (min)	Dielectric Constant (ε) of Pure Solvent[269]
Toluene	110	2.4
Tetrahydrofuran	55	7.6
Acetonitrile	17	37.5

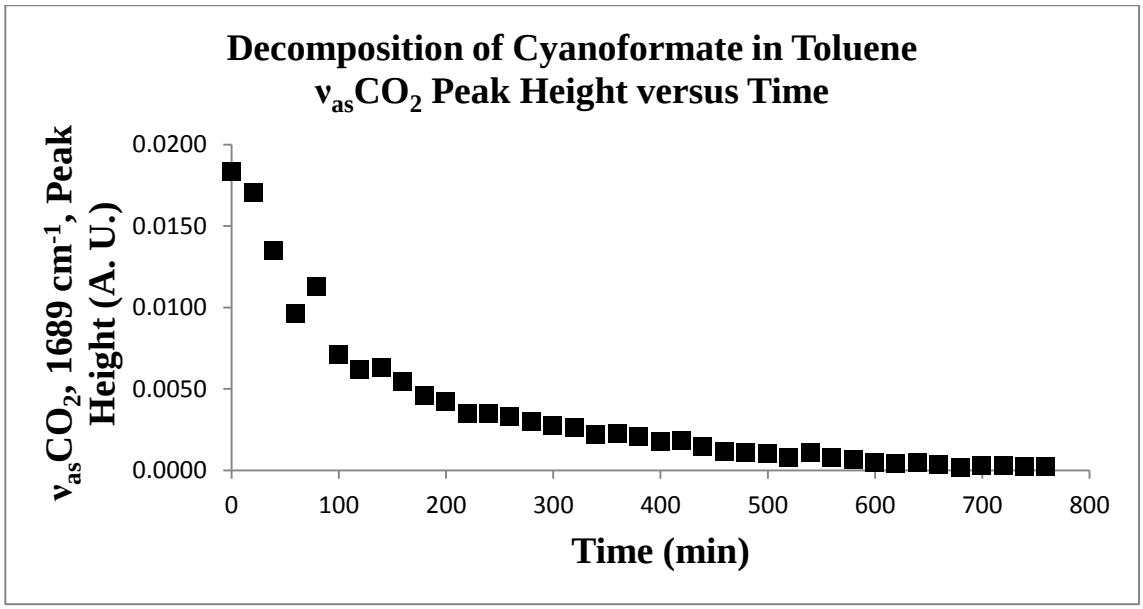

Figure 37: Decomposition plot of an IL solution of cyanoformate diluted in toluene as a function of the $\nu_{as}CO_2$ peak height (1689 cm^{-1} in toluene).

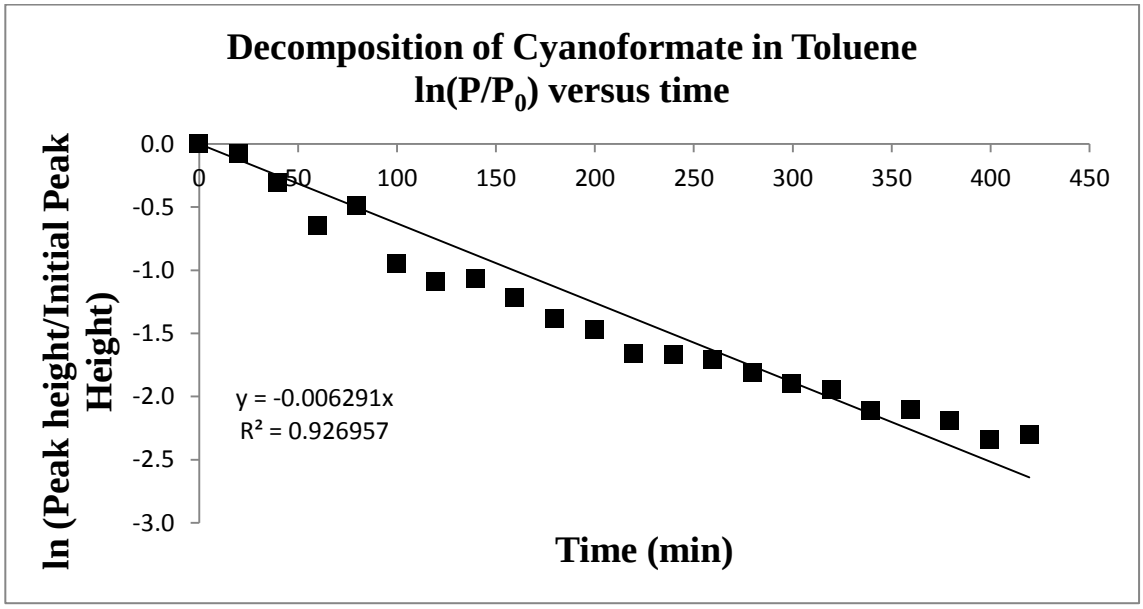

Figure 38: Decomposition plot of cyanoformate in toluene. Only data up to a remaining peak height of 10% of the initial peak height were included in the regression analysis.

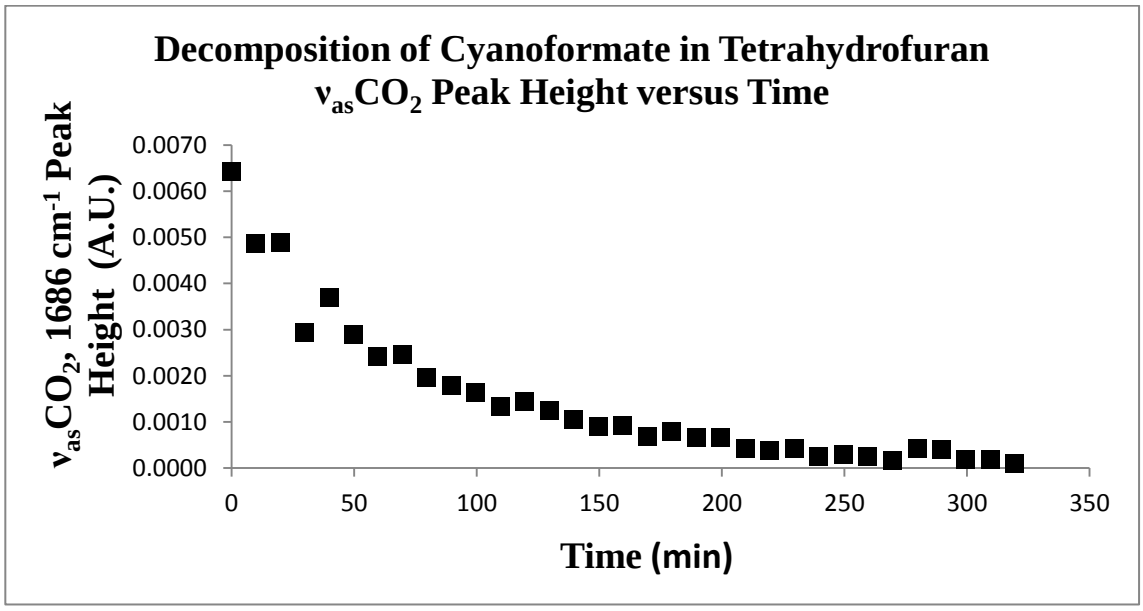

Figure 39: Decomposition plot of an IL solution of cyanoformate diluted in THF as a function of the $\nu_{as}CO_2$ peak height (1686 cm^{-1} in THF).

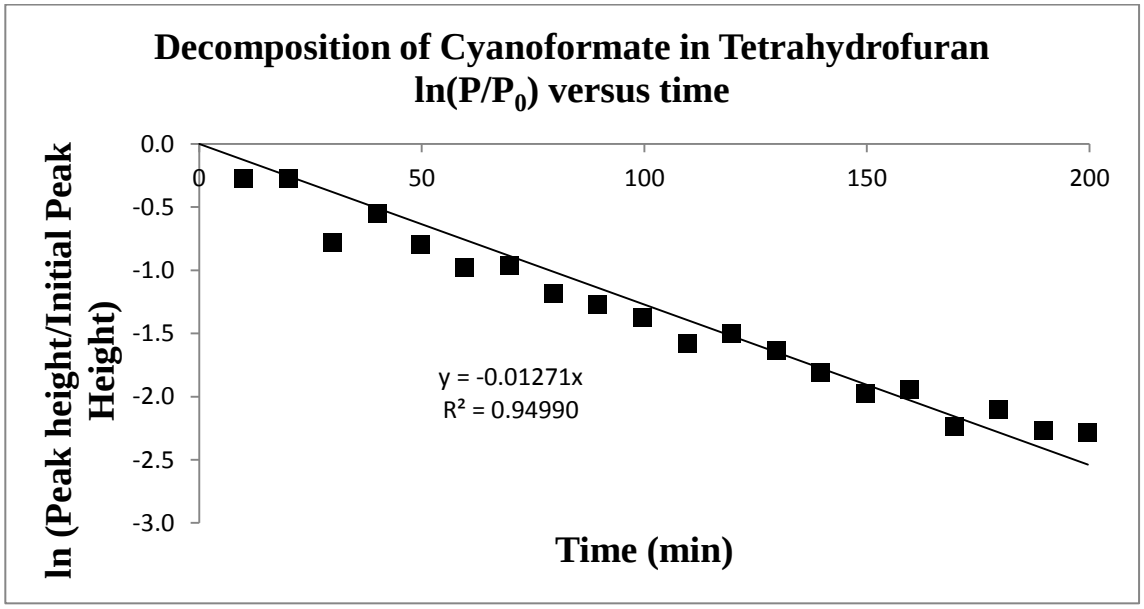

Figure 40: Decomposition plot of cyanoformate in THF. Only data up to a remaining peak height of 10% of the initial peak height were included in the regression analysis.

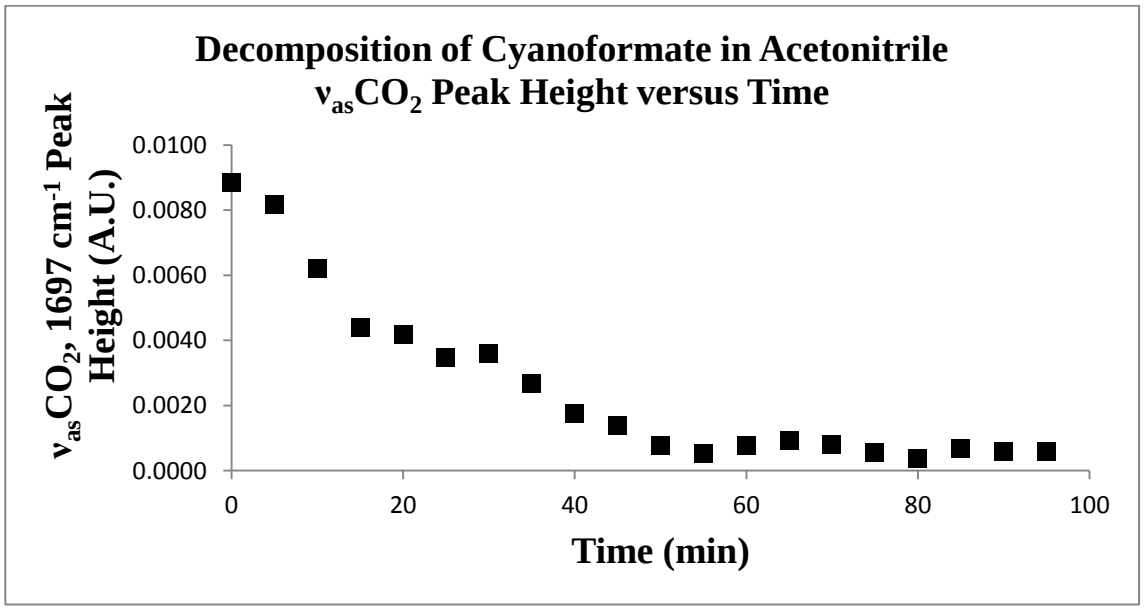

Figure 41: Decomposition plot of an IL solution of cyanoformate diluted in acetonitrile as a function of the $\nu_{as}CO_2$ peak height (1697 cm^{-1} in acetonitrile).

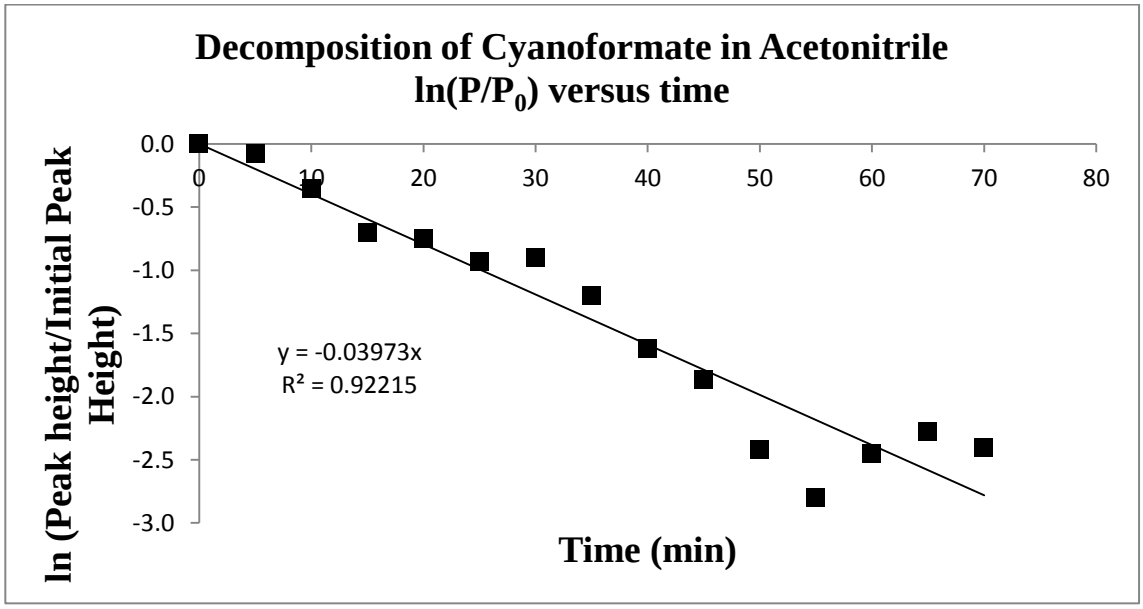

Figure 42: Decomposition plot of cyanoformate in acetonitrile. Only data up to a remaining peak height of 10% of the initial peak height was included in the regression analysis.

Based on the *in situ* IR data collected, it is clear that the cyanoformate ion is markedly more stable in the IL/toluene mixture than in the IL/THF mixture and especially in the IL/acetonitrile mixture. Dissociation of cyanoformate to thermodynamically stable CO_2 and to cyanide can be expected to be promoted in polar solvents due to their enhanced ability to solvate the small cyanide ion. While acetonitrile is the only polar solvent studied thus far, it is expected that a similar result would be obtained for other polar solvents (e.g. DMSO or DMF). Acetonitrile was chosen due to the few absorbances present in its IR spectrum, their location in regions of low interference, as well as the low expected reactivity of acetonitrile with cyanide or cyanoformate, and the absence of acidic protons. The use of acetone, for example, was undesirable because of the large carbonyl stretching frequency in the IR which would undoubtedly interfere with that of

cyanoformate. Furthermore, it was also anticipated that the produced cyanide ion would react with the electrophilic carbonyl-carbon atom of acetone.

Dielectric constants of the active sites of enzymes have been determined to be quite low, one study provides values of ε = 2-3.[120] While the dielectric constant of the active site of ACC oxidase has not been specifically reported, it is reasonable to assume that it should not be markedly different from other enzymes. Therefore, based on the measured stability of cyanoformate in the low dielectric IL/toluene solution, cyanoformate would be expected to be stable at the active site of the enzyme. After it is produced, cyanoformate can then be 'shuttled' away from the active site, to the much higher dielectric cytosol, where the complex will be far less stable, and will undergo dissociation to produce CO_2 and cyanide.

To obtain computational solution state data to bolster the experimental results obtained from the *in situ* IR study, the thermodynamics of the reaction generating cyanoformate were re-evaluated in the presence of a number of different solvents (water, acetonitrile, methanol, THF and toluene) at the PBE0/aug-cc-pVTZ and ωB97X-D/aug-cc-pVTZ levels of theory. The data obtained is shown in Table 9. The dielectric constants used for each solvent were; H_2O, ε = 78.3553; MeCN, ε = 35.688; MeOH, ε = 32.613; THF, ε = 7.4257 and PhMe, ε = 2.3741.

Table 9: DFT level thermochemical data [kJ mol^{-1}] for the reaction $CO_2 + CN^- \rightarrow [NCCO_2]^-$ in the presence of a solvent field (H_2O, MeCN, MeOH, THF and PhMe).

PBE0/aug-cc-pVTZ	**H_2O**	**MeCN**	**MeOH**	**THF**	**PhMe**
$\Delta_a H°$	11.3	10.5	10.4	5.0	-9.1
$\Delta_a G°$	42.9	42.1	43.7	36.6	21.9
$\Delta_r H°$	-39.5	-40.3	-40.4	-46.0	-61.3
$\Delta_r G°$	-1.2	-2.1	-2.2	-7.8	-23.1
ωB97X-D/aug-cc-pVTZ	**H_2O**	**MeCN**	**MeOH**	**THF**	**PhMe**
$\Delta_a H°$	22.2	21.3	21.2	15.4	-0.2
$\Delta_a G°$	54.6	53.7	53.6	47.9	31.8
$\Delta_r H°$	-21.7	-22.5	-22.6	-28.1	-43.3
$\Delta_r G°$	16.6	15.8	15.6	10.1	-5.1

The acquired data suggests that $[NCCO_2]^-$ is thermodynamically stable with respect to fragmentation in toluene ($\Delta_r G°$ = -23.1 and -5.1 kJ mol^{-1} at the PBE0 and ωB97X-D levels, respectively). However, in medium (tetrahydrofuran) and high dielectric solvents (water, acetonitrile and methanol) the anion becomes thermodynamically unstable. It should also be noted that the calculated enthalpy change, $\Delta_r H°$, is negative irrespective of solvent.

The inclusion of solvent effects using a polarizable continuum model introduces notable changes to the energy profile of the reaction between CO_2 and cyanide in the gas-phase (see Table 3 for data *in vacuo*). First, even though an ion-dipole complex can be located on the potential energy surface, its Gibbs energy is always higher than that of free CN^- and CO_2. This is due to favourable solvent-solute interactions that significantly outweigh any ion-dipole interaction between CN^- and CO_2. Second, the calculated activation energy, $\Delta_a G°$, is now distinctly positive and depends strongly on the dielectric constant of the solvent, as suggested by the experimental study. $\Delta_a G°$ is 31.8 and 47.9 kJ

mol^{-1} for toluene and tetrahydrofuran, respectively, and roughly 54 kJ mol^{-1} for the other solvents studied (water, acetonitrile and methanol) at the ωB97X-D/aug-cc-pVTZ level of theory. Third, as already noted above, the reaction Gibbs energy, $\Delta_r G°$, is negative only when toluene is used as the solvent; the cyanoformate anion is calculated to be thermodynamically unstable in all the other solvents investigated. However, the anion is *kinetically* stabilized in all media as breaking the C-C bond has an activation energy of approximately 40 kJ mol^{-1} at the ωB97X-D/aug-cc-pVTZ level of theory. The calculated reaction profiles for the formation of cyanoformate from cyanide and carbon dioxide in water, acetonitrile, THF, toluene and *in vacuo* are represented graphically in Figure 43.

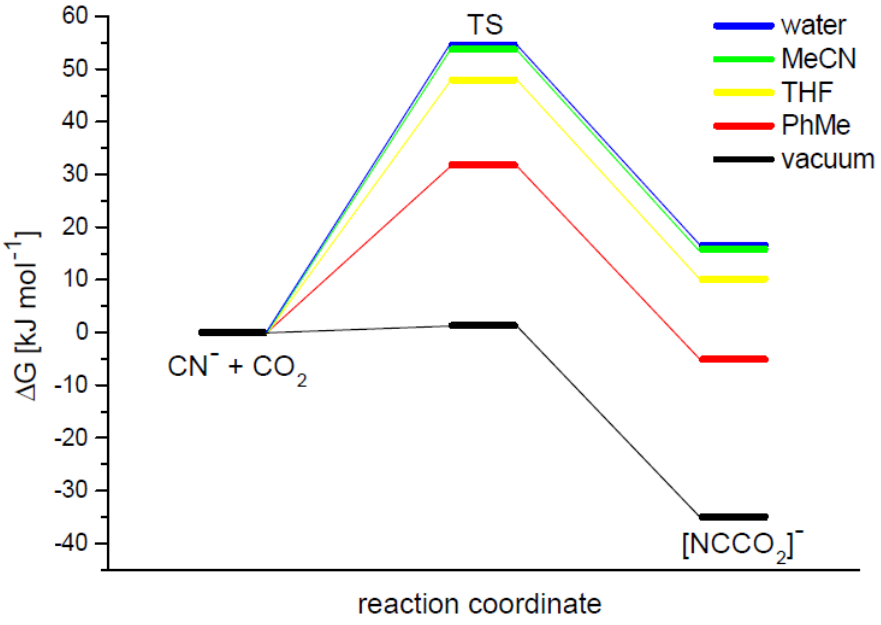

Figure 43: Calculated reaction profile for the formation of $[NCCO_2]^-$ from CN^- and CO_2 at ωB97X-D/aug-cc-pVTZ level of theory with different solvent models.

Our experimental work has clearly shown that cyanoformate is relatively easily converted to bicarbonate (and HCN) in the presence of water. In our early attempts to

isolate the cyanoformate salt, crystals of tetraphenylphosphonium bicarbonate were often obtained instead. The crystal structure and a packing diagram of tetraphenylphosphonium bicarbonate hydrate are shown in Figures 44 and 45, respectively. The salt was only confirmed crystallographically (though multiple times) and no additional effort, other than through infrared spectroscopy, were made to further characterize it.

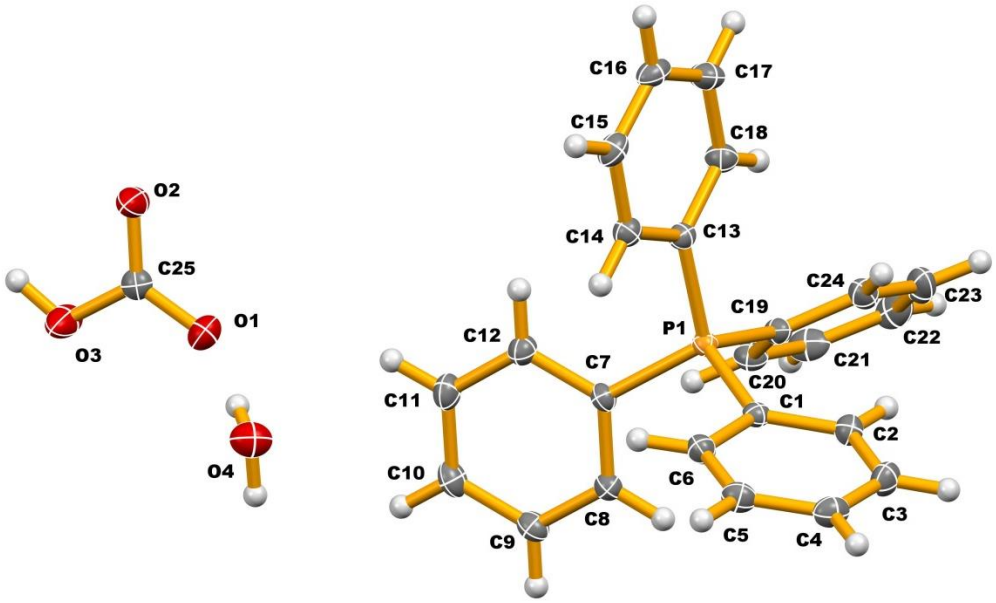

Figure 44: Structural diagram of $[PPh_4][HCO_3]\cdot H_2O$. Ellipsoids are drawn at the 50% probability level.

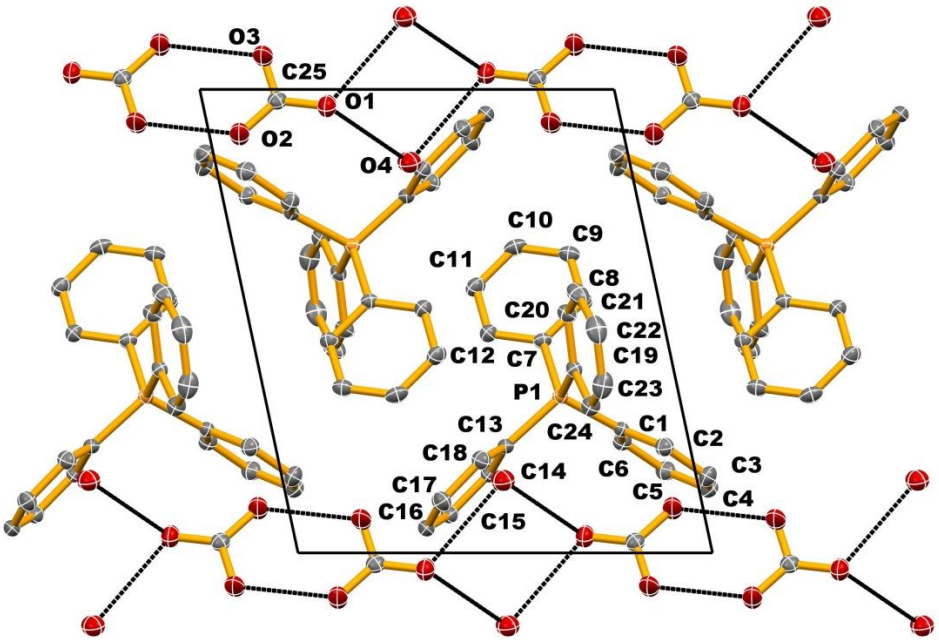

Figure 45: Packing diagram of $[PPh_4][NCCO_2]\cdot H_2O$ viewed down the *x* axis. Ellipsoids are drawn at the 50% probability level. Hydrogen atoms have been removed for clarity. Crystallographically unique atoms have been labelled. The dashed lines represent H-bonding interactions shown between oxygen atoms of the bicarbonate ions and solvating water.

One can easily envisage the production of HCN and HCO_3^- from the addition of one equivalent of water to the cyanoformate salt as illustrated in Scheme 15. In fact, in the ^{13}C NMR study, the presence of a peak at 162.3 ppm (Figure 35) is certainly attributable to the presence of bicarbonate. The position of this peak correlates very well with that reported for other bicarbonate salts in the literature.[267] The notion that the bicarbonate originates from the added CO_2 rather than another source is also supported by the large size of this peak relative to others in the same spectrum, as the CO_2 used in this

particular sample was ^{13}C-enriched. The behaviour of the cyanoformate anion in an aqueous environment was investigated in more detail by performing geometry optimizations at the ωB97X-D/aug-cc-pVTZ level of theory. These included explicit H_2O molecules in addition to the bulk solvent (polarizable continuum model, as with the other theoretical solvent studies described earlier). In all cases, the calculations yielded minimum structures displaying hydrogen bonding to the terminal oxygen and nitrogen atoms of the cyanoformate anion; no spontaneous hydrolysis was observed.

Potential energy surface scans in which an oxygen atom of a molecule of H_2O was gradually forced closer to the carbon atom at the CO_2 moiety led to a steep increase in energy. Ultimately, a C-OH bond was formed, generating bicarbonate, along with a concomitant transfer of a proton to the released cyanide anion. The energy required for this process, however, was much higher than that calculated for the dissociation of cyanoformate into CN^- and CO_2. Furthermore, despite numerous efforts, all attempts to locate a transition state for this transformation were unsuccessful. Consequently, the theoretical investigations find no support for a *concerted* hydrolysis of cyanoformate in water.

A *sequential* pathway for the hydrolysis of cyanoformate in water can easily be envisioned, however. As illustrated from the solution stability study, and the theoretical calculations that accompany it, cyanoformate readily dissociates into CN^- and CO_2 in high dielectric media. The produced cyanide anion is an excellent nucleophile that would be readily protonated in water. This process generates hydroxide ions that, in turn, can

attack the electrophilic carbon of the dissociated CO_2 to yield the observed bicarbonate anion, HCO_3^-, as illustrated in Scheme 15.

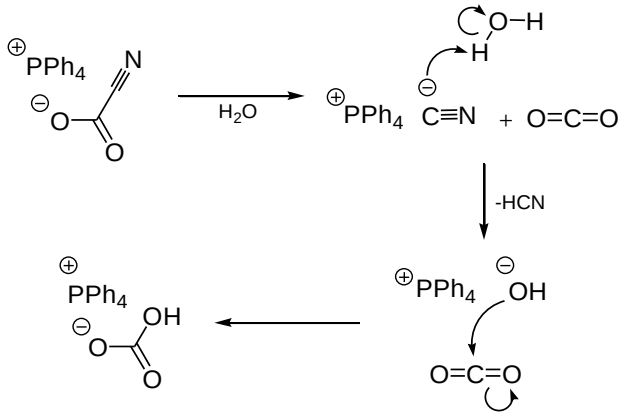

Scheme 15: Stepwise hydrolysis of tetraphenylphosphonium cyanoformate to give tetraphenylphosphonium bicarbonate and hydrogen cyanide.

The behaviour of the cyanoformate anion in a protic environment was also investigated by explicitly optimizing the structure of NCCOOH (cyanoformic acid) at the ωB97X-D/aug-cc-pVTZ level of theory, including a continuum model for solvent effects (water). The results show that charge neutralization with a proton leads to no other changes in the molecular geometry other than the non-equality of the two C-O bonds as well as the shortening (and simultaneous strengthening) of the C-C bond by roughly 0.07 Å. This is entirely expected as heterolytic cleavage of the bond would then yield CN^- and $COOH^+$, which would be a very unfavourable process due to the obvious instability of the latter species.

It appears unlikely, however, that cyanoformate would be protonated in a bulk aqueous environment to any major extent as the estimated pKa value of cyanoformic acid is -3.5 at the ωB97X-D/aug-cc-pVTZ level of theory. This value was obtained using the

pKa of trifluoroacetic acid (0.5 in an aqueous environment) as a reference point and calculating the pKa of cyanoformic acid relative to that. Although the accurate calculation of absolute pKa values is a very demanding computational task (an error of *ca.* 5 kJ mol^{-1} in relative energy translates to an error of 1 pKa unit[270]) trends in relative strengths of acids can be calculated with much greater precision, justifying the comparison between cyanoformic and trifluoroacetic acid. It also appears that if cyanoformate were to be protonated, it would actually be protonated at the nitrogen end according to additional calculations. The calculated energies at the ωB97X-D/aug-cc-pVTZ level indicate that protonation at the nitrogen is energetically preferred by 23.1 kJ mol^{-1}, likely because of the increased entropy contribution that comes with dissociation of the anion. Rather than dissociation to CN^- and the highly unstable $COOH^+$ ion, protonation at nitrogen would lead to its dissociation into CO_2 and hydrogen isocyanide, HNC.

To illustrate the cyanoformate salt's sensitivity to hydrolysis experimentally, a 2 mL aliquot of the $[Bu_4N]CN$ solution in $[P_{66614}][TFSI]$ saturated with CO_2 from the decomposition study was added to a 20 mL scintillation vial, open to the air and equipped with the ReactIR probe. The peak at 1689 cm^{-1} ($\nu_{as}CO_2$ of the cyanoformate anion) was monitored as 4 mL of reagent grade 1-propanol was added to the stirred solution. As illustrated in Figure 46, the peak at 1689 cm^{-1} rapidly diminished while concomitantly a peak appeared at 1652 cm^{-1}, corresponding to bicarbonate.[271] This latter peak reached a maximum after one reading and then gradually diminished as well. We feel, however, that this decrease was simply due to dilution incurred by the mixing process. The new peak also gradually shifted from a value of 1652 cm^{-1} to 1645 cm^{-1} during the data collection.

Over the course of two minutes, $\nu_{as}CO_2$ for cyanoformate disappeared completely, while the bicarbonate peak reached a steady absorbance.

It is worth noting that bicarbonate has been repeatedly identified as an activator of the enzyme responsible for the in the generation of ethylene from ACC.[90,91] The fact that cyanoformate is ultimately hydrolyzed to bicarbonate (and HCN) in the presence of water is added support for these observations.

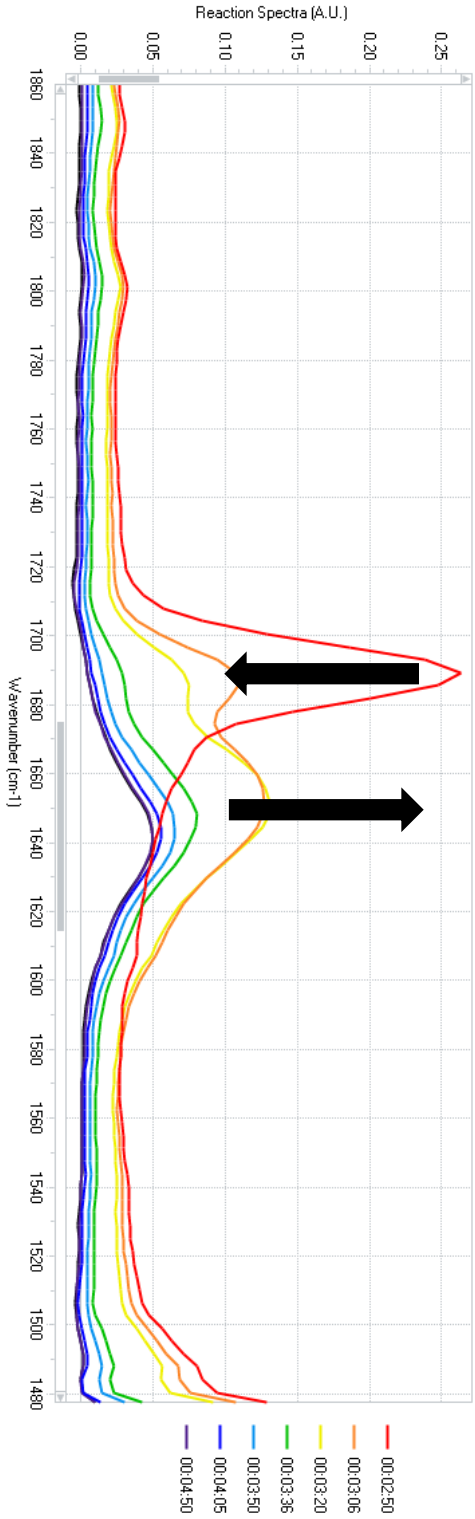

Figure 46: *In situ* infrared analysis of cyanoformate hydrolysis. Time points are indicated in the legend on the right. The spectrum for 1-propanol has been subtracted from the data.

To investigate the thermal stability of tetraphenylphosphonium cyanoformate, thermogravimetric analysis (TGA) was performed. Figure 47 shows the mass loss curve (upper) and heat flow curve (lower) for a sample of tetraphenylphosphonium cyanoformate. In the mass spectrum (not shown) for 44 amu a broad signal was observed from approximately 65°C to 160°C, indicating gradual evolution of CO_2 over this range. Unfortunately the mass loss was not quantitative (if all the possible CO_2 was evolved from a sample, a mass loss of 10.7% would be expected), so no other conclusion may be drawn except for evolution of some amount of CO_2 from the sample over the above temperature range. This is likely due in part to decomposition of the sample into other byproducts through exposure to atmospheric conditions during data collection. No significant signals were observed in the spectra at 26 amu (CN^-) or 27 amu (HCN).

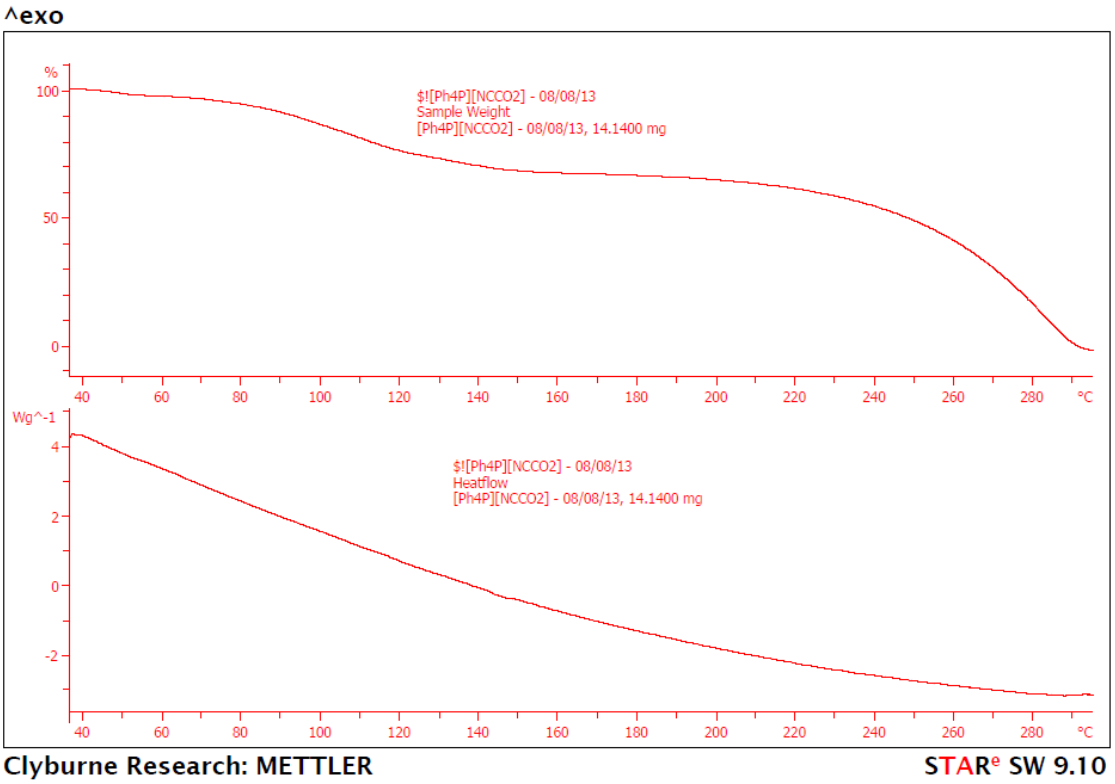

Figure 47: Mass loss curve (upper) and heat flow curve (lower) for a 14.14 mg sample of $[PPh_4][NCCO_2]$ over a temperature range of 25-300°C.

4.6 Theoretical Analysis of Bonding in Cyanoformate

An energy decomposition analysis of $[NCCO_2]^-$ in terms of CN^- and CO_2 at the PBE0/TZ2P level showed that the instantaneous interaction energy between the fragments (that is, CN^- and bent CO_2) is -317.8 kJ mol^{-1}. This consists of Pauli repulsion (1356.5 kJ mol^{-1}), quasi-classical electrostatic interaction (-780.8 kJ mol^{-1}) and orbital interactions (-893.5 kJ mol^{-1}). Although the instantaneous interaction energy is considerably more than the calculated interaction energy at the PBE0/aug-cc-pVTZ level of theory (-94.8 kJ mol^{-1}), the considerable energetic penalty (preparation energy) associated with the bending of the CO_2 molecule (approximately 200.0 kJ mol^{-1}) explains most of the energy difference.[272] Because of symmetry, the orbital interaction term can be expressed as a sum of σ- and π-type contributions. This analysis shows that the σ-contribution constitutes 89% of the stabilizing orbital interaction energy, whereas the corresponding percentages for the two possible π-contributions are 4 and 5%. The frontier orbitals (at the PBE0/aug-cc-pVTZ level) most relevant to the C-C bond formation are shown graphically in Figure 48.

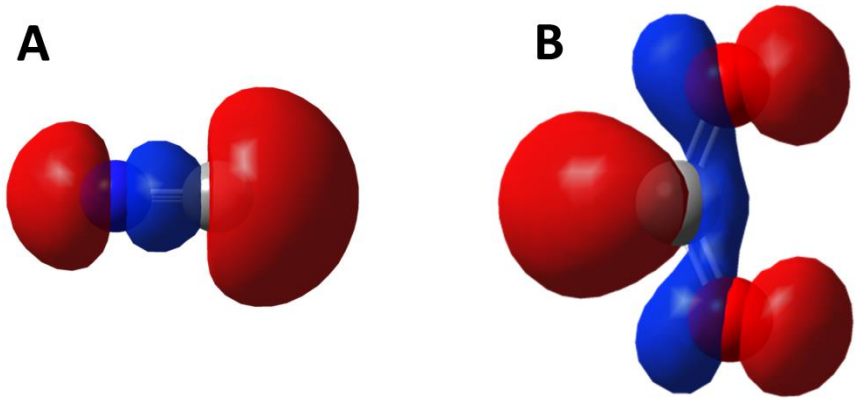

Figure 48: (A) The HOMO of the CN^-fragment and (B) the LUMO of the CO_2 fragment of $[NCCO_2]^-$ calculated at the PBE0/aug-cc-pVTZ level of theory.

The analysis of the electron localisation function of $[NCCO_2]^-$ at the ωB97X-D/aug-cc-pVTZ level of theory shows a distinct disynaptic V(C,C) bond basin at mid-bond (Figure 49A) with an average population of 2.42 electrons. This is consistent with the description of the bond as a covalent donor-acceptor interaction. For comparison, the disynaptic V(F,C) bond basin is merged with the two monosynaptic V(F) basins in $[FCO_2]^-$ (Figure 49B) and has an average population of 0.83 electrons (3.48 electrons for each of the V(F) basins). This suggests that the bond in $[FCO_2]^-$ is significantly more ionic in nature, as expected.

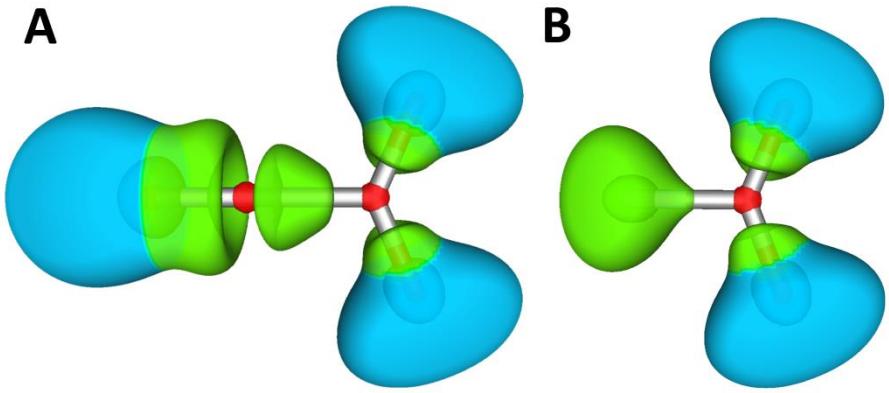

Figure 49: The electron localisation functions of (A) $[NCCO_2]^-$ and (B) $[FCO_2]^-$ (at the ωB97X-D/aug-cc-pVTZ level). Colour code: core basin (red), disynaptic valence basin (green), monosynaptic valence basin (blue).

The effect of coordinated CO_2 on cyanide can be visualized by superimposing maps of the electrostatic potential on the total electron density of both cyanide and cyanoformate ions. Plots such as these aid in the assessment of reactivity, in particular with prediction of potential sites of attack for nucleophilic and electrophilic species. For instance, a region of high-electron density will likely show an increased propensity for attraction to electrophilic sites, while the opposite can be said for the regions of low-electron density. Figure 50 shows the changes in electrostatic potential between (A) the cyanide ion and (B) the cyanoformate ion.

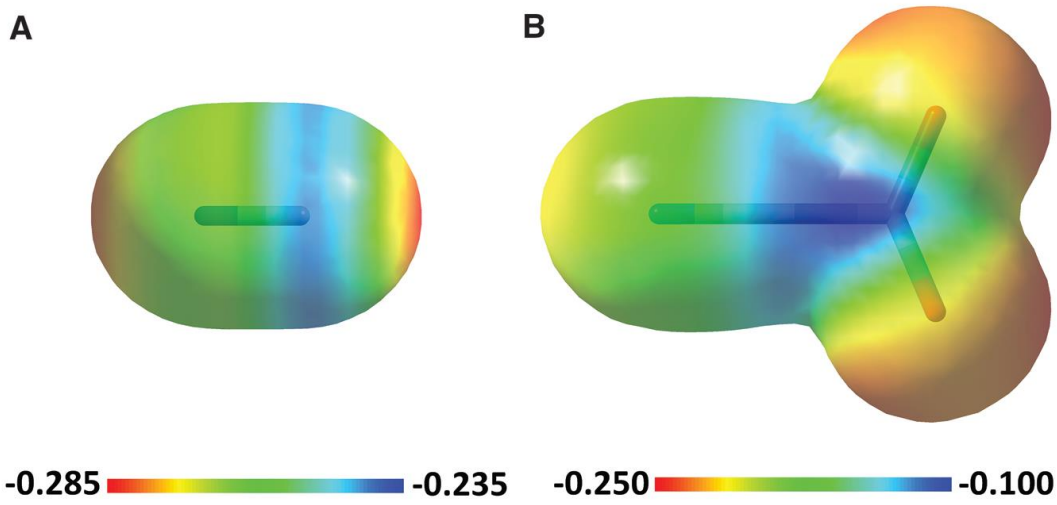

Figure 50: Electrostatic potentials (atomic units (au)) superimposed on the total electron density isosurface (0.01 au) of (A) NC^- and (B) $[NCCO_2]^-$ at the ωB97X-D/aug-cc-pVTZ level of theory.

In Figure 50, regions of high electron density are shown in red, while regions of low electron density are in blue. For the cyanide ion (A), the nitrogen atom is oriented to the left. The surface around the carbon atom is electron poor in comparison to the nitrogen atom, however, directly on the bond axis of both atoms are electron-rich areas. This is expected, considering the two possible coordination modes of cyanide (i.e. through carbon to form nitriles, or through nitrogen to form isonitriles).

In the cyanoformate ion, however, it is clear that the electrostatic potential of the cyano fragment is drastically altered from its precursor. The formerly electron-rich nitrogen end of the molecule is now much less-so, with the area around the oxygen atoms becoming the electron-rich part of the ion. This suggests that the carboxylate end of cyanoformate will favour interaction with electrophilic sites (such as the iron center in the active site of ACC oxidase) rather than the cyano end. This supports the notion that coordination of cyanide to carbon dioxide has fundamentally altered the reactivity of the

potentially toxic precursor substance and may preclude toxic deactivation of ACC oxidase.

Chapter 5 – Conclusions

In the introduction to this thesis, a review of various crystallographically-characterized complexes of carbon dioxide reported in the literature is provided. These include such compounds as inclusion complexes, carbamates, imidazol-2-carboxylates and FLP-CO_2 complexes. It has been observed that most of these complexes possess some form of stabilizing interactions to the carboxylate fragment, most commonly in the form of hydrogen-bonds. As a result it is rationalized that the preparation of CO_2 complexes with fewer such stabilizing interactions may lead to interesting, weak, CO_2 adducts which could possess unusual properties and have important uses.

In the short study investigating CO_2 uptake in solutions of DETA, or the ionic liquid, [DETAH]NO_3, in PEG 200, both solutions were found to have an optimum operating concentration under the conditions studied. This concentration was much lower for [DETAH]NO_3 than DETA, with a measured CO_2 uptake rate of 8.57 ppm/min in a 10% (v/v) solution of the former. The corresponding solution of DETA, meanwhile, exhibited an uptake rate of 4.72 ppm/min. DETA alone was found to have a higher uptake rate at 20% (v/v), with a rate of 9.29 ppm/min. In both examples (10% [DETAH]NO_3 and 20% DETA), the CO_2 concentration of the 90 L chamber was reduced to 50 ppm in two to three hours.

Cyanoformate, the elusive complex of cyanide with carbon dioxide, which has long been postulated as an intermediate in the biological production of ethylene, was finally isolated and fully characterized. Despite the theoretically and experimentally

determined fragility of this complex, cyanoformate was successfully crystallised as its tetraphenylphosphonium salt and its crystal structure was determined by X-ray diffraction. The spectroscopic (IR, Raman, ^{13}C NMR), crystallographic and theoretical data contained herein fully support the formulation of the isolated salt as $[PPh_4][NCCO_2]$.

The stability of cyanoformate in solution was investigated computationally, and through an *in situ* spectroscopic study. By spectroscopic monitoring of the rate of decrease of the $\nu_{as}CO_2$ stretching vibration of cyanoformate in various solvent mixtures, it was found that with increasing solvent dielectric, the stability of cyanoformate decreased drastically. Half-lives of cyanoformate were determined in toluene (110 min), tetrahydrofuran (55 min) and acetonitrile (17 min). Theoretical analysis using a polarizable continuum model for solvents of varying dielectric constant gave an analogous trend to that obtained in the experimental study. Cyanoformate was also observed to be quite sensitive to hydrolysis, giving the corresponding bicarbonate salt with concomitant production of HCN. A sequential pathway of dissociation and then addition of H^+ and OH^- to the constituents, was postulated based on theoretical calculations. All of these findings support the notion that cyanoformate generated during the ACC oxidase-catalyzed production of ethylene in plants, remains in complexed form at the low dielectric active site of the enzyme. Then, as the ion migrates into the higher dielectric cytosol, it breaks down giving the oft observed products, cyanide and CO_2, thereby limiting the concentration of cyanide produced in the vicinity of the sensitive iron center of the active site.

Overall, the nature of the C-C bond in cyanoformate has been shown computationally to be a donor-acceptor interaction, much like the C-C interactions found in adducts of CO_2 with *N*-heterocyclic carbenes. The observation that the stability of a particular bond is highly sensitive to changes in solvent dielectric should spawn further research into other, similar, systems. It will aid in the discovery of new chemical techniques for the low-energy, easily-reversible, activation of carbon dioxide. Exploration in this field is invaluable as the ability to use carbon dioxide as a feedstock for the synthesis of value-added products is one of the major techniques being investigated for mitigating rising CO_2 concentrations in the atmosphere and the resulting global climate change.

Chapter 6– Experimental

6.1 Experimental Preface

****CAUTION**** ***Cyanide salts and their corresponding reaction products are highly toxic and can easily undergo hydrolysis to produce poisonous and volatile hydrogen cyanide gas. Every precaution should be taken to ensure no accidental ingestion/inhalation/injection occurs. Any material (surfaces, glassware, etc.) in contact with cyanide should be washed vigorously with bleach and disposed of properly.***

Diethylenetriamine (99.9%), poly(ethylene glycol) (MW = 200), potassium cyanide, potassium cyanide (99 atom % ^{13}C), carbon-^{13}C dioxide (99 atom % ^{13}C, <3 atom % ^{18}O) and tetraethylammonium cyanide (94%) were supplied by Sigma Aldrich. Reagent grade nitric acid was supplied by ACP chemicals. Tetraphenylphosphonium bromide (>98.0%) was supplied by TCI America. Carbon dioxide (99.8%), ultra high purity nitrogen and argon were provided by Praxair Inc. Trihexyl(tetradecyl)phosphonium bis(trifluoromethylsulfonyl)imide was provided by IOLITEC, inc. Reagent grade acetonitrile and methanol were supplied by Caledon Laboratory Chemicals. Purification of reagents and solvents was not performed, nor found to be essential, unless otherwise stated.

6.2 Preparation of Relevant Compounds

$[PPh_4]CN$ – Tetraphenylphosphonium cyanide was prepared according to known literature procedures.[257] X-ray quality crystals were grown from a concentrated acetonitrile solution prepared at room temperature and then cooled to -15 °C. mp. 185-90 °C (dec), 52% yield. IR (KBr, cm^{-1}): 3468 (vs, br), 3086 (m), 3066 (s), 2684 (w), 2584 (w), 2367 (vw), 2346 (vw), 2200 (w), 2069 (m), 2001 (w), 1920 (w), 1831 (w), 1786

(vw), 1636 (s), 1586 (s), 1484 (s), 1442 (vs), 1341 (s), 1318 (s), 1195 (s), 1160 (w), 1106 (vs), 1028 (m), 998 (s), 761 (vs), 722 (vs), 695 (vs), 529 (vs).

$[PPh_4][NCCO_2]$ – A concentrated solution of $[PPh_4]CN$ in acetonitrile (0.7 g in approximately 2 mL) was exposed to an atmosphere of carbon dioxide, immediately resulting in the formation of clear colourless crystals. mp. 136-50 °C (dec), 31% yield. IR (KBr, cm^{-1}): 3469 (m, br), 3084 (w), 3056 (m), 2682 (vw), 2580 (vw), 2365 (vw), 2346 (vw), 2204 (w), 2069 (w), 1982 (w), 1911 (w), 1831 (w), 1697 (vs), 1629 (s), 1585 (s), 1481 (s), 1435 (vs), 1375 (m), 1341 (m), 1311 (s), 1266 (s), 1185 (s), 1164 (m), 1108 (vs), 1072 (m), 1025 (m), 995 (s), 924 (w), 856 (w), 836 (w), 798 (s), 755 (vs), 723 (vs), 691 (vs), 615 (m), 527 (vs). Elemental analysis calcd. [%] for $C_{26}H_{20}NO_2P$: C 76.27, H 4.92, N 3.42, O 7.82; found C 75.76, H 5.22, N 2.92, O 7.13.

$[PPh_4][N^{13}C^{13}CO_2]$ – $[PPh_4]CN$ and an equivalent of $K^{13}CN$ were stirred for one hour in methanol to induce partial anion exchange. The solution was evaporated to dryness and extracted with 5 mL acetonitrile. The solution was vacuum filtered, concentrated and placed under an atmosphere of $^{13}CO_2$ for crystallisation as with the unlabelled analogue. IR (KBr, cm^{-1}): 3476 (w, br), 3056 (vs), 2895 (vw), 2862 (vw), 2367 (vw), 2346 (vw), 2204 (vw), 1654 (s), 1585 (m), 1480 (m), 1436 (s), 1364 (w), 1341 (w), 1313 (w), 1289 (w), 1250 (m), 1185 (w), 1108 (s), 1072 (w), 995 (m), 857 (w), 811 (w), 785 (m), 756 (s), 723 (s), 691 (s), 527 (vs).

$[DETAH]NO_3$ - $[DETAH]NO_3$ was prepared by reaction of DETA with one equivalent of 10M nitric acid. Water was removed by rotary evaporation and the product was dried under vacuum to obtain a viscous transparent orange liquid (74% yield). X-ray quality

crystals were grown from dH_2O and the structure was confirmed to be $[DETAH]NO_3$. mp: 32-5°C. IR (NaCl, cm^{-1}): 3496 (m, bd), 3350 (s), 3291 (s), 2945 (w), 2362 (m), 2100 (w, bd), 1749 (w), 1603 (s), 1538 (s), 1459 (s), 1340 (s), 1120 (s), 1039 (s), 953 (s), 828 (s), 777 (m), 716 (w), 642 (w), 586 (w).

$[DETAH_2\text{-}CO_2]NO_3$ - $[DETAH]NO_3$ was dissolved in a minimum of dH_2O in a 20mL scintillation vial. The vial was placed in a desiccator which was put under an atmosphere of CO_2 to give $[DETAH_2\text{-}CO_2]NO_3$ in 98% yield. X-ray quality crystals were grown and the structure was confirmed to be $[DETAH_2\text{-}CO_2]NO_3$. mp: 93-7°C. IR (KBr, cm^{-1}): 3020 (s, bd), 2601 (s), 2361 (m), 2343 (m), 2186 (m), 2081 (w), 1629 (s), 1549 (s), 1479 (s), 1424 (s), 1384 (s), 1321 (s), 1233 (s), 1158 (s), 1120 (m), 1083 (s), 1042 (m), 1029 (m), 996 (m), 951 (m), 924 (s), 864 (w), 831 (m), 808 (s), 765 (m), 664 (s), 613 (m), 585 (w), 513 (m).

6.3 Vapour Pressure Measurements

Vapour pressure of solutions of DETA in PEG 200 (as well as neat DETA and neat PEG 200) were collected using LoggerPro v.3.8.5.1 software and then plotted in Microsoft Excel. Approximately 70 mL of each solution to be tested was placed in a 100 mL 3-neck round bottom flask, equipped with a Vernier pressure sensor and temperature probe and connected to a double-manifold vacuum line. The flask was put under vacuum, but not left open to vacuum, during the course of data collection. Using a sand bath the flask was heated with continuous stirring and pressure readings were taken every second

until a temperature of 130 °C was attained. Measurements were performed on neat PEG 200, neat DETA and 10% and 20% (v/v) solutions of DETA in PEG 200.

6.4 CO_2 Uptake Studies

All CO_2 uptake studies were performed in a sealed Plexiglas box (~90 L volume) equipped with a Vernier temperature probe and CO_2 sensor, a fan for circulation and an Hagen Elite 800 brand aquarium pump (flow rate 1.5L/min) to bubble the box atmosphere into the capture solution.

Capture solutions of both DETA and [DETAH]NO_3 were prepared in polyethylene glycol (PEG200) supplied by Sigma-Aldrich at v/v% concentrations of approximately 5, 10, 15 and 20%. 5mL of DETA and [DETAH]NO_3 were used in each run for consistency, as well as to ensure that there would be adequate CO_2 absorption (5 mL is an excess based on an approximate ambient CO_2 concentration of 400 ppm in a 90 L container). These solutions were prepared under ambient conditions, sealed in a 100 mL graduated cylinder with parafilm to limit exposure to CO_2 prior to analysis and inverted to mix. LoggerPro v.3.8.5.1 software was used for all data collection. The sample rate for each solution was set to 1 sample every 4 seconds. The time required for the CO_2 concentration to reach a minimum varied with concentration. Initial rates of CO_2 absorption were taken as the slopes of lines derived from linear regression of the data for the first ten minutes of each run. Data were plotted in Microsoft Excel.

6.5 Infrared and Raman Spectroscopy

Infrared spectra were collected using a Bruker Vertex 70 Infrared Spectrometer using samples prepared as KBr pellets unless otherwise specified. Data processing was completed using the OPUS 6.0 software suite and spectra were plotted in Microsoft Excel 2010.

Raman spectra were collected using a DXR SmartRaman spectrometer (Thermo Scientific). For all but one sample, a 532 nm wavelength diode-pumped solid state laser (DPSS), with a full-range grating (3500-50 cm^{-1}) and a laser power of 10 mW, were used. For the samples containing an ionic liquid (Figure 30), a 780 nm laser (multiple transverse mode, narrow spectrum diode) with a range of 3300-50 cm^{-1} and a power of 150 mW had to be utilized. A 180 Degree sampling accessory was used to hold the samples. For all acquisitions a spectral resolution of 5.0 cm^{-1} at FWHM, with a nominal laser spot size at the sample of 10 μm, and an acquisition time of 30 s were used. Origin 9.0 software (Origin Lab Corporation, Northampton, MA, USA) was used for spectral data processing. All spectra were smoothed using the 8 points Adjacent-Averaging method. All collection and processing of Raman spectra were performed by Scott Harroun, and instrumentation was provided by Dr. Christa Brosseau of the Department of Chemistry at Saint Mary's University.

6.6 Solid-State ^{13}C CP/MAS NMR Spectroscopy

All NMR experiments were carried out on a Bruker Avance DSX NMR spectrometer with a 9.4 T magnet (400.24 MHz proton Larmor frequency, 100.64 MHz

^{13}C Larmor frequency) and a Bruker Avance NMR spectrometer with a 16.4 T magnet (700.28 MHz proton Larmor frequency, 176.08 MHz ^{13}C Larmor frequency) using probe heads for rotors of 4 mm diameter. Samples were packed into the rotors under a nitrogen atmosphere. They were kept under nitrogen and at -15 °C prior to data collection. Since the samples, particularly the cyanoformate salt, were susceptible to decomposition, care was taken to minimise the amount of time between sample preparation and data collection.

^{1}H NMR spin lattice relaxation times, T_1, for the protons were determined by inversion-recovery sequences and ranged up to approximately 60 seconds. The recycle delays for the ^{13}C cross-polarisation (CP) / magic angle spinning (MAS) experiments were chosen to be up to 180 seconds. The other parameters for the ^{13}C CP/MAS experiments with TPPM proton decoupling were optimised on glycine whose carbonyl resonance also served as an external, secondary chemical shift standard at 176.1 ppm. For the final ^{13}C CP/MAS NMR spectra up to 32 scans were acquired. The samples were spun between 7 and 10 kHz around the magic angle to identify spinning sidebands. The cross-polarisation contact times were 2.6 ms and 2.0 ms for the 9.4 T and 16.4 T magnets, respectively. All NMR data collection and processing was performed by Dr. Ulrike Werner-Zwanziger of the Department of Chemistry and Institute for Research in Materials at Dalhousie University in Halifax, Nova Scotia.

6.7 Solution Stability Studies

A solution of tetrabutylammonium cyanide, $[Bu_4N]CN$, (3.4 g) dissolved in an ionic liquid (IL), trihexyl(tetradecyl)phosphonium bis(trifluoromethylsulfonyl)imide,

$[P_{66614}][TFSI]$, (47 mL) was prepared and then diluted in the chosen solvent for each measurement. The stock solution was stored under a nitrogen atmosphere and CO_2 was bubbled into each aliquot for 10 minutes at ambient temperature and pressure prior to analysis.

The presence of cyanide and/or cyanoformate in the stock IL solution was confirmed using FTIR and Raman spectroscopy. In the Raman, a peak at 2051 cm^{-1}, corresponding to νCN, was observed for the cyanide containing solution. For the same solution saturated with CO_2, the peaks observed at 2051 cm^{-1} and 2193 cm^{-1} correspond to νCN of cyanide and cyanoformate, respectively. The symmetric CN stretch of the cyanoformate ion is not observed in the IR. The weak absorption of νCN of cyanide in the IR and the relatively low concentration of cyanide in the solution meant that this peak was not observed either. However, $\nu_{as}CO_2$ of cyanoformate was plainly visible, appearing at 1689 cm^{-1} in the IL solution, and it is this absorbance that was monitored throughout each kinetic study.

A Mettler-Toledo EasyMax Reactor equipped with a ReactIR probe was used for all of the kinetic measurements. The solvent to be studied, 9 mL of toluene, acetonitrile or THF, was added to a 50 mL glass reactor vessel. Toluene and acetonitrile were dispensed from an MBraun MB-SPS-800 solvent purification unit, while anhydrous THF was purchased - all solvents were handled under a dry, inert atmosphere. The reactor was then purged with argon as the ReactIR probe and an EasyMax stirrer were added to the system. The reactor was stoppered and kept under argon for the duration of the measurements. One mL of the $[Bu_4N]CN$ solution, saturated with CO_2, was quickly added to the reactor

via syringe, to give a 10% IL solution by volume in the studied solvent. The solution was stirred initially to ensure adequate mixing, but during data collection the stirrer was turned off. The solid state value of $\nu_{as}CO_2$ (1697 cm^{-1}) was observed to shift depending on the solvent used; in toluene, $\nu_{as}CO_2$ = 1689 cm^{-1}, in THF, $\nu_{as}CO_2$ = 1686 cm^{-1}, and in acetonitrile, $\nu_{as}CO_2$ = 1697 cm^{-1}. Rates of decomposition were measured as a function of the $\nu_{as}CO_2$ peak height versus time.

Peak heights were determined from the difference between the peak maximum and an appropriately chosen baseline position nearby. Peak heights in each experiment were adjusted by subtracting the minimum peak height from all measured values to facilitate the calculation of half-lives. This adjustment does not affect the calculated rate, but is necessary in order to obtain a linear plot passing through the origin for fitting of the equation shown below.

$$\ln\left(\frac{P}{P_0}\right) = -\left(\frac{\ln 2}{T_{1/2}}\right)t$$

Half-lives were determined by plotting $\ln(P/P_0)$, the ratio of peak height (P) to initial peak height (P_0), versus time (t). Linear plots were obtained and linear regression, fixing the y-intercept at the origin, was used to obtain a relationship equivalent to that of Equation 1, allowing calculation of the half-life, $T_{1/2}$, of the cyanoformate ion in each solvent. Only data from t = 0 to the time corresponding to 10 % of the initial peak height remaining were included in the regression analyses.

6.8 Thermogravimetric Analysis/Mass Spectrometry

Thermogravimetric analysis and mass spectrometry (TGA/MS) measurements were completed on a TGA/DSC 1 Star^{e} System from Mettler Toledo equipped with a GC 200 Gas Controller. The TGA furnace was coupled to a Pfeiffer Vacuum ThermoStar Gas Analysis System for mass spectrometry measurements. Nitrogen was used as the purge and carrier gases for all measurements. 100 μL aluminium crucibles with pierced aluminium lids, a heating rate of 1.00 °C per minute and a nitrogen flow rate of 50 mL per minute were used for all TGA/MS measurements. Samples were dried under vacuum for several hours prior to analysis. MS measurements were performed as trend scans, which monitor M/Z over time. In each sample M/Z = 18 amu (H_2O), 26 amu (CN), 27 amu (HCN) and 44 amu (CO_2) were monitored for the duration of the analysis.

6.9 Computational Details

All computations and were performed and interpreted by Heikki Tuononen and Jani Moilanen of the Department of Chemistry at the University of Jyväskylä in Jyväskylä, Finland. All calculations were performed with Gaussian09.[273] The geometries of the studied compounds were optimised in vacuum at the MP2,[274] PBE0,[275-277] ωB97X-D[278]and CCSD(T)[279] levels of theory in combination with triple-ζ valence correlation consistent basis sets augmented with polarisation and diffuse functions (aug-cc-pVTZ).[280,281] Frequency analyses were performed for all optimised structures to ensure that they corresponded to either true minima (no imaginary frequencies) or to transition states (one imaginary frequency) on the potential energy hypersurface. CCSD(T) single point energy calculations were done on the CCSD(T)/aug-cc-pVTZ optimised geometries

in conjunction with aug-cc-pVQZ and aug-cc-pV5Z basis sets[280,281] in order to obtain energies at the complete basis set (CBS) limit using an extrapolation procedure.[282] The acquired CBS energies were further corrected by zero-point and thermal corrections calculated at the CCSD(T)/aug-cc-pVTZ level (T = 298.15 K, P = 101.325 kPa, ideal gas/rigid rotor/harmonic oscillator approximations). All DFT calculations performed in this work were also done in a solvent system, investigating different solvents with differing dielectric constants (H_2O, $\varepsilon = 78.3553$; MeCN, $\varepsilon = 35.688$; MeOH, $\varepsilon = 32.613$; THF $\varepsilon = 7.4257$ and PhMe, $\varepsilon = 2.3741$). The presence of solvent was taken into account using the integral equation formalism variant of the polarisable continuum model (IEFPCM) as implemented in Gaussian09;[283] due to theoretical limitations, the PCM calculations could not be performed at the CCSD(T)/aug-cc-pVTZ level of theory. An energy decomposition analysis[284-286] of $[NCCO_2]^-$ was performed with the program ADF 2012.1[287] at the PBE0/TZ2P level of theory[288] using the geometry of the anion at the PBE0/aug-cc-pVTZ level (the ωB97X-D functional is not implemented in the ADF code); the electronic distribution in $[NCCO_2]^-$ was also investigated by plotting the ωB97X-Daug-cc-pVTZ electron density with the calculated electrostatic potential as well as performing an electron localisation function analysis[289] with the program code TopMoD-09.[290]

6.10 X-ray Crystallographic Details

X-ray crystallographic analysis was performed by Dr. Katherine Robertson at Saint Mary's University. The sample crystals were clear and colourless, and grew in the form of thick plates. A rectangular piece was cut from one of the plates and attached to

the tip of a 300 μm MicroLoop with paratone-N oil. Measurements were made on a Bruker APEXII CCD equipped diffractometer (30 mA, 50 mV) using monochromated Mo Kα radiation (λ= 0.71073 Å) at room temperature.[291] The initial orientation and unit cell were indexed using a least-squares analysis of a random set of reflections collected from three series of 0.5° ω-scans, 10 seconds per frame and 12 frames per series, that were well distributed in reciprocal space. For data collection, four ω-scan frame series were collected with 0.5° wide scans, 45 second frames and 366 frames per series at varying φ angles (φ = 0°, 90°, 180°, 270°). The crystal to detector distance was set to 6 cm and a complete sphere of data was collected. Cell refinement and data reduction were performed with the Bruker SAINT software,[292] which corrects for beam inhomogeneity, possible crystal decay, Lorentz and polarisation effects. A multi-scan absorption correction was applied (SADABS).[293] The structure was solved using direct methods (SHELXS-2013)[294]and refined using a full-matrix least-squares method on F^2 with SHELXL-2013.[294] The non-hydrogen atoms were refined anisotropically. Hydrogen atoms bonded to carbon were included at geometrically idealised positions and were not refined. The isotropic thermal parameters of the hydrogen atoms were fixed at $1.2U_{eq}$ of the parent carbon atom. The oxygen atom in the anion was weakly restrained to give more isotropic behavior of its thermal parameters.

During the data processing it was noted that the first 250 frames collected in run 1 did not integrate properly with the rest of the data (likely due to a shift in the crystal position in the X-ray beam). They were removed from the data processing. This was not overly problematic as the data set was still massively redundant. Several attempts were

made to collect low temperature data sets for this structure with little success. The crystals showed a tendency to be affected in some way in the cold stream but what was happening (phase transition, decomposition or other) could not be ascertained.

Two of the three unique atoms in the anion, C(7) and N(1), with occupancies of 0.5 and 0.25 respectively, lie on an S_4 rotation axis in the unit cell, parallel to the *Z* axis on the 0,0,*z* edge of the cell. They do not lie directly on the -4 special position but slightly removed from it. The position of C(7) is (0,0,0.0995) so that application of the -4 symmetry operation generates the two different carbon atoms of the anion (50% occupied) in its two different orientations. The one nitrogen atom of each anion is generated in identical fashion. The length of the *Z* axis is 7.4430(14) Å so it is an easy matter to calculate the length of the C-C bond in the anion. Carbon to the origin is 0.0995 fractional units, so C to C will be 2(0.0995) or 0.1989 in fractional coordinates which corresponds to 0.1989(7.4430) Å or 1.480(9) Å. Similarly, the coordinates of N(1) are (0,0,0.2414) so it lies 0.1419 from carbon along the *Z* axis in fractional coordinates, which corresponds to 0.1419(7.4430) Å or 1.056(12) Å. The unique oxygen atom O(1), which has a occupancy of 0.5, lies on a general position off of the rotation axis and is bonded to C(7). The other 3 positions it occupies (50% in each case) are again generated by symmetry. The large thermal ellipsoid of the oxygen atom shows that it is more able to vibrate/rotate in the off-axis position it occupies. The final characteristic bond length of the anion C-O is 1.181(9) Å, possibly shortened slightly by the observed thermal motion. The bond angles in the anion are as expected. The N-C-C angle is 180° as dictated by symmetry. The two equivalent C-C-O angles, 117.3(6)°, are smaller than the O-C-O angle of 125.4(12)°, which is opened up by the larger, more electronegative oxygen atoms.

Crystallographic data for $[PPh_4][NCCO_2]$ and $[PPh_4][HCO_3]\cdot H_2O$ are included in Tables 10 to 23.

Table 10: Crystal data and structure refinement for $[PPh_4][NCCO_2]$.

Identification code	$[PPh_4][NCCO_2]$
Empirical formula	$C_{26}\ H_{20}\ N_1\ O_2\ P_1$
Formula weight	409.4
Temperature	299(2) K
Wavelength	0.71073 Å
Crystal system	Tetragonal
Space group	I_4^-
Unit cell dimensions	a = 11.948(2) Å α = 90°
	b = 11.948(2) Å β = 90°
	c = 7.4430(14) Å γ = 90°
Volume	1062.5(4) $Å^3$
Z	2
Density (calculated)	1.280 Mg m^{-3}
Absorption coefficient	0.152 mm^{-1}
F(000)	428
Crystal size	0.21 x 0.14 x 0.12 mm^3
Theta range for data collection	2.411 to 28.760°
Index ranges	-16<=h<=15, -15<=k<=15, -10<=l<=9
Reflections collected	5291
Independent reflections	1301 [R(int) = 0.0188]
Completeness to theta = 25.242°	99.80%
Absorption correction	Semi-empirical from equivalents
Max. and min. transmission	0.7457 and 0.6861
Refinement method	Full-matrix least-squares on F^2
Data / restraints / parameters	1301 / 6 / 76
Goodness-of-fit on F2	1.059
Final R indices [I>2sigma(I)]	R1 = 0.0337, wR2 = 0.0919
R indices (all data)	R1 = 0.0372, wR2 = 0.0951
Absolute structure parameter	0.01(4)
Extinction coefficient	not refined
Largest diff. peak and hole	0.121 and -0.103 e.$Å^{-3}$

Table 11: Atomic coordinates (x 10^4) and equivalent isotropic displacement parameters ($Å^2$ x 10^3) for $[PPh_4][NCCO_2]$. U(eq) is defined as one third of the trace of the orthogonalised U^{ij} tensor.

	x	y	z	U(eq)
P(1)	0	5000	2500	45(1)
C(1)	961(2)	4280(2)	1057(3)	49(1)
C(2)	2105(2)	4478(2)	1110(3)	55(1)
C(3)	2797(2)	3946(2)	-125(4)	67(1)
C(4)	2368(2)	3222(2)	-1362(4)	73(1)
C(5)	1233(3)	3001(3)	-1401(4)	78(1)
C(6)	530(2)	3544(2)	-213(3)	65(1)
C(7)	0	0	995(6)	79(1)
N(1)	0	0	2414(16)	125(4)
O(1)	312(14)	821(8)	1722(14)	212(5)

Table 12: Bond lengths [Å] and angles [°] for $[PPh_4][NCCO_2]$.

Bond Length	**Å**
P(1)-C(1)	1.792(2)
P(1)-C(1)#1	1.792(2)
P(1)-C(1)#2	1.792(2)
P(1)-C(1)#3	1.792(2)
C(1)-C(2)	1.388(3)
C(1)-C(6)	1.390(3)
C(2)-C(3)	1.390(3)
C(2)-H(2)	0.93
C(3)-C(4)	1.363(4)
C(3)-H(3)	0.93
C(4)-C(5)	1.382(4)
C(4)-H(4)	0.93
C(5)-C(6)	1.381(4)
C(5)-H(5)	0.93
C(6)-H(6)	0.93
C(7)-N(1)	1.056(12)
C(7)-O(1)	1.181(9)
C(7)-O(1)#4	1.181(9)
C(7)-C(7)#5	1.480(9)

Bond Angle	°
C(1)-P(1)-C(1)#1	111.04(6)
C(1)-P(1)-C(1)#2	106.38(13)
C(1)#1-P(1)-C(1)#2	111.04(6)
C(1)-P(1)-C(1)#3	111.04(6)
C(1)#1-P(1)-C(1)#3	106.38(13)
C(1)#2-P(1)-C(1)#3	111.04(6)
C(2)-C(1)-C(6)	119.5(2)
C(2)-C(1)-P(1)	122.14(16)
C(6)-C(1)-P(1)	118.31(16)
C(1)-C(2)-C(3)	119.3(2)
C(1)-C(2)-H(2)	120.4
C(3)-C(2)-H(2)	120.4
C(4)-C(3)-C(2)	120.9(2)
C(4)-C(3)-H(3)	119.6
C(2)-C(3)-H(3)	119.6
C(3)-C(4)-C(5)	120.3(2)
C(3)-C(4)-H(4)	119.8
C(5)-C(4)-H(4)	119.8
C(6)-C(5)-C(4)	119.5(3)
C(6)-C(5)-H(5)	120.2
C(4)-C(5)-H(5)	120.2
C(5)-C(6)-C(1)	120.5(2)
C(5)-C(6)-H(6)	119.7
C(1)-C(6)-H(6)	119.7
O(1)-C(7)-O(1)#4	125.4(12)
N(1)-C(7)-C(7)#5	180
O(1)-C(7)-C(7)#5	117.3(6)
O(1)#4-C(7)-C(7)#5	117.3(6)
Symmetry transformations used to generate equivalent atoms: #1 -y+1/2,x+1/2,-z+1/2 #2 -x,-y+1,z #3 y-1/2,-x+1/2,-z+1/2 #4 -x,-y,z #5 y,-x,-z	

Table 13: Anisotropic displacement parameters ($Å^2$ x 10^3) for $[PPh_4][NCCO_2]$. The anisotropic displacement factor exponent takes the form: $-2\pi^2[h^2a^{*2}U^{11} + ... + 2 h k a^* b^* U^{12}]$.

	U^{11}	U^{22}	U^{33}	U^{23}	U^{13}	U^{12}
P(1)	45(1)	45(1)	47(1)	0	0	0
C(1)	51(1)	48(1)	49(1)	3(1)	1(1)	6(1)
C(2)	52(1)	50(1)	64(1)	4(1)	3(1)	2(1)
C(3)	55(1)	67(1)	79(2)	6(1)	12(1)	11(1)
C(4)	75(2)	76(2)	68(1)	-5(1)	13(1)	21(1)
C(5)	83(2)	87(2)	66(2)	-23(1)	-3(1)	14(1)
C(6)	57(1)	77(2)	62(1)	-15(1)	-4(1)	6(1)
C(7)	80(3)	89(3)	67(3)	0	0	18(2)
N(1)	130(8)	187(14)	58(5)	0	0	25(9)
O(1)	338(13)	161(8)	138(7)	-67(6)	-94(8)	30(7)

Table 14: Hydrogen coordinates (x 10^4) and isotropic displacement parameters ($Å^2$ x 10^3) for $[PPh_4][NCCO_2]$.

	x	y	z	U(eq)
H(2)	2405	4961	1963	66
H(3)	3562	4087	-108	80
H(4)	2841	2876	-2183	87
H(5)	944	2489	-2221	94
H(6)	-237	3416	-263	78

Table 15: Torsion angles [°] for $[PPh_4][NCCO_2]$.

C(1)#1-P(1)-C(1)-C(2)	-0.12(17)
C(1)#2-P(1)-C(1)-C(2)	120.81(18)
C(1)#3-P(1)-C(1)-C(2)	-118.3(2)
C(1)#1-P(1)-C(1)-C(6)	-176.74(19)
C(1)#2-P(1)-C(1)-C(6)	-55.81(17)
C(1)#3-P(1)-C(1)-C(6)	65.12(15)
C(6)-C(1)-C(2)-C(3)	0.8(3)
P(1)-C(1)-C(2)-C(3)	-175.75(17)
C(1)-C(2)-C(3)-C(4)	-1.1(3)
C(2)-C(3)-C(4)-C(5)	-0.3(4)
C(3)-C(4)-C(5)-C(6)	2.0(5)
C(4)-C(5)-C(6)-C(1)	-2.2(4)
C(2)-C(1)-C(6)-C(5)	0.8(4)
P(1)-C(1)-C(6)-C(5)	177.5(2)
O(1)#4-C(7)-N(1)-O(1)	180.001(1)
O(1)-C(7)-N(1)-O(1)#4	179.999(1)
O(1)#4-N(1)-O(1)-C(7)	-0.001(1)
O(1)#4-C(7)-O(1)-N(1)	0.001(1)
C(7)#5-C(7)-O(1)-N(1)	180.000(1)
Symmetry transformations used to generate equivalent atoms: #1 -y+1/2,x+1/2,-z+1/2 #2 -x,-y+1,z #3 y-1/2,-x+1/2,-z+1/2 #4 -x,-y,z #5 y,-x,-z	

Table 16: Hydrogen bonds for $[PPh_4][NCCO_2]$ [Å and °].

D-H···A	**d(D-H)**	**d(H···A)**	**d(D···A)**	**<(DHA)**
C(2)-H(2) ···O(1)#1	0.93	2.37	3.121(11)	137.4
Symmetry transformations used to generate equivalent atoms: #1 -y+1/2,x+1/2,-z+1/2				

Table 17: Crystal data and structure refinement for $[PPh_4][HCO_3]\cdot H_2O$.

Identification code	LM028
Empirical formula	$C_{25}H_{23}O_4P$
Formula weight	418.4
Temperature	127(2) K
Wavelength	0.71073 Å
Crystal system	Triclinic
Space group	*P*-1
Unit cell dimensions	*a* = 9.3501(17) Å α = 77.810(2)°
	b = 10.0575(18) Å β = 79.722(2)°
	c = 11.677(2) Å γ= 87.698(2)°
Volume	1056.1(3) $Å^3$
Z	2
Density (calculated)	1.316 Mg/m^{-3}
Absorption coefficient	0.159 mm^{-1}
F(000)	440
Crystal size	0.180 x 0.170 x 0.140 mm^3
Theta range for data collection	1.812 to 28.795°
Index ranges	-12<=h<=12, -12<=k<=13, -15<=l<=15
Reflections collected	12707
Independent reflections	5043 [R(int) = 0.0190]
Completeness to theta = 25.242°	99.80%
Absorption correction	Semi-empirical from equivalents
Max. and min. transmission	0.7457 and 0.7059
Refinement method	Full-matrix least-squares on F^2
Data / restraints / parameters	5043 / 0 / 283
Goodness-of-fit on F2	1.036
Final R indices [I>2sigma(I)]	R1 = 0.0352, wR2 = 0.0853
R indices (all data)	R1 = 0.0419, wR2 = 0.0899
Extinction coefficient	n/a
Largest diff. peak and hole	0.363 and -0.296 $e.Å^{-3}$

Table 18: Atomic coordinates (x 10^4) and equivalent isotropic displacement parameters ($Å^2$ x 10^3) for $[PPh_4][HCO_3]\cdot H_2O$. U(eq) is defined as one third of the trace of the orthogonalized U^{ij} tensor.

	x	y	z	U(eq)
P(1)	5325(1)	7129(1)	6627(1)	16(1)
C(1)	5823(1)	8427(1)	7334(1)	17(1)
C(2)	4825(1)	9385(1)	7712(1)	22(1)
C(3)	5240(2)	10284(1)	8348(1)	26(1)
C(4)	6628(2)	10236(1)	8611(1)	26(1)
C(5)	7631(2)	9296(1)	8229(1)	24(1)
C(6)	7234(1)	8395(1)	7587(1)	21(1)
C(7)	6763(1)	6987(1)	5422(1)	18(1)
C(8)	7215(1)	8170(1)	4571(1)	20(1)
C(9)	8218(1)	8073(1)	3559(1)	23(1)
C(10)	8791(2)	6811(2)	3408(1)	26(1)
C(11)	8372(2)	5648(2)	4260(1)	26(1)
C(12)	7344(1)	5726(1)	5265(1)	22(1)
C(13)	5063(1)	5558(1)	7699(1)	18(1)
C(14)	6216(1)	5032(1)	8283(1)	21(1)
C(15)	6010(2)	3857(1)	9164(1)	24(1)
C(16)	4665(2)	3221(1)	9467(1)	25(1)
C(17)	3525(2)	3724(1)	8886(1)	26(1)
C(18)	3718(1)	4896(1)	7997(1)	22(1)
C(19)	3686(1)	7596(1)	6044(1)	18(1)
C(20)	3650(2)	7721(1)	4832(1)	23(1)
C(21)	2357(2)	8078(2)	4412(1)	30(1)
C(22)	1120(2)	8336(2)	5185(2)	33(1)
C(23)	1156(2)	8208(2)	6380(2)	31(1)
C(24)	2420(1)	7819(1)	6823(1)	24(1)
C(25)	9340(1)	1814(1)	238(1)	22(1)
O(1)	8963(1)	2990(1)	359(1)	29(1)
O(2)	8884(1)	733(1)	964(1)	34(1)
O(3)	10309(1)	1699(1)	-720(1)	40(1)
O(4)	10278(1)	4684(1)	1570(1)	34(1)

Table 19: Bond lengths [Å] and angles [°] for $[PPh_4][HCO_3]\cdot H_2O$.

Bond Length	**(Å)**
P(1)-C(7)	1.7899(13)
P(1)-C(19)	1.7923(13)
P(1)-C(13)	1.7927(13)
P(1)-C(1)	1.8018(13)
C(1)-C(2)	1.3975(18)
C(1)-C(6)	1.4002(18)
C(2)-C(3)	1.3905(19)
C(2)-H(2)	0.95
C(3)-C(4)	1.383(2)
C(3)-H(3)	0.95
C(4)-C(5)	1.390(2)
C(4)-H(4)	0.95
C(5)-C(6)	1.3900(18)
C(5)-H(5)	0.95
C(6)-H(6)	0.95
C(7)-C(12)	1.3946(18)
C(7)-C(8)	1.4047(17)
C(8)-C(9)	1.3896(18)
C(8)-H(8)	0.95
C(9)-C(10)	1.391(2)
C(9)-H(9)	0.95
C(10)-C(11)	1.385(2)
C(10)-H(10)	0.95
C(11)-C(12)	1.3920(18)
C(11)-H(11)	0.95
C(12)-H(12)	0.95
C(13)-C(18)	1.3992(18)
C(13)-C(14)	1.4039(17)
C(14)-C(15)	1.3878(18)
C(14)-H(14)	0.95
C(15)-C(16)	1.389(2)
C(15)-H(15)	0.95
C(16)-C(17)	1.386(2)
C(16)-H(16)	0.95
C(17)-C(18)	1.3908(19)

C(17)-H(17)	0.95
C(18)-H(18)	0.95
C(19)-C(24)	1.3999(18)
C(19)-C(20)	1.4002(18)
C(20)-C(21)	1.3904(19)
C(20)-H(20)	0.95
C(21)-C(22)	1.386(2)
C(21)-H(21)	0.95
C(22)-C(23)	1.379(2)
C(22)-H(22)	0.95
C(23)-C(24)	1.3838(19)
C(23)-H(23)	0.95
C(24)-H(24)	0.95
C(25)-O(1)	1.2499(16)
C(25)-O(2)	1.2656(16)
C(25)-O(3)	1.3311(17)
O(3)-H(3A)	0.92(3)
O(4)-H(4A)	0.84(2)
O(4)-H(4B)	0.89(2)
Bond Angle	**(°)**
C(7)-P(1)-C(19)	108.80(6)
C(7)-P(1)-C(13)	111.10(6)
C(19)-P(1)-C(13)	109.79(6)
C(7)-P(1)-C(1)	107.81(6)
C(19)-P(1)-C(1)	110.38(6)
C(13)-P(1)-C(1)	108.93(6)
C(2)-C(1)-C(6)	119.66(11)
C(2)-C(1)-P(1)	122.27(10)
C(6)-C(1)-P(1)	117.89(9)
C(3)-C(2)-C(1)	119.61(12)
C(3)-C(2)-H(2)	120.2
C(1)-C(2)-H(2)	120.2
C(4)-C(3)-C(2)	120.58(13)
C(4)-C(3)-H(3)	119.7
C(2)-C(3)-H(3)	119.7
C(3)-C(4)-C(5)	120.17(12)
C(3)-C(4)-H(4)	119.9
C(5)-C(4)-H(4)	119.9

C(4)-C(5)-C(6)	119.88(13)
C(4)-C(5)-H(5)	120.1
C(6)-C(5)-H(5)	120.1
C(5)-C(6)-C(1)	120.10(12)
C(5)-C(6)-H(6)	120
C(1)-C(6)-H(6)	120
C(12)-C(7)-C(8)	120.14(11)
C(12)-C(7)-P(1)	121.41(10)
C(8)-C(7)-P(1)	118.23(9)
C(9)-C(8)-C(7)	119.64(12)
C(9)-C(8)-H(8)	120.2
C(7)-C(8)-H(8)	120.2
C(8)-C(9)-C(10)	119.88(12)
C(8)-C(9)-H(9)	120.1
C(10)-C(9)-H(9)	120.1
C(11)-C(10)-C(9)	120.51(12)
C(11)-C(10)-H(10)	119.7
C(9)-C(10)-H(10)	119.7
C(10)-C(11)-C(12)	120.21(12)
C(10)-C(11)-H(11)	119.9
C(12)-C(11)-H(11)	119.9
C(11)-C(12)-C(7)	119.58(12)
C(11)-C(12)-H(12)	120.2
C(7)-C(12)-H(12)	120.2
C(18)-C(13)-C(14)	120.27(12)
C(18)-C(13)-P(1)	121.03(10)
C(14)-C(13)-P(1)	118.63(9)
C(15)-C(14)-C(13)	119.53(12)
C(15)-C(14)-H(14)	120.2
C(13)-C(14)-H(14)	120.2
C(14)-C(15)-C(16)	119.80(12)
C(14)-C(15)-H(15)	120.1
C(16)-C(15)-H(15)	120.1
C(17)-C(16)-C(15)	121.04(12)
C(17)-C(16)-H(16)	119.5
C(15)-C(16)-H(16)	119.5
C(16)-C(17)-C(18)	119.77(13)
C(16)-C(17)-H(17)	120.1

C(18)-C(17)-H(17)	120.1
C(17)-C(18)-C(13)	119.58(12)
C(17)-C(18)-H(18)	120.2
C(13)-C(18)-H(18)	120.2
C(24)-C(19)-C(20)	119.89(12)
C(24)-C(19)-P(1)	118.97(10)
C(20)-C(19)-P(1)	121.14(10)
C(21)-C(20)-C(19)	119.54(13)
C(21)-C(20)-H(20)	120.2
C(19)-C(20)-H(20)	120.2
C(22)-C(21)-C(20)	120.13(14)
C(22)-C(21)-H(21)	119.9
C(20)-C(21)-H(21)	119.9
C(23)-C(22)-C(21)	120.24(13)
C(23)-C(22)-H(22)	119.9
C(21)-C(22)-H(22)	119.9
C(22)-C(23)-C(24)	120.65(14)
C(22)-C(23)-H(23)	119.7
C(24)-C(23)-H(23)	119.7
C(23)-C(24)-C(19)	119.50(13)
C(23)-C(24)-H(24)	120.3
C(19)-C(24)-H(24)	120.3
O(1)-C(25)-O(2)	124.94(13)
O(1)-C(25)-O(3)	117.14(12)
O(2)-C(25)-O(3)	117.91(12)
C(25)-O(3)-H(3A)	112.1(15)
H(4A)-O(4)-H(4B)	105(2)

Table 20: Anisotropic displacement parameters ($Å^2$ x 10^3)for $[PPh_4][HCO_3]\cdot H_2O$. The anisotropic displacement factor exponent takes the form: $-2p^2$ [$h^2a^{*2}U^{11}$ + ... + 2 h k a* b* U^{12}].

	U^{11}	U^{22}	U^{33}	U^{23}	U^{13}	U^{12}
P(1)	16(1)	16(1)	14(1)	-3(1)	-2(1)	0(1)
C(1)	20(1)	16(1)	14(1)	-2(1)	-1(1)	-2(1)
C(2)	23(1)	22(1)	22(1)	-5(1)	-4(1)	2(1)
C(3)	31(1)	23(1)	26(1)	-10(1)	-3(1)	3(1)
C(4)	34(1)	24(1)	21(1)	-7(1)	-4(1)	-5(1)
C(5)	24(1)	26(1)	23(1)	-5(1)	-6(1)	-5(1)
C(6)	19(1)	23(1)	22(1)	-5(1)	-1(1)	-1(1)
C(7)	16(1)	21(1)	15(1)	-4(1)	-1(1)	1(1)
C(8)	20(1)	20(1)	20(1)	-4(1)	-1(1)	0(1)
C(9)	23(1)	27(1)	18(1)	-2(1)	-1(1)	-2(1)
C(10)	24(1)	35(1)	18(1)	-10(1)	1(1)	1(1)
C(11)	29(1)	26(1)	23(1)	-10(1)	-2(1)	6(1)
C(12)	25(1)	20(1)	20(1)	-5(1)	-2(1)	2(1)
C(13)	22(1)	17(1)	14(1)	-3(1)	-2(1)	0(1)
C(14)	22(1)	20(1)	21(1)	-5(1)	-4(1)	0(1)
C(15)	32(1)	20(1)	20(1)	-5(1)	-8(1)	6(1)
C(16)	40(1)	16(1)	17(1)	-2(1)	-2(1)	-1(1)
C(17)	29(1)	22(1)	24(1)	-2(1)	-1(1)	-7(1)
C(18)	23(1)	22(1)	22(1)	-4(1)	-5(1)	-2(1)
C(19)	17(1)	17(1)	19(1)	-2(1)	-4(1)	-1(1)
C(20)	24(1)	23(1)	21(1)	-1(1)	-5(1)	-3(1)
C(21)	33(1)	29(1)	29(1)	2(1)	-16(1)	-4(1)
C(22)	24(1)	27(1)	51(1)	-4(1)	-19(1)	3(1)
C(23)	18(1)	30(1)	48(1)	-14(1)	-5(1)	1(1)
C(24)	20(1)	25(1)	26(1)	-7(1)	-2(1)	-2(1)
C(25)	22(1)	24(1)	21(1)	-6(1)	-6(1)	0(1)
O(1)	34(1)	23(1)	31(1)	-7(1)	-7(1)	4(1)
O(2)	41(1)	24(1)	31(1)	-6(1)	12(1)	-3(1)
O(3)	60(1)	24(1)	27(1)	-3(1)	14(1)	0(1)
O(4)	41(1)	34(1)	28(1)	-5(1)	-7(1)	-7(1)

Table 21: Hydrogen coordinates (x 10^4) and isotropic displacement parameters (Å^2 x 10^3) for $[PPh_4][HCO_3]\cdot H_2O$.

	x	y	z	U(eq)
H(2)	3869	9421	7536	26
H(3)	4564	10937	8603	31
H(4)	6896	10848	9054	31
H(5)	8586	9268	8406	29
H(6)	7922	7757	7320	26
H(8)	6838	9032	4687	24
H(9)	8511	8867	2971	28
H(10)	9476	6747	2715	31
H(11)	8786	4793	4158	31
H(12)	7041	4925	5841	26
H(14)	7131	5478	8076	25
H(15)	6787	3490	9559	29
H(16)	4523	2427	10083	30
H(17)	2614	3270	9095	31
H(18)	2943	5245	7594	27
H(20)	4504	7563	4300	27
H(21)	2321	8145	3594	36
H(22)	245	8601	4892	40
H(23)	304	8389	6903	37
H(24)	2429	7705	7651	28
H(3A)	10520(30)	800(30)	-750(20)	79(8)
H(4A)	9880(20)	4160(20)	1250(20)	57(6)
H(4B)	10510(20)	5430(20)	1000(20)	63(7)

Table 22: Torsion angles [°] for $[PPh_4][HCO_3]\cdot H_2O$.

Angle	(°)
C(7)-P(1)-C(1)-C(2)	138.47(11)
C(19)-P(1)-C(1)-C(2)	19.75(12)
C(13)-P(1)-C(1)-C(2)	-100.87(11)
C(7)-P(1)-C(1)-C(6)	-46.44(11)
C(19)-P(1)-C(1)-C(6)	-165.15(10)
C(13)-P(1)-C(1)-C(6)	74.22(11)
C(6)-C(1)-C(2)-C(3)	-0.78(19)
P(1)-C(1)-C(2)-C(3)	174.24(10)
C(1)-C(2)-C(3)-C(4)	-0.2(2)
C(2)-C(3)-C(4)-C(5)	0.8(2)
C(3)-C(4)-C(5)-C(6)	-0.4(2)
C(4)-C(5)-C(6)-C(1)	-0.5(2)
C(2)-C(1)-C(6)-C(5)	1.13(19)
P(1)-C(1)-C(6)-C(5)	-174.10(10)
C(19)-P(1)-C(7)-C(12)	-108.69(11)
C(13)-P(1)-C(7)-C(12)	12.29(12)
C(1)-P(1)-C(7)-C(12)	131.58(11)
C(19)-P(1)-C(7)-C(8)	65.95(11)
C(13)-P(1)-C(7)-C(8)	-173.07(9)
C(1)-P(1)-C(7)-C(8)	-53.78(11)
C(12)-C(7)-C(8)-C(9)	1.59(19)
P(1)-C(7)-C(8)-C(9)	-173.12(10)
C(7)-C(8)-C(9)-C(10)	-1.48(19)
C(8)-C(9)-C(10)-C(11)	0.0(2)
C(9)-C(10)-C(11)-C(12)	1.5(2)
C(10)-C(11)-C(12)-C(7)	-1.4(2)
C(8)-C(7)-C(12)-C(11)	-0.17(19)
P(1)-C(7)-C(12)-C(11)	174.37(10)
C(7)-P(1)-C(13)-C(18)	-122.04(11)
C(19)-P(1)-C(13)-C(18)	-1.64(12)
C(1)-P(1)-C(13)-C(18)	119.34(11)
C(7)-P(1)-C(13)-C(14)	61.08(11)
C(19)-P(1)-C(13)-C(14)	-178.52(10)
C(1)-P(1)-C(13)-C(14)	-57.54(11)
C(18)-C(13)-C(14)-C(15)	-0.52(19)

P(1)-C(13)-C(14)-C(15)	176.39(10)
C(13)-C(14)-C(15)-C(16)	-0.57(19)
C(14)-C(15)-C(16)-C(17)	1.3(2)
C(15)-C(16)-C(17)-C(18)	-0.9(2)
C(16)-C(17)-C(18)-C(13)	-0.1(2)
C(14)-C(13)-C(18)-C(17)	0.87(19)
P(1)-C(13)-C(18)-C(17)	-175.96(10)
C(7)-P(1)-C(19)-C(24)	-177.51(10)
C(13)-P(1)-C(19)-C(24)	60.72(11)
C(1)-P(1)-C(19)-C(24)	-59.39(11)
C(7)-P(1)-C(19)-C(20)	3.34(12)
C(13)-P(1)-C(19)-C(20)	-118.44(11)
C(1)-P(1)-C(19)-C(20)	121.45(11)
C(24)-C(19)-C(20)-C(21)	0.53(19)
P(1)-C(19)-C(20)-C(21)	179.68(10)
C(19)-C(20)-C(21)-C(22)	1.3(2)
C(20)-C(21)-C(22)-C(23)	-1.6(2)
C(21)-C(22)-C(23)-C(24)	-0.1(2)
C(22)-C(23)-C(24)-C(19)	2.0(2)
C(20)-C(19)-C(24)-C(23)	-2.20(19)
P(1)-C(19)-C(24)-C(23)	178.63(10)

Table 23: Hydrogen bonds for $[PPh_4][HCO_3]\cdot H_2O$ [Å and °].

D-H···A	**d(D-H)**	**d(H···A)**	**d(D···A)**	**<(DHA)**
O(3)-H(3A)...O(2)#1	0.92(3)	1.67(3)	2.5893(16)	172(2)
O(4)-H(4A)...O(1)	0.84(2)	2.03(2)	2.8667(16)	176(2)
O(4)-H(4B)...O(1)#2	0.89(2)	2.00(2)	2.8960(16)	176(2)
Symmetry transformations used to generate equivalent atoms: #1 -x+2,-y,-z #2 -x+2,-y+1,-z				

References

[1]Larkin, D.W.; Caldwell, T.A.; Lobban, L.L.; Mallinson, R.G. *Energy & Fuels* **1998**, 12, 740-4.

[2]Buckingham, A.D.; Disch, R.L. *Proc. R. Soc. Lond. A* **1963**, 273, 1353, 275-89.

[3]Kendall, J.L.; Canela, D.A.; Young, J.L.; DeSimone, J.M. *Chem. Rev.* **1999**, 99, 543-63.

[4]DeSimone, J.M.; Guan, Z.; Elsbernd, C.S. *Science* **1992**, 257, 5072, 945-7.

[5]Tans, P.; Keeling, R. *Trends in Atmospheric Carbon Dioxide.* http://www.esrl.noaa.gov/gmd/ccgg/trends/ (accessed February 2014).

[6] Siegenthaler, U.; Stocker, T. F.; Monnin, E.; Luethi, D.; Schwander, J.; Stauffer, B.; Raynaud, D.; Barnola, J.-M.; Fischer, H.; Masson-Delmotte, V.; Jouzel, J. *Science* **2005**, 310, 5752, 1313-7.

[7]Karl, T.R.; Trenberth, K.E. Science **2003**, 302, 1719-23.

[8]Zeebe, R.E.; Wolf-Gladrow, D. *CO_2 in Seawater: Equilibrium, Kinetics, Isotope*; Elsevier Science B.V.: Amsterdam, The Netherlands, 2001.

[9]Jacobson, M.Z. *J. Geophys. Res.* **2005**, 110, D7.

[10]Fabry. V.J.; Seibel, B.A.; Feely, R.A.; Orr, J.C. *ICES J. Mar. Sci.* **2008**, 65, 3, 414-32.

[11]Munday, P.L.; Donelson, J.M.; Dixson, D.L.; Endo, G.G.K. *Proc. R. Soc. B* **2009**, 276, 3275-83.

[12]Pachauri, R.K., Reisinger, A., Climate Change **2007**: Synthesis Report. Eds.; IPCC, Geneva, Switzerland.

[13]Gasda, S.E.; Nordbotten, J.M.; Celia, M.A. *Comput. Geosci.* **2009**, 13, 469-81.

[14]Kling, G.W.; Clark, M.A.; Wagner, G.N.; Compton, H.R.; Humphrey, A.M.; Devine, J.D.; Evans, W.C.; Lockwood, J.P.; Tuttle, M.L.; Koenigsberg, E.J. *Science* **1987**, 236, 4798, 169-75.

[15]Yang, H.; Xu, Z.; Fan, M.; Gupta, R.; Slimane, R.B.; Bland, A.E.; Wright, I. *J. Environ. Sci.* **2008**, 20, 14-27.

[16]Brunetti, A.; Scura, F.; Barbieri, G.; Drioli, E. *J. Membr. Sci.* **2010**, 359, 115-25.

[17]Ho, M.T.; Allinson, G.W.; Wiley, D.E. *Ind. Eng. Chem. Res.* **2008**, 47, 1562-8.

[18]Oelkers, E.H.; Gislason, S.; Matter, J. *Elements* **2008**, 4, 5, 333-7.

[19]Kelemen, P.B.; Matter, J.; Streit, E.E.; Rudge, J.F.; Curry, W.B.; Blusztajn, J. *Annual Review of Earth and Planetary Sciences* **2011**, 39, 545-76.

[20]Kelemen, P.B.; Matter, J. *Proc. Natl. Acad. Sci. USA* **2008**, 105, 45, 17295-300.

[21]Siriwardane, R.V.; Shen, M.S.; Fisher, E.P.; Poston, J.A. *Energy & Fuels* **2001**, 15, 2, 279-84.

[22]Xu, X.; Song, C.; Andresen, J.M.; Miller, B.G.; Scaroni, A.W. *Energy & Fuels* **2002**, 16, 6, 1463-9.

[23]Goeppert, A.; Czaun, M.; May, R.B.; Surya Prakash, G.K.; Olah, G.A.; Narayanan, S.R. *J. Am. Chem. Soc.* **2011**, 133, 20164-7.

[24]Xu, X.; Song, C.; Miller, B.G.; Scaroni, A.W. *Energy & Fuels* **2002**, 16, 1463-9.

[25]Zeleňák, V.; Badanicová, M.; Halamova, D.; Čejka, J.; Zukal, A.; Murafa, N.; Goerigk, G. *Chem. Eng. J.* **2008**, 144, 2, 336-42.

[26]Dybtsev, D.N.; Chun, H.; Yoon, S.H.; Kim, D.; Kim, K. *J. Am. Chem. Soc.* **2004**, 126, 32-3.

[27]Ockwig, N.W.; Delgado-Friedrichs, O.; O'Keeffe, M.; Yaghi, O.M. *Acc. Chem. Res.* **2005**, 36, 176-82.

[28]James, S.L. *Chem. Soc. Rev.* **2003**, 32, 276-88.

[29]Forrest, K.A.; Pham, T.; Hogan, A.; McLaughlin, K.; Tudor, B.; Nugent, P.; Burd, S.D.; Mullen, A.; Cioce, C.R.; Wojtas, L.; Zaworotko, M.J.; Space, B.; *J. Phys. Chem. C* **2013**, 117, 17687-98.

[30]Nugent, P.; Belmabkhout, Y.; Burd, S.D.; Cairns, A.J.; Luebke, R.; Forrest, K.; Pham, T.; Ma, S.; Space, B.; Wojtas, L.; Eddaoudi, M.; Zaworotko, M. J. *Nature* **2013**, 495, 80-4.

[31]Arstad, B.; Fjellvåg, H.; Kongshaug, K.O.; Swang, O.; Blom, R. *Adsorption* **2008**, 14, 6, 755-62.

[32]Vaidhyanathan, R.; Iremonger, S.S.; Shimizo, G.K.H.; Boyd, P.G.; Alavi, S.; Woo, T.K. *Science* **2010**, 330, 650-3.

[33]Sumida, K.; Rogow, D.L.; Mason, J.A.; McDonald, T.M.; Bloch, E.D.; Herm, Z.R.; Bae, T.-H.; Long, J.R. *Chem. Rev.* **2011**, 112, 2, 724-81.

[34]Li, H.; Eddaoudi, M.; Groy, T.L.; Yaghi, O.M. *J. Am. Chem. Soc.* **1998**, 120, 8571-2.

[35]Perry, J.J. IV.; Perman, J.A.; Zaworotko, M.J. *Chem. Soc. Rev.* **2009**, 38, 1400-17.

[36]Ma, S.; Sun, D.; Ambrogio, M.; Fillinger, J.A.; Parkin, S.; Zhou, H. *J. Am. Chem. Soc.* **2007**, 129. 1858-9.

[37]Ma, L.; Abney, C.; Lin, W. *Chem. Soc. Rev.* **2009**, 38, 1248-56.

[38]Sun, D.; Ke, Y.; Collins, D.J.; Lorigan, G.A.; Zhou, H. *Inorg Chem.* **2007**, 46, 2725-

34.

[39]Benemann, J. *Energy Convers. Manage.* **1997**, 38, S475-9.

[40]Usui, N.; Ikenouchi, M. *Energy Convers. Manage.* **1997**, 38, S487-92.

[41]Huntley, M.E.; Redalje, D.G. *Mitigation and Adaptation Strategies for Global Change* **2007**, 12, 573-608.

[42]Feller, U.; Anders, I.; Mae, T. *J. Exp. Bot.* **2008**, 59, 7, 1615-24.

[43]King, W.A.; Gready, J.E.; Andrew, T.J. *Biochem.* **1998**, 37, 15414-22.

[44]Stephenson, P.G.; Moore, C.M.; Terry, M.J.; Zubkov, M.V.; Bibby, T.S. *Trends Biotechnol.* **2011**, 29, 12, 615-23.

[45]Spreitzer, R.J.; Salvucci, M.E. *Annu. Rev. Plant. Biol.* **2002**, 53, 449-75.

[46]Hambourger, M.; Moore, G.F.; Kramer, D.M.; Gust, D.; Moore, A.L.; Moore, T.A. *Chem. Soc. Rev.* **2009**, 38, 1, 25-35.

[47]Rochelle, G.T. *Science* **2009**, 325, 5948, 1652-4.

[48]Cifre, P.G.; Brechtel, K.; Hoch, S.; Garcia, H.; Asprion, N.; Hasse, H.; Scheffknecht, G. *Fuel* **2009**, 88, 2481-8.

[49]Bonenfant, D.; Mimeault, M.; Hausler, R. *Ind. End. Chem. Res.* **2003**, 42, 3179-84.

[50]Strazisar, B.R.; Anderson, R.R.; White, C.M. *Energy & Fuels* **2003**, 17, 1034-9.

[51]Freguia, S.; Rochelle, G.T. *AIChE Journal* **2003**, 49. 7, 1676-86.

[52] Blanchon le Bouhelec, E.; Mougin, P.; Barreau, A.; Solimando, R. *Energy & Fuels* **2007**, 21, 4, 2044-55.

[53]Harper, N.D.; Nizio, K.D.; Hendsbee, A.D.; Masuda, J.D.; Robertson, K.N.; Murphy, L.J.; Johnson, M.B.; Pye, C.C.; Clyburne, J.A.C. *Ind. Eng. Chem. Res.*

2011, 50, 2822-30.

[54]Francesconi, R.; Bigi, A.; Rubini, K.; Comelli, F. *J. Chem. Eng. Dat.* **2007**, 52, 2020-5.

[55] Ilioudis, C.A.; Georganopoulou, D.G.; Steed, J.W. *J. Mater. Chem.* **2002**, 4, 6, 26-36

[56]Ilioudis, C.A.; Hancock, K.S.B.; Georganopoulou, D.G.; Steed, J.W. *New J. Chem.* **2000**, 24, 787-98.

[57]Burdon, J.; Lallu, N.; Billing, D.; Burmeister, D.; Yearsley, C.; Wang, M.; Gunson, A.; Young, H. *Postharvest Biology and Technology* **2005**, 65, 2, 133-41.

[58]Burg, S.P.; Burg, E.A. *Plant Physiol.* **1967**, 42, 1, 144-52.

[59]Lelièvre, J.-M.; Latche, A.; Jones, B.; Bouzayen, M.; Pech, J.-C. *Physiol. Planta.* **1997**, 101, 4, 727-39.

[60]Theologis, A. *Cell* **1992**, 70, 2, 181-4.

[61]Alexander, L.; Grierson, D. *J. Exp. Bot.* **2002**, 53, 377, 2039-55.

[62]Rothan, C.; Duret, S.; Chevalier, C.; Raymond, P. *Plant Physiol.* **1997**, 114, 1, 255-63.

[63]Munoz, M.T.; Aguado, P.; Ortega, N.; Escribano, M.I.; Merodio, C. *Functional Plant Biology* **1999**, 26, 3, 201-9.

[64]Kao, C. H.; Yang, S.F. *Planta* **1982**, 155, 3, 261-6.

[65]Knee, M., Ed. *Fruit quality and its biological basis*. Vol. 9. CRC Press: Boca Raton, FL, U.S.A., 2002.

[66]Agar, I.T.; Massantini, R.; Hess-Pierce, B.; Kader, A.A. *J. Food Sci.* **1999**, 64, 3, 433-40.

[67]Burg, S.P.; Clagett, C.O. *Biochem. Biophys. Res. Commun.* **1967**, 27, 125-30.

[68]Murr, D.P.; Yang, S.F. *Phytochemistry* **1975**, 14, 1291-2

[69]Adams, D.O.; Yang, S.F. *Plant Physiol.* **1977**, 60, 892-6

[70]Adams, D.O.; Yang, S.F. *Proc. Natl. Acad. Sci. USA* **1979**, 76, 1, 170-4.

[71]Salaiin, J.; Bairtr, M.S. *Curr. Med. Chem.* **1995**, 2, 511-42.

[72]Yeong-Biau, Y.; Adams, D.O.; Yang, S.F. *Archives of Biochemistry and Biophysics* **1979**, 198, 1, 280-6.

[73]Boller, T.; Herner, R.C.; Kende, H. *Planta* **1979**, 145, 3, 293-303.

[74]Jones, J.F.; Kende, H. *Planta* **1979**, 146, 5, 649-56.

[75]Yu, Y.-B.; Yang, S.F. *Plant Physiol.* **1979**, 64, 6, 1074-7.

[76]Konze, J.R.; Kende, H. *Planta* **1979**, 146, 3, 293-301.

[77]Konze, J.R.; Kwiatkowski, G.M.K. *Planta* **1981**, 151, 4, 320-6.

[78]Lurssen, K.; Naumann, K., Schröder, R. *Naturwissenschaften* **1979**, 66, 5, 264-5.

[79]Adlington, R.M.; Baldwin, J.E.; Rawlings, B.J. *J. Chem. Soc., Chem. Commun.* **1983**, 6, 290-92.

[80]Adams, D.O.; Yang, S.F. *Trends Biochem. Sci.***1981**, 6, 161-4.

[81]Pirrung, M.C.; McGeehan, G.M. *J. Org. Chem.* **1983**, 48, 25, 5143-4.

[82]Pirrung, M.C. *J. Am. Chem. Soc.* **1983**, 105, 24, 7207-9.

[83]Peiser, G.D.; Wang, T.-T.; Hoffman, N.E.; Yang, S.F.; Liu, H.-W.; Walsh, C.T. *Proc. Natl. Acad. Sci.* **1984**, 81, 10, 3059-63.

[84]Pirrung, M.C. *Bioorganic Chemistry* **1985**, 13, 3, 219-26.

[85]Dong, J.G.; Fernandez-Maculet, J.C.; Yang, S.F. *Proc. Natl. Acad. Sci.* **1992**, 89, 20, 9789-93.

[86]Ververidis, P.; John, P. *Phytochemistry* **1991**, 30, 3, 725-7.

[87]Fernández-Maculet, J.C.; Yang, S.F. *Plant Physiol.* **1992**, 99, 2, 751-4.

[88]Hamilton, A.J.; Bouzayen, M.; Grierson, D. *Proc. Natl. Acad. Sci.***1991**, 88, 16, 7434-7.

[89]Vioque, B.; Castellano, J.M. *Physiol. Planta.* **1994**, 90, 2, 334-8.

[90]McRae, D.G.; Coker, J.A.; Legge, R.L.; Thompson, J.E. *Plant Physiol.* **1983**, 73, 3, 784-90.

[91]Smith, J.J.; John, P. *Phytochemistry* **1993**, 32, 6, 1381-6.

[92]Rocklin, A.M.; Tierney, D.L.; Kofman, V.; Brunhuber, N.M.W.; Hoffman, B.M.; Christoffersen, R.E.; Reich, N.O.; Lipscomb, J.D.; Que, L. *Proc. Natl. Acad. Sci.* **1999**, 96, 14, 7905-9.

[93]Zhang, Z.; Barlow, J.N.; Baldwin, J.E.; Schofield, C.J. *Biochem.* **1997**, 36, 50, 15999-16007.

[94]Pirrung, M.C. *Acc. Chem. Res.* **1999**, 32, 8, 711-8.

[95]Costas, M.; Mehn, M.P.; Jensen, M.P.; Que, L. *Chem. Rev.* **2004**, 104, 2, 939-86.

[96]Tierney, D.L.; Rocklin, A.M.; Lipscomb, J.D.; Que, L.; Hoffman, B.M. *J. Am. Chem. Soc.* **2005**, 127, 19, 7005-13.

[97]Zhou, J.; Rocklin, A.M.; Lipscomb, J.D.; Que, L.; Solomon, E.I. *J. Am. Chem. Soc.* **2002**, 124, 17, 4602-9.

[98]Zhang, Z.; Ren, J.-S.; Clifton, I.J.; Schofield, C.J. *Chem. Biol.* **2004**, 11, 10, 1383-94.

[99]Bruijnincx, P.C.A.; van Koten, G.; Klein Gebbink, R.J.M. *Chem. Soc. Rev.* **2008**, 37, 2716-44.

[100]Mirica, L.M.; Klinman, J.P. *Proc. Natl. Acad. Sci.* **2008**, 105, 6, 1814-9.

[101]Thrower, J.S.; Blalock, R.; Klinman, J.P. *Biochem.* **2001**, 40, 32, 9717-24.

[102]Rocklin, A.M.; Kato, K.; Liu, H.-W.; Que, L.; Lipscomb, J.D. *J. Biol. Inorg. Chem.* **2004**, 9, 2, 171-82.

[103]Hiyama, T.; Koide, H.; Noazki, H. *Bull. Chem. Soc. Jpn.* **1975**, 48, 2918-21

[104]Peiser, G.D.; Wang, T.-T.; Hoffman, N.E.; Yang, S.F.; Liu, H.-W.; Walsh, C.T. *Proc. Natl. Acad. Sci.* **1984**, 81, 10, 3059-63

[105]Yang, S.F.; Dong, J.G. *Bot. Bull. Acad. Sin.* **1993**, 34, 89-101.

[106]Bassan, A.; Borowski, T.; Schofield, C.J.; Siegbahn, P.E.M. *Chem. Eur. J.* **2006**, 12, 8835-46.

[107]Pirrung, M.C. *J. Org. Chem.* **1987**, 52, 19, 4179-84.

[108]Brunhuber, N.M.W.; Mort, J.L.; Christoffersen, R.E.; Reich, N.O. *Biochem.* **2000**, 39, 35, 10730-8.

[109]Lee, S.C.; Scott, M.J.; Kauffmann, K.; Münck, E.; Holm, R.H. *J. Am. Chem. Soc.* **1994**, 116, 1, 401-2.

[110]Lurie, S.; Arie, R.B.; Faust, M. *Biochemical and Physiological Aspects of Ethylene Production in Lower and Higher Plants*, Springer: Netherlands, **1989**; pp 81-90.

[111]Wurtele, E.S.; Nikolau, B.J.; Conn, E.E. *Plant Physiol.* **1984**, 75, 4, 979-82.

[112]Manning, K. *Planta* **1986**, 168, 1, 61-66.

[113]Lurie, S.; Klein, J.D. *J. Plant. Phys.* **1990**, 135, 5, 518-21.

[114]McMahon, S.; Arteca, R.N. *Physiol. Planta.* **2000**, 109, 2, 180-7.

[115]Maruyama, A.; Ishizawa, K.; Takagi, T.; Esashi, Y. *Plant. Cell Phys.***1998**, 39, 7, 671-80.

[116]García, I.; Castellano, J.M.; Vioque, B.; Solano, R.; Gotor, C.; Romero, L.C. *The Plant Cell Online* **2010**, 22, 10, 3268-79.

[117]Pirrung, M.C.; Brauman, J.I. *Plant. Phys. Biochem.* **1987**, 25, 1, 55-61.

[118]Dilley, D.R.; Wang, Z.; Kadirjan-Kalbach, D.K.; Ververidis, F.; Beaudry, R.; Padmanabhan, K. *AoB Plants* **2013**, 5.

[119]Leavesley, H.B.; Li, L.; Prabhakaran, K.; Borowitz, J.L.; Isom, G.E. *Toxilogic. Sci.* **2008**, 101, 1, 101-11.

[120]Gilson, M.K.; Honig, B.H. *Nature* **1987**, 330, 6143, 84-6.

[121]García-Moreno, B.E.; Dwyer, J.J.; Gittis, A.G.; Lattman, E.E.; Spencer, D.S.; Stites, W.E. *Biophys. Chem.* **1997**, 64, 1, 211-24.

[122]Shoukry, M.M.; Hassan, S.S. *Cent. Eur. J. Chem.* **2014**, 12, 3, 318-24.

[123]Masoud, M.S.; Abdallah, A.A. *J. Chem. Eng. Data* **1982**, 27, 1, 60-2.

[124]Sigel, H.; Martin, R.B.; Tribolet, R.; Häring, U.K.; Malini-Balakrishnan, R. *Eur. J. Biochem.* **1985**, 152, 1, 187-93.

[125]Snyder, S.E.; Carey, J.R.; Shvets, A.B.; Pirkle, W.H. *J. Org. Chem.* **2005**, 70, 10, 4073-81.

[126]Zhang, X.; Gross, U.; Seppelt, K. *Angew. Chem. Int. Ed. Engl.* **1995**, 34, 17, 1858-60.

[127]Hermann, W.A.; Elison, M.; Fischer, J.; Koecher, C.; Artus, G.R.J. *Angew. Chem. Int. Ed. Engl.* **1995**, 34, 21, 2371-4.

[128]Dyker, C.A.; Lavallo, V.; Donnadieu, B.; Bertrand, G. *Angew. Chem.* **2008**, 120, 17, 3250-3.

[129]Tonner, R.; Frenking, G. *Chem. Eur. J.* **2008**, *14*, 3260-72.

[130]Gies, H.; Gerke, H.; Liebau, F. *Neues Jahrb. Mineral. Monatsh.* **1982**, 3, 119-24.

[131]Gies, H. *Z. Kristallogr.* **1983**, 164, 247-57.

[132]Hirotsu, K.; Kamitori, S.; Higuchi, T.; Tabushi, I.; Yamamura, K.; Nonoguchi, H. *J. Inclu. Phenom.* **1984**, 2, 215-22.

[133]Férey, G. *Chem. Soc. Rev.* **2008**, 37, 191-214.

[134]Kitagawa, S.; Kaitaura, R.; Noro, S.-I. *Angew. Chem. Int. Ed.* **2004**, 43, 18, 2334-75.

[135]Li, J.-R.; Kuppler, R.J.; Zhou, H.-C. *Chem. Soc. Rev.* **2009**, 38, 1477-504.

[136]Rowsell, J.L.C.; Yaghi, O.M. *Angew. Chem. Int. Ed.* **2005**, 44, 30, 4670-9.

[137]Cornia, A.; Caneschi, A.; Dapporto, P.; Fabretti, A.C.; Gatteschi, D.; Malavasi, W.; Sangregorio, C.; Sessoli, R. *Angew. Chem. Int. Ed.* **1999**, 38, 12, 1780-2.

[138]Tian, Y.-Q.; Zhao, Y.-M.; Xu, H.-J.; Chi, C.-Y. *Inorg. Chem.* **2007**, 46, 1612-6.

[139]Takamizawa, S.; Nakata, E.-I.; Saito, T.; Kojima, K. *Angew. Chem. Int. Ed.* **2003**, 42, 4331-4.

[140]Takamizawa, S.; Nakata, E.-I.; Saito, T., Kojima, K. *Cryst. Eng. Comm.* **2003**, 5, 72, 411-3.

[141]Takamizawa, S.; Nakata, E.-I.; Saito, T. *Inorg. Chem. Commun.* **2004**, 7, 1-3.

[142]Takamizawa, S.; Takasaki, Y.; Miyake, R. *Chem. Commun.* **2009**, 43, 6625-7.

[143]Takamizawa, S.; Nataka, E.-I.; Akatsuka, T.; Miyake, R.; Kakizaki, Y.; Takeuchi, H.; Maruta, G. Takeda, S. *J. Am. Chem. Soc.* **2010**, 132, 3783-92.

[144]Plonka, A.M.; Banerjee, D.; Woerner, W.R.; Zhang, Z.; Nijem, N.; Chabal, Y.J.; Li, J. Parise, J.B. *Angew. Chem. Int. Ed.* **2013**, 52, 1692-5.

[145]Takamizawa, S.; Kojima, K.; Akatsuka, T. *Inorg. Chem.* **2006**, 45, 12, 4580-2.

[146]Takamizawa, S.; Kohbara, M.-A. *Dalton Trans.* **2007**, 33, 3640-5.

[147]Zhang, J.-P.; Kitagawa, S. *J. Am. Chem. Soc.* **2008**, 130, 907-17.

[148]Tsue, H.; Takahashi, H.; Ishibashi, K.; Inoue, R.; Shimizu, S.; Takahashi, D.; Tamura, R. *CrystEngComm* **2012**, 14, 1021-6.

[149]Maji, T.; Mostafa, G.; Matsuda, R.; Kitagawa, S. *J. Am. Chem. Soc.* **2005**, 127, 17152-3.

[150]Kim, H.; Kim, Y.; Yoon, M.; Lim, S.; Park, S.M.; Seo, G.; Kim, K. *J. Am. Chem. Soc.* **2010**, 132, 12200-2.

[151]Legrand, Y.-M.; van der Lee, A.; Barboiu, M. *Science* **2010**, 329, 299-302.

[152]Miyahara, Y.; Abe, K.; Inazu, T. *Angew. Chem. Int. Ed.* **2002**, 41, 16, 3020-3.

[153]Udachin, K.A.; Moudrakovski, I.L.; Enright, G.D.; Ratcliffe, C.I.; Ripmeester, J.A. *Phys. Chem. Chem. Phys.***2008**, 10, 4636-43.

[154]Zhang, J.-P.; Chen, X.-M. *J. Am. Chem. Soc.* **2009**, 131, 5516-21.

[155]Lin, J.-B.; Xue, W. Zhang, J.-P.; Chen, X.-M. *Chem. Commun.* **2011**, 47, 926-8.

[156]Liao, P.-Q.; Zhou, D.-D.; Zhu, A.-X.; Jiang, L.; Lin, R.-B.; Zhang, J.-P.; Chen, X.-M. *J. Am. Chem. Soc.* **2012**, 134, 17380-3.

[157]Planas, N.; Dzubak, A.L.; Poloni, R.; Lin, L-C.; McManus, A.; McDonald, T.M.; Neaton, J.B.; Long, J.R.; Smit, B.; Gagliardi, L. *J. Am. Chem. Soc.* **2013**, 135, 7402-5.

[158]Saint Martin, S.; Marre, S.; Guionneau, P.; Cansell, F.; Renouard, J.; Marchetto, V.; Aymonier, C. *Chem. Eur. J.* **2010**, 16, 13473-8.

[159]Wriedt, M.; Sculley, J.P.; Yakovenko, A.A.; Ma, Y.; Halder, G.J.; Balbuena, P.B.; Zhou, H-C. *Angew. Chem. Int. Ed.* **2012**, 57, 9804-8.

[160]Jacobs, T.; Lloyd, G.O.; Gertenbach, J.-A.; Müller-Nedebock, K.K.; Esterhuysen, C.; Barbour, L.J. *Angew. Chem. Int. Ed.* **2012**, 51, 4913-6.

[161]Dietzel, P.D.C.; Johnsen, R.E.; Fjellvåg, H.; Bordiga, S. *Chem. Commun.* **2008**, 5125-7.

[162]Castro-Rodriguez, I.; Nakai, H.; Zakharov, L.H.; Rheingold, A.L.; Meyer, K. *Science* **2004**, 305, 1757-9.

[163]Xie, L.-H.; Lin, J.-B.; Liu, X.-M.; Wang, Y.; Zhang, W.-X.; Zhang, J.-P.; Chen, X.-M. *Inorg. Chem.* **2010**, 49, 1158-65.

[164]Arduengo, A.J., III; Harlow, R.L.; Kline, M. *J. Am. Chem. Soc.* **1991**, 113, 1, 361-3.

[165]Kuhn, N.; Steimann, M.; Weyers, G. *Z. Naturforsch.* **1999**, 54b, 427-33.

[166]Holbrey, J.D.; Reichert, W.M.; Tkatchenko, I.; Bouajila, E.; Walter, O.; Tommasi, I.; Rogers, R.D. *Chem. Commun.* **2003**, 1, 28-9.

[167]Kuhn, N.; Maichle-Mößmer, C.; Weyers, G. *Z. Anorg. Allg. Chem.* **1999**, 625, 851-6.

[168]Petz, W.; Kutschera, C.; Heitbaum, M.; Frenking, G.; Tonner, R.; Neumüller, B. *Inorg. Chem.* **2005**, 44, 1263-74.

[169]Petz, W.; Köhler, K.; Mörschel, P.; Neumüller, B. *Z. Anorg. Allg. Chem.* **2005**, 631, 1779-84.

[170]Petz, W.; Neumüller, B. *Z. Anorg. Allg. Chem.* **2012**, 638, 6, 987-91.

[171]Duong, H.A.; Tekavec, T.N.; Arif, A.M.; Louie, J. *Chem. Commun.* **2004**, 1, 112-3.

[172]Smiglak, M.; Holbrey, J.D.; Griffin, S.T.; Reichert, W.M.; Swatloski, R.P.; Katritzky, A.R.; Yang, H.; Zhang, D.; Kirichenko, K.; Rogers, R.D. *Green Chem.* **2007**, 9, 90-8.

[173]Feroci, M.; Chiarotto, I.; Forte, G.; Inesi, A. *J. CO_2 Util.* **2013**, 2, 29-34.

[174]Van Ausdall, B.R.; Glass, J.L.; Wiggins, K.M.; Aarif, A.M.; Louie, J. *J. Org. Chem.* **2009**, 74, 7935-42.

[175]Ajitha, M.J.; Suresh, C.H. *J. Org. Chem.* **2012**, 1087-94.

[176]Zhou, H.; Zhang, W.-Z.; Liu, C.-H.; Qu, J.-P.; Lu, X.-B. *J. Org. Chem.* **2008**, 73, 8039-44.

[177]Zhou, H.; Wang, Y.-M.; Zhang, W.-Z.; Qu, J.-P.; Lu, X.-B. *Green Chem.* **2011**, 13, 644-50.

[178]Ueno, A.; Kayaki, Y.; Ikariya, T. *Green. Chem.* **2013**, 15, 425-30.

[179]Bantu, B.; Pawar, G.M.; Wurst, K.; Decker, U.; Schmidt, A.M.; Buchmeiser, M.R. *Eur. J. Inorg. Chem.* **2009**, 13, 1970-6.

[180]Van Ausdall, B.R.; Poth, N.F.; Kincaid, V.A.; Arif, A.M.; Louie, J. *J. Org. Chem.* **2011**, 76, 8413-20.

[181]Pinaud, J.; Vignolle, J.; Gnanou, Y.; Taton, D. *Macromolecules* **2011**, 44, 1900-8.

[182]Feroci, M.; Chiarotto, I.; Ciprioti, S.V.; Inesi, A. *Electrochim. Acta* **2013**, 109, 95-101.

[183]Reitz, A.; Wilhelm, R.; Kuckling, D. *Macromol. Symp.* **2013**, 334, 92-7.

[184]Brulé, E.; Guérineau, V.; Vermaut, P.; Prima, F.; Balogh, J.; Maron, L.; Slawin, A.M.Z.; Nolan, S.P.; Thomas, C.M. *Polym. Chem.* **2013**, 4, 2414-23.

[185]Tretyakov, E.; Fokin, S.; Ovcharenko, V.; Romanenko, G.; Shvedenkov, Y. *Polyhedron* **2005**, 2176-84.

[186]Walter, O. *Acta. Cryst. E.* **2013**, E69, o1611.

[187]Blake, A.J.; Hill, S.J.; Hubberstey, P. *Acta. Cryst. E.* **2001**, E57, o1258-60.

[188]Krawczyk, S.; Gdaniec, M.; Sączewski, F. *Acta. Cryst. E.* **2005**, E61, o4185-7.

[189]Yao, X.-J.; Yuan, Q. *Acta. Cryst. E.* **2011**, E67, o1399.

[190]Xia, Z.; Wei, Q.; Yang, Q.; Qiao, C.; Chen, S.; Xie, G.; Zhang, G.; Zhou, C.; Gao, S. *CrystEngComm* **2013**, 15, 86-99.

[191]Gurau, G.; Rodríguez, H.; Kelley, S.P.; Janiczek, P.; Kalb, R.S.; Rogers, R.D. *Angew. Chem. Int. Ed.* **2011**, 50, 12024-6.

[192]Wang, Y.-B.; Wang, Y.-M.; Zhang, W.-Z.; Lu, X.-B. *J. Am. Chem. Soc.* **2013**, 135, 11996-2003.

[193]Wright, H.B.; Moore, M.B. *J. Am. Chem. Soc.* **1948,** 70, 11, 3865-6.

[194]Aresta, M.; Ballivet-Tkatchenko, D.; Dell'Amico, D.B.; Bonnet, M.C.; Boschi, D.; Calderazzo, F.; Faure, R.; Labella, L.; Marchetti, F. *Chem. Commun.* **2000**, 13, 1099-100.

[195]Berkessel, A.; Schröder, M.; Sklorz, C.A.; Tabanella, S.; Vogl, N.; Lex, J.; Neudörfl, J.M. *J. Org. Chem.* **2004**, 69, 3050-6.

[196]Berkessel, A.; Roland, K.; Schröder, M.; Neudörfl, J.M.; Lex, J. *J. Org. Chem.* **2006**, 71, 9312-8.

[197]Esparza-Ruiz, A.; Herrmann, C.; Chen, J.; Patrick, B.O.; Polishchuk, E.; Orvig, C. *Inorg. Chim. Acta* **2012**, 393, 276-83.

[198]Kuhn, N.; Ströbele, M.; Meyer, H.-J. *Z. Anorg. Allg. Chem.* **2007**, 633, 653-6.

[199]Adams, J.M.; Small, R.W.H. *Acta Cryst. B* **1973**, B29, 2317-9.

[200]Baisch, U.; Pagano, S.; Zeuner, M.; Schnick, W. *Eur. J. Inorg. Chem.* **2006**, 17, 3517-24.

[201]Jo, E.; Jhon, Y.H.; Choi, S.B.; Shim, J.-G.; Kim, J.-H.; Lee, J.H.; Lee, I.-Y.; Jang, K.-R.; Kim, J. *Chem. Commun.* **2010**, 46, 48, 9158-60.

[202]Im, J.; Hong, S.Y.; Cheon, Y.; Lee, J.; Lee, J.S.; Kim, H.S.; Cheong, M.; Park, H. *Energy Environ. Sci.* **2011**, 4, 4284-9.

[203]Garbauskas, M.F.; Goehner, R.P.; Davis, A.M. *Acta Cryst. C* **1983**, C39, 1684-6.

[204]Shao, B.; Wang, H.-B. *Acta Cryst. E* **2011**, E67, o3201.

[205]Shi, P.-F.; Xu, T.-T.; Xu, X.-Y.; Niu, S.-R. *Acta. Cryst. E* **2006**, E62, o5191-3.

[206]Lee, B.; Kang, S.H.; Kang, D.; Lee, K.H.; Cho, J.; Nam, W.; Han, O.C.; Hur, N.H. *Chem. Commun.* **2011**, 47, 11219-21.

[207]Teague, C. M.; Dai, S.; Jiang D.-E. *J. Phys. Chem. A* **2010**, 114, 11761.

[208]Chang, C.-C.; Srinivas, B.; Wu, M.-L.; Chiang, W.-H.; Chiang, M.Y.; Hsiung, C.-S. *Organometallics* **1995**, 14, 5150-9.

[209]Yang, K.-C.; Chang, C.-C.; Yeh, C.-S.; Lee, G.-H.; Peng, S.-M. *Organometallics* **2001**, 20, 126-37.

[210]Ruben, M.; Walther, D.; Knake, R.; Görls, H.; Beckert, R. *Eur. J. Inorg. Chem.* **2000**, 5, 1055-60.

[211]Tang, Y.; Zakharov, L.N.; Rheingold, A.L.; Kemp, R.A. *Organometallics* **2004**, 23, 4788-91.

[212]Caudle, M.T.; Brennessel, W.W.; Young, V.G., Jr. *Inorg. Chem.* **2005**, 44, 3233-40.

[213]Davies, R.P.; Raithby, P.R.; Snaith, R. *Organometallics* **1996**, 15, 4355-6.

[214]Kennedy, A.R.; Mulvey, R.E.; Oliver, D.E.; Robertson, S.D. *Dalton Trans.* **2010**, 39, 6190-7.

[215]Kulangara, S.V.; Mason, C.; Juba, M.; Yang, Y.; Thapa, I.; Gambarotta, S.; Korobkov, I.; Duchateau, R. *Organometallics* **2012**, 31, 6438-49.

[216]Dell'Amico, D.B.; Calderazzo, F.; Labella, L.; Marchetti, F. *Inorg. Chem.* **2008**, 47, 5372-6.

[217]Knabel, K.; Krossing, I.; Nöth, H.; Schwenk-Kircher, H.; Schmidt-Amelunxen, M.; Selfert, T. *Eur. J. Inorg. Chem.* **1998**, 1095-114.

[218]Habereder, T.; Nöth, H.; Paine, R.T. *Eur. J. Inorg. Chem.* **2007**, 27, 4298-305.

[219]Feier-Iova, O.; Linti, G. *Z. Anorg. Allg. Chem.* **2008**, 634, 559-64.

[220]Klunker, J.; Biedermann, M.; Schäfer, W.; Hartung, H. *Z. Anorg. Allg. Chem.* **1998**, 624, 1503-8.

[221]Horley, G.A.; Mahon, M.F.; Molloy, K.C. *Inorg. Chem.* **2002**, 51, 5052-8.

[222]Stewart, C.A.; Dickie, D.A.; Tang, Y.; Kemp, R.A. *Inorg. Chim. Acta* **2011**, 376, 73-9.

[223]Cavell, R.G.; The, K.I.; Vande Griend, L. *Inorg. Chem.* **1981**, 20, 3813-8.

[224]Cavell, R.G.; Vande Griend, L. *Phosphorus and Sulfur and Relat. Elem.* **1983**, 18, 1-3, 89-92.

[225]Dickie, D.A.; Coker, E.N.; Kemp, R.A. *Inorg. Chem.* **2011**, 50, 11288-90.

[226]Dickie, D.A.; Ulibarri-Sanchez, R.P., III; Jarman, P.J.; Kemp, R.A. *Polyhedron* **2013**, 58, 92-8.

[227]Courtemanche, M.-A.; Larouche, J.; Légaré, M.-A.; Bi, W.; Maron, L.; Fontaine, F.-G. *Organometallics* **2013**, 32, 6804-11.

[228]Tam, E.C.Y.; Johnstone, N.C.; Ferro, L.; Hitchcock, P.B.; Fulton, J.R. *Inorg. Chem.* **2009**, 48, 8971-6.

[229]Boudreau, J.; Courtemanche, M.-A.; Fontaine, F.-G. *Chem. Commun.* **2011**, 47, 11131-3.

[230]Bertini, F.; Hoffman, F.; Appelt, C.; Uhl, W.; Ehlers, A.W.; Slootweg, J.C.; Lammertsma, K. *Organometallics* **2013**, 32, 6764-9.

[231]Kwon, H.J.; Kim, H.W.; Rhee, Y.M. *Chem. Eur. J.* **2011**, 17, 6501-7.

[232]Ménard, G.; Stephan, D.W. *Angew. Chem.* **2011**, 50, 8396-9.

[233]Ménard, G.; Gilbert, T.M.; Hatnean, J.A.; Kraft, A.; Krossing, I.; Stephan, D.W. *Organometallics* **2013**, 32, 4416-22.

[234]Ménard, G.; Stephan, D.W. *J. Am. Chem. Soc.* **2010**, 132, 1796-7.

[235]Mömming, C.M.; Otten, E.; Kehr, G.; Fröhlich, R.; Grimme, S.; Stephan, D.W.; Erker, G. *Angew. Chem.* **2009**, 48, 6643-6.

[236]Bertini, F.; Lyaskovskyy, V.; Timmer, B.J.J.; de Kanter, F.J.J.; Lutz, M.; Ehlers, A.W.; Slootweg, J.C.; Lammertsma, K. *J. Am. Chem. Soc.* **2012**, 134, 201-4.

[237]Theuergarten, E.; Schlösser, J.; Schlüns, D.; Freytag, M.; Daniliuc, C.G.; Jones, P.G.; Tamm, M. *Dalton Trans.* **2012**, 41, 9101-10.

[238]Peuser, I.; Neu, R.C.; Zhao, X.; Ulrich, M.; Schirmer, B.; Tannert, J.A.; Kehr, G.; Fröhlich, R.; Grimme, S.; Erker, G.; Stephan, D.W. *Chem. Eur. J.* **2011**, 17, 9640-50.

[239]Naqvi, R.R.; Wheatley, P.J.; Forest-Serantoni, E. *J. Chem. Soc. A* **1971**, 2751-4.

[240]Heift, D.; Benkö, Z.; Grützmacher, H. *Dalton Trans.* **2014**, 43, 831-40.

[241]Gershikov, A.G.; Spiridonov, V.P. *J. Mol. Struct.* **1982**, 96, 141-9.

[242]Villiers, C.; Dognon, J.-P.; Pollet, R.; Thuéry, P.; Ephritikhine, M. *Angew. Chem.* **2010**, 49, 1-5.

[243]Ma, J.; Zhang, X.; Zhao, N.; Al-Arifi, A.S.N.; Aouak, T.; Al-Othman, Z.A.; Xiao, F.; Wei, W.; Sun, Y. *J. Mol. Catal. A* **2010**, 315, 76-81.

[244]Pérez, E.R.; Santos, R.H.A.; Gambardella, M.T.P.; de Macedo, L.G.M.; Rodrigues-Filho, U.P.; Launay, J.-C.; Franco, D.W. *J. Org. Chem.* **2004**, 69, 8005-11.

[245]Pereira, F.S.; da Silva Agostini, D.L.; do Espírito Santo, R.D.; deAzevedo, E.R.; Bonagamba, T.J.; Job, A.E.; Pérez González, E.R. *Green Chem.* **2011**, 13, 2146-53.

[246]Edwards, P.R.; Hiscock, J.R.; Gale, P.A.; Light, M.E. *Org. Biomol. Chem.* **2010**, 8, 100-6.

[247]Endo, T.; Nagai, D.; Monma, T.; Yamaguchi, H.; Ochiai, B. *Macromol.* **2004**, 37, 2007-9.

[248]Gomes, C.D.N.; Jacquet, O.; Villiers, C.; Thuéry, P.; Ephritikhine, M.; Cantat, T. *Angew. Chem.* **2012**, 51, 187-90.

[249]Jessop, P.G.; Heldebrant, D.J.; Li, X.; Eckert, C.A.; Liotta, C.L. *Nature* **2005**, 436, 1102.

[250]Jessop, P.G.; Subramaniam, B. *Chem. Rev.* **2007**, 107, 2666-94.

[251] Aschenbrenner, O.; Supasitmongkol, S.; Taylor, M.; Styring, P. *Green. Chem.* **2009**, 11, 1217-21.

[252] Li, X.; Hou, M.; Zhang, Z.; Han, B.; Yang, G.; Wang, X.; Zou, L. *Green Chem.* **2008**, 10, 879-84.

[253]D'Alessandro, D.M.; Smit, B.; Long, J.R. *Angew. Chem., Int. Ed.* **2010**, 49, 35, 6058-82.

[254]Stolaroff, J.K.; Keith, D.W.; Lowry, G.V. *Environ. Sci. Technol.* **2008**, 42, 2728-35.

[255]Larson, J.W.; McMahon, T.B. *J. Am. Chem. Soc.* **1987**, 109, 6230-6.

[256]MacIntosh, I.S.; Sherren, C.N.; Robertson, K.N.; Masuda, J.D.; Pye, C.C.; Clyburne, J.A.C. *Organometallics* **2010**, 29, 9, 2063-8.

[257]Gloaguen, F.; Lawrence, J.D.; Schmidt, M.; Wilson, S.R.; Rauchfuss, T.B. *J. Am. Chem. Soc.* **2001**, 123, 50, 12518-27.

[258]Aldridge, S.; Warwick, P.; Evans, N.; Vines, S. *Chemosphere* **2007**, 66, 4, 672-6.

[259]Allen, F.H. *Acta Crystallogr., Sect. B: Struct. Sci.* **2002**, 58, 380-8.

[260]Drück, U.; Becker, W.; Becker, G. *Z. Kristallogr*. **1984**, 167, 131.

[261]Alcock, N.W. *Acta Crystallogrp., Sect. C: Cryst. Struct. Commun* **1985**, 41, 1549-50.

[262]Schweizer, E.E.; Baldacchini, C.J.; Rheingold, A.L. *Acta Crystallogr., Sect. C: Cryst. Struct. Commun.* **1989**, 45, 1236-9.

[263]Köckerling, M.; Willems, J.B. *Z. Kristallogr.- New. Cryst. Struct.* **1999**, 214, 460.

[264]Bernsdorf, A.; Köckerling, M. *Z. Kristallogr.- New. Cryst. Struct.* **2012**, 227, 85.

[265]Williams, D.H.; Fleming, I. *Spectroscopic methods in organic chemistry*, McGraw-Hill: United Kingdom, **1989**; pp. 42.

[266]Horenstein, B.A. *J. Am. Chem. Soc.* **1997**, 119, 1101-7.

[267]Mani, F.; Peruzzini, M.; Stoppioni, P. *Green Chem.* **2006**, 8, 995-1000.

[268]Cook, F.L.; Bowers, C.W.; Liotta, C.L. *J. Org. Chem.* **1974**, 39, 23, 3416-8

[269]Budavari, S.; O'Neil, M.J.; Smith, A.; Heckelman, P.E. *The Merck Index, an Encyclopedia of Chemicals, Drugs and Biologicals*, 2nd ed.; Merck Co., Inc.: New Jersey, **1989**.

[270]Alongi, K.S.; Shields, G.C. *Annu. Rep. Comp. Chem.* **2010**, 6, 113-38.

[271]Miller, F.A.; Wilkins, C.H. *Anal. Chem.* **1952**, 24, 8, 1253-94.

[272]Alabugin, I.V.; Gold, B.; Shatruk, M,; Kovnir, K, *Science* **2010**, 330, 1047.

[273]Frisch, M.J.; Trucks, G.W.; Schlegel, H.B.; Scuseria, G.E.; Robb, M.A.; Cheeseman, J.R.; Scalmani, G. *et al.*, Gaussian 09, Revision A.1. Gaussian, Inc., Wallingford CT (**2009**).

[274]Møller, C.; Plesset, M.S. *Phys. Rev*. **1934**, 46, 7, 618-22.

[275]Perdew, J.P.; Burke, K.; Ernzerhof, M. *Phys. Rev. Lett.* **1996**, 77, 18, 3865-8.

[276]Perdew, J.P.; Burke, K.; Ernzerhof, M. *Phys. Rev. Lett.* **1997**, 78, 1396.

[277]Adamo, C.; Barone, V. *J. Chem. Phys*. **1999**, 110, 13, 6158-70.

[278]Chai, J.-D.; Head-Gordon, M. *Phys. Chem. Chem. Phys.* **2008**, 10, 44, 6615-20.

[279]Watts, J.D.; Gauss, J.; Bartlett, R.J. *J. Chem. Phys.* **1993**, 98, 11, 8718-33.

[280]Dunning, T.H. *J. Chem. Phys.* **1989**, 90, 2, 1007-23.

[281]Kendall, R.A.; Dunning, T.H.; Harrison, R.J. *J. Chem. Phys.* **1992**, 96, 9, 6796-806.

[282]Halkier, A.; Helgaker, T.; Jørgensen, P.; Klopper, W.; Koch, H.; Olsen, J.; Wilson, A.K. *Chem. Phys. Lett.* **1998**, 286, 3, 243-52.

[283]Tomasi, J.; Mennucci, B.; Cammi, R. *Chem. Rev*. **2005**, 105, 8, 2999-3094.

[284]Morokuma, K. *J. Chem. Phys.* **1971**, 55, 3, 1236-44.

[285]Kitaura, K.; Morokuma, K. *Int. J. Quantum Chem.* **1976**, 10, 2, 325-40.

[286]Ziegler, T.; Rauk, A. *Theoret. Chim. Acta* **1977**, 46, 1, 1-10.

[287]ADF2012.01, SCM, Theoretical Chemistry, Vrije Universiteit, Amsterdam, The Netherlands, http://www.scm.com.

[288]Van Lenthe, E.; Baerends, E.J. *J. Comp. Chem.* **2003**, 24, 9, 1142-56.

[289] Silvi, B.; Savin, A. *Nature* **1994**, 371, 6499, 683-6.

[290]Noury, S.; Krokidis, X.; Fuster, F.; Silvi, B. TopMoD-09, Laboratoire de Chimie Théorique, Université P. & M. Curie, Paris, France, 2009.

[291]APEX2 (Bruker, 2008) Bruker AXS Inc., Madison, Wisconsin, USA

[292]SAINT (Bruker, 2008) Bruker AXS Inc., Madison, Wisconsin, USA

[293]SADABS (Bruker, 2009) Bruker AXS Inc., Madison, Wisconsin, USA.

[294]Sheldrick, G.M. *Acta Crystallogr., Sect. A: Found. Cryst.* **2008**, 64, 1, 112-22.